Master's thesis part 1:

Evaluation of NEMO–PISCES v2 biogeochemical model with field data from a north-south gradient in the Northeast Atlantic Ocean

Utrecht University

university of groningen

Royal Netherlands Meteorological Institute
Ministry of Infrastructure and the Environment

Nomikos Skyllas

Supervisors:

prof. dr. Jack Middelburg (UU)

prof. dr. Anita Buma (RUG)

prof. dr. Richard Bintanja (KNMI - RUG)

dr. Willem van de Poll (RUG)

July 10, 2018

Abstract

Global ocean biogeochemical models are powerful tools that help to study the carbon cycle and to predict its future climate and biogeochemical changes. Recently, the EC-Earth model was supplemented with the community ocean model NEMO (Nucleus for European Modelling of the Ocean) coupled to PISCES (Pelagic Interactions Scheme for Carbon and Ecosystem Studies). Yet, validation of model outcomes was urgently needed. It was the aim of the present study to validate EC-Earth runs using a dataset on water column physics, chemistry and phytoplankton biomass along a transect in the North Atlantic ocean. To this end the capability of the model to simulate vertical profiles of the aforementioned parameters along this transect was studied. During a first model run, water column characteristics were compared to depth field data for salinity, temperature, density, Chl a and nutrient concentrations. In a second run several NEMO-related physical parameters had been modified and the response of phytoplankton dynamics to the new conditions was investigated.

At high latitudes, the first model run did not realistically predict Mixed Layer Depths (MLD). This resulted in a failure to predict the correct timing and magnitude of the phytoplankton spring bloom. In contrast, the "sensitive" MLD criterion used by the model to work well at low latitudes. The 2nd model run improved both phytoplankton dynamics and nutrients distribution, implying that the adjustments in water column physics had improved model calculations. Finally, a constant overestimation by the model regarding relative diatom abundance in nutrient-rich and coastal regions was observed. The present study contributed to the validation of NEMO-PISCES v2 model in the North Atlantic. It also underlines the need for more validation studies, especially in the crucial high-latitude sections of the North Atlantic, where the quality of model calculations was found to be relatively poor.

Contents

List of Figures

37

Chapter 1

Introduction and objectives

Global ocean biogeochemical models are powerful tools that help study the carbon cycle and also predict its response to future and past climate and chemical changes. Attention has shifted to the development of Earth System Models (ESMs) that go beyond the more 'traditional' state-of-the-art coupled atmosphere-ocean general circulation models (AOGCMs).

These ESMs include various climate components such as ocean biogeochemistry, dynamic vegetation, atmospheric chemistry, carbon cycle components and dynamic ice sheets. In the coming decade, ESMs will thus enable us to study the Earth's climate system and its response to perturbations in the broadest sense, with the interactions among the various subsystems most likely resulting in increased accuracy of climate predictions as well as in valuable new insights in climate variability and interactions. In addition, there is rising interest in predicting the impacts of anthropogenic climate change and natural climate variability beyond seasonal to interannual time scales.

A few years ago, it was decided by the European Centre for Medium-range Weather Forecast (ECMWF) member states to develope an ESM (EC-Earth), and the ECMWF weather prediction model was chosen as a starting point. While the current version of EC-Earth is essentially a state-of-the-art AOGCM, a number of additional components are currently under development and will be added to EC-Earth in the coming years. These include dynamic vegetation, ocean biogeochemistry, carbon cycle components and dynamic ice sheets. EC-Earth uses the community ocean model NEMO (Nucleus for European Modelling of the Ocean) coupled to PISCES (Pelagic Interactions Scheme for Carbon and Ecosystem Studies).

The PISCES model simulates marine biological productivity and describes the biogeochemical cycles of carbon and of the main nutrients (P, N, Si, Fe). It falls within the category of Monod models, meaning that it assumes a constant Redfield ratio and phytoplankton growth depends on the external nutrient concentration [2]. PISCES is currently embedded into two modeling systems: NEMO and Regional Ocean Modeling System - Adaptive Grid Refinement In Fortran (ROMS_AGRIF). It has in total 24 compartments: 5 modeled limiting nutrients for phytoplankton growth, 4 living compartments and 3 non-living compartments. The development of PISCES started in 1997 with the release of the P3ZD model which was a simple Nutrient - Phytoplankton - Zooplankton - Detritus (NPZD) model with semi-labile dissolved organic matter (DOM) [2].

As the model kept improving and became more complex with time, the issue of the lack of data for validation was risen [2]. Therefore it was the aim of the present study to compare model runs with field observations, obtained from two cruises in the North Atlantic Ocean. This validation effort would then help to determine possible model deviations, weak points and points of improvement in the model runs. In order to address this issue, it was initiated to compare the output from a test run of PISCES-v2 standalone by the Swedish Meteorological and Hydrological Institute (SMHI) for the current climate, of which the years 2006-2015 were compared with equivalent data taken from both cruises called STRATIPHYT I (2009) and STRATIPHYT II (2011).

Both cruises covered a transect between 29^{o}N and 63^{o}N in the North Atlantic Ocean. The North Atlantic Ocean was chosen because of its key role in global climate and ocean circulation. For example, North Atlantic deep water formation, accounts for 20% of the net ocean

uptake of CO_2 [43]. Another advantage of this transect is that it provides a meridional gradient in stratification with permanent stratification in the subtropics and seasonal stratification in the temperature zones. This gradient allowed to define three different phytoplankton states: Deep Chlorophyll Maxima (southern stations), Upper Chlorophyll Maxima (mid-latitudes) and Deep Mixing (northernmost stations). Thus the STRATIPHYT transect allowed us to study water column characteristics as well as phytoplankton biomass under various conditions.

The main objective of the present project was to make a thorough comparison/validation of the NEMO-PISCES v2 standalone run by SMHI for the years 2006-2015, with the data collected by the STRATIPHYT cruises (2009 and 2011) from the Northeast Atlantic transect. In the case of chlorophyll a surface concentrations, remote sensing data (MODIS aqua and ESA-MERIS) were additionally used. We expected to make a useful contribution to establish where (and where not) PISCES-v2 has biases that need to be addressed in the development towards a full-blown ESM (Earth System Model).

In practice, our focus was on spatial (along the transect), interannual and seasonal variability with respect to Chlorophyll a concentration, nutrients (N, P) and water column physics (temperature, salinity, density and vertical mixing). Another important issue is the capability of the model to simulate vertical profiles of the various variables, and how this depends on vertical mixing (vertical temperature profile).

Chapter 2

Theory

2.1 Ocean Mixing

Upper mixed layer

According to the classical view, the ocean is divided into two layers: an upper layer where temperature and salinity are homogeneously mixed and a deeper, more stable layer (deep ocean) [17, 18]. The upper, mixed layer (ML) is where all the atmosphere - ocean interactions take place. Most oceanic motions have their source in this exchange of momentum, mass and energy between the air and the sea occurring in the ML [17, 18, 29]. These interactions include wind, surface cooling, wave energy, the current shear and other physical phenomena which cause vertical mixing of the ML, thus making it a uniform surface region with respect to density (or temperature) [52, 33]. One of the most important concepts regarding the ocean is the Mixed Layer Depth (MLD). The depth of this homogeneous and neutrally buoyant ML, can be highly variable [33, 29] and is a balance between stabilizing (e.g. heating) and destabilizing forces (e.g. cooling during the night) [26, 52]. The MLD can be further divided into an actively Mixing Layer, a daily remnant layer and the underlying water layers. Yet, in this study only the overall term MLD was used which is defined as "*the layer that has been actively mixed within the past day or few days*" [17, 9].

MLDs are extremely variable: in the summer hemisphere they can be shallower than 20m while during winter, especially at high latitudes they can reach more than 500m of water depth [17]. The reason behind this variability is the combination of many different processes: surface forcing, lateral advection, internal waves, etc [17]. At some locations, in winter, MLs can be as deep as 2000m (see section 2.1.2 - Convective Mixing) [29]. The MLD concept is arbitrary and represents averages over different timescales: days, months etc [17]. Many different definitions for the MLD estimation can be found in the literature, but the ones that are mainly used are based on a temperature or density criterion [33], for example a difference of 0.3^{o}C (ΔT=0.3^{o}C) between the MLD and the surface.

The ML is crucial for various oceanic processes, for example it helps to drive ocean circulation by wind stress [29]. Additionally, it is very important for biology, firstly because it is rich in nutrients in winter, before the spring bloom (mainly due to the convective mixing, explained in the next section) and secondly because it keeps phytoplankton confined in a layer close to the sunlit surface layer, potentially triggering the phytoplankton bloom [17, 46], leading to rapid utilization of the available nutrients.

Sverdrup [51] created first a theoretical framework regarding the onset of phytoplankton blooms, the "critical depth hypothesis". This hypothesis relies on the assumption that winter mixing is so deep that it causes light limitation to phytoplankton cells, hindering their growth. The springtime shoaling of the ML removes the light limitation as cells can now reach the well - lit surface waters. The critical depth is right where growth matches exactly the losses of phytoplankton and as soon as the MLD becomes shallower than that, the spring bloom is initiated [51]. During the last 65 years, research has lead to advances of the "critical depth hypothesis" adding more factors that affect algal growth than just light limitation [49, 4, 37].

Convective Mixing

The ocean in general, is for a large part stratified. Unstable regions can be found mainly at high latitudes, where the cool surface waters become dense enough to cause vertical instability resulting in sinking [60, 41]. These special places, located in the North Atlantic ocean, in the Southern ocean and in the Northwestern Mediterranean sea, are weakly stratified and in the winter they experience a deep, convective mixing down to the deep ocean [41]. This phenomenon follows an annual cycle, and is followed by restratification of the water column [41].

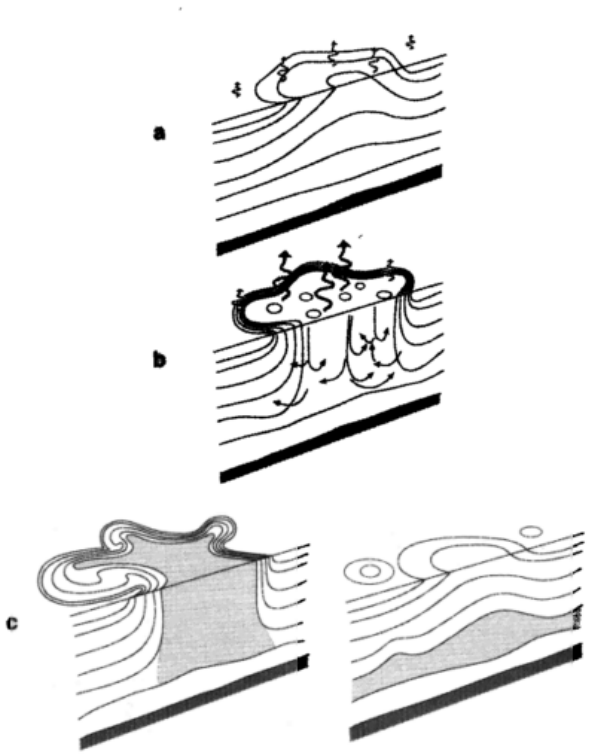

Figure 2.1: Diagram of the 3 phases of deep convective mixing: (a) preconditioning, (b) deep convection and (c) lateral exchange and spreading. Curly arrows represent the buoyancy flux through the sea surface, continuous lines represent stratification and the grey color is the water mass which has been mixed by convection. Adapted from Marshall & Schott (1999) [41].

Convection can be described, in a simplistic way, as a mixing between light and heavy water which change places or become homogeneous [60]. This type of mixing takes place in small areas and in short timescales and can reach depths of more than 1000m [17] affecting the properties of the deep ocean [29]. It can be explained using 3 steps, as shown in Fig.2.1: (a) "Preconditioning" happens at a large scale, meaning hundreds of km and during this phase weakly stratified waters from the inner ocean are brought up to the surface (Fig.2.1(a)). (b) During the second phase of "convective mixing", the water column is mixed in many plumes, by a process triggered by a buoyancy loss of the surface waters because of the winter conditions. This intense mixing of the heavy and cold surface waters with deeper waters is more localized and its depth and intensity vary greatly among years and even decades. (c) After a certain period of time, on the scale of days, the vertical mixing stops and gets replaced by horizontal mixing from eddies. The recently mixed waters disintegrate under the influence of eddies and gravity and after weeks (or months in some cases) are completely homogenized with the surrounding waters [41].

The North Atlantic ocean is critical for Earth's climate. Deep convection in this part of the world is the driving force behind the thermohaline circulation, which transports heat and salt around the global oceans. Additionally, convection is what makes the North Atlantic such an important CO_2 sink, as the dense water formation and sinking to immense depths (more than 1000m) can take up significant parts of the anthropogenic CO_2 emissions [55, 41].

2.2 Phytoplankton Dynamics

The oceans play a critical role in the regulation of the carbon cycle and this role is mainly controlled by the ocean's solubility and the biological pumps, meaning organisms that can export carbon to the deep ocean or the sea floor [2]. The North Atlantic spring bloom is characterized by an impressive seasonal increase in phytoplankton biomass. Blooms found here are capable of fueling the marine food web of the entire area while additionally taking up vast amounts of CO_2 [42]. Phytoplankton takes up CO_2 at the ocean surface, through photosynthesis, and produces organic matter part of which is exported to the deep ocean, in a process known as the "biological pump". Phytoplankton is responsible for almost 50% of global photosynthesis and

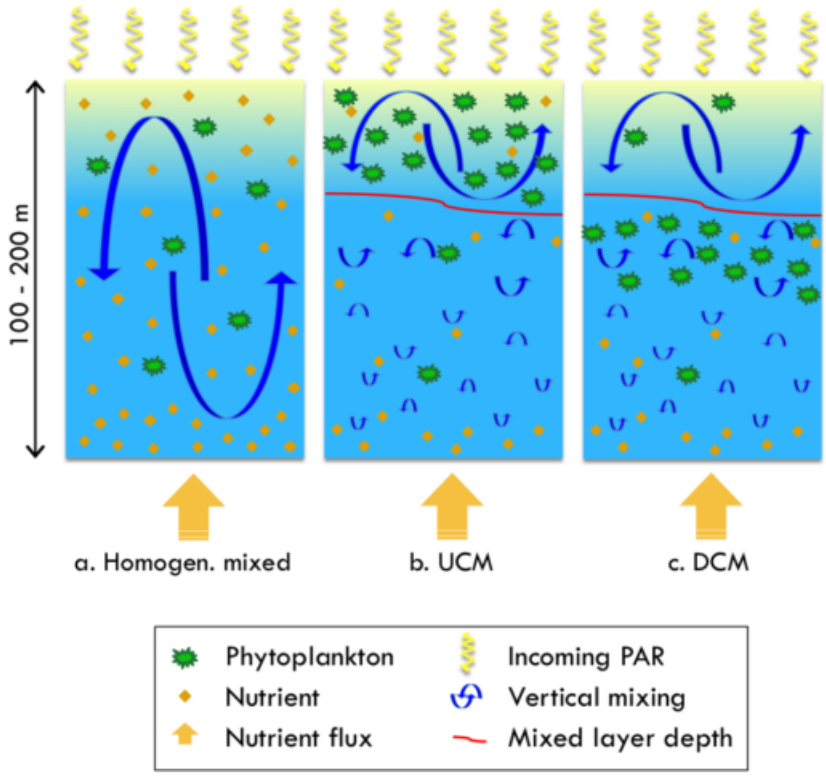

Figure 2.2: The 3 main phytoplankton growth states: a) homogeneously mixed over the water column, b) restricted to the mixed layer in an Upper Chlorophyll Maximum (UCM), and c) restricted by nutrient limitation to grow below the mixed layer in a Deep Chlorophyll Maximum (DCM). Adapted from Hahn-woernle et al. (2016) [26]

stores carbon in the deep ocean over long time periods, therefore regulating the climate [19]. Its (and consequently chlorophyll-a) concentrations vary on annual or even decadal timescales which correlate to climatic variations regulating the availability of light, nutrients, grazers and the sinking speed of the cells [59, 25]. It is therefore clear that understanding the mechanisms controlling the phytoplankton dynamics is vital in predicting the future of marine ecosystems under the changing climate.

Vertical mixing is the controlling mechanism behind phytoplankton growth, since it determines the availability of light and nutrients [31, 25], as explained in the former section. The 3 main growth states can be described as follows: In winter (Fig.2.2(a)) the deep convection mixes nutrients and algal cells down to a few hundred meters (in some cases even 600m), resulting in a nutrient-rich water column. Phytoplankton cells are diluted and spend most of the time in darkness and therefore show extremely low (to no) growth [25, 59]. In spring (Fig.2.2(b)) the shoaling of the mixed layer (ML) confines phytoplankton close to the surface where it is exposed to sufficient Photosynthetically Active Radiation (PAR) under nutrient replete conditions (derived from deep winter mixing). Therefore, in this Upper Chlorophyll Maximum (UCM) state, cells grow at very high rates and as a result they may form a "spring bloom". The termination of the winter convection and the onset of the spring stratification is a crucial point which can determine the phytoplankton dynamics of the entire year [59, 42]. After the spring bloom (Fig.2.2(c)), later in the warm season, the ML becomes nutrient-depleted (nitrate, phosphate) thereby limiting growth. Phytoplankton sinks deeper until it meets a nutrient-rich layer where PAR can still penetrate. This Deep Chlorophyll Maximum (DCM) state dominates the permanently stratified regions (e.g. Subtropical Atlantic) and also appears in the seasonally-stratified regions like the mid-latitude Atlantic ocean [25]. However, phytoplankton productivity is low here, due to the overall low light levels at depth, in combination with low nutrient levels.

Models predict a further future increase in surface warming. This will result in the expansion of (permanently as well as temporarily) stratified regions. This will have major consequences for nutrient and irradiance dynamics, essential for phytoplankton growth. As a result, carbon

sequestration, the biological pump, as well as local ecosystems will be significantly affected [59, 43]. For example, primary production may increase initially in high latitude, light-limited regions, in the short run, but a prolonged stratification can result in a depletion of nutrients in the surface layer, affecting ecosystems and reducing their carbon export capacity [43]. Earth system models may help us to understand how complex interactions associated with climate change may impact future ocean physics, chemistry and finally also biology, with all the potential feedback mechanisms. As stated above, the present validation project will hopefully contribute to a realistic model design, such that reliable future predictions can eventually be made.

2.3 Modelling

EC-Earth

It is becoming clear that in order to accurately understand the Earth's global climate response, all the interactions between its subsystems must be studied. Therefore, a shift to the development of Earth System Models (ESM) is observed, meaning models that include various climate components: ocean biochemistry, dynamic vegetation, atmospheric chemistry, carbon cycle components and dynamic ice sheets. In the near future ESMs will allow us to study the Earth's climate system in a larger scale and take into account all the interactions between its subsystems. Hopefully, this will lead to an increased accuracy in climate prediction, weather prediction and better estimations of the anthropogenic climate change in large timescales. Not many years ago it was decided by the members of the European Centre for Medium-range Weather Forecast (ECMWF) to develope a European ESM based on the existing ECMWF weather prediction model. The result was a model supported by 32 institutes from 12 European countries: the EC-Earth model. A number of EC-Earth climate components are still under development and will be added in the coming years but regarding ocean biogeochemistry, the NEMO - PISCES v2 coupled model is already being used [8].

NEMO-PISCES v2

The Nucleus for European Modelling of the Ocean (NEMO) has been built on the OPA (Ocean PArallélisé) ocean general circulation model and is used for a variety of different applications, small- or large-scale as ocean model or even coupled with other models in order to study the interactions between the climate subsystems. It consists of the OPA model, the LIM2 (Louvain-la- Neuve Ice Model v2) ice model and the PISCES v2(Pelagic Interactions Scheme for Carbon and Ecosystem Studies volume 2) biogeochemical model [39, 56].

The development of PISCES global biogeochemical model started in 1997 with the introduction of the P3ZD model and its target was to simulate marine biological productivity, by including two phytoplankton and two zooplankton classes, and the biogeochemical cycles of carbon and the main nutrients: P, N, Si and Fe. PISCES is incorporated into two different models, NEMO and ROMS_AGRIF, and is being used for studying a wide variety of spatial scales and timescales, reaching up to simulations of thousands of years [2].

2.4 In Situ Observations of Mixing and Chlorophyll a

Understanding the mechanisms controlling the phytoplankton dynamics in different vertical stability regimes, permanently stratified, seasonally stratified and convective mixing, is crucial to estimating the response of marine ecosystems to climate change [43]. Different stratification responses are expected by different Atlantic ocean regions: subtropical, mid-latitude and subpolar [59]. Unfortunately, most of the phytoplankton studies have focused on the oligotrophic (subtropical) ocean and neglected temperate and subpolar regions [59]. The same goes for microprofiler studies, focusing in the physical parameters of the ocean, which are usually carried

out in the Pacific ocean and very rarely in the Atlantic [31], which is a key region for the global climate, as explained earlier.

What is unique about the North Atlantic, is the fact that it offers a meridional gradient in stratification: Permanently stratified in subtropical latitudes, seasonally stratified in midlatitude and winter convection in subpolar latitudes [43]. In order to investigate how changes in stratification in these 3 regions affect primary productivity, 2 STRATIPHYT boat cruises were organized by the Royal Netherlands Institute for Sea Research (NIOZ, https://www.nioz.nl). The first cruise, STRATIPHYT-I (Las Palmas, Reykjavik, 15 July to 9 August 2009) provided measurements of mixing, phytoplankton and nutrients along a North Atlantic transect. Exactly the same procedure was followed by the second cruise as well, STRATIPHYT-II (Las Palmas– Reykjavik, 6 April–3 May 2011), only in a different season this time. This way, datasets from 2 different seasons and 3 different stratification regimes were obtained, facilitating the understanding of these under-studied oceanic regions [31].

Chapter 3

Methodology

3.1 STRATIPHYT project

Two cruises took place along a transect from the Canary islands (29^{o}N) to Iceland (63^{o}N): STRATIPHYT I in the summer of 2009 (July-August) and STRATIPHYT II in the spring of 2011 (April-May) (Fig.3.1). Samples were collected, on board of the R/V Pelagia, from 32 stations for each cruise, over the course of 1 month and an effort was made for the stations to be separated by 100km. The water samples were collected from the top 250m of the water column and they were more than 10 per station. During the 2009 cruise 24 plastic samplers (General Oceanics type Go-Flow, 10 L) were used and during the 2011 cruise they were replaced by 24 Teflon samplers (NIOZ design Pristine Bottles, 27 L). The bottles were mounted on a trace-metal free titanium frame carrying a CTD (Seabird 91; standard conductivity, temperature, and pressure sensors) and auxiliary sensors for chlorophyll autofluorescence (Chelsea Aquatracka Mk III), light transmission (Wet-Labs C-star) and PAR (Satlantic) [43, 59].

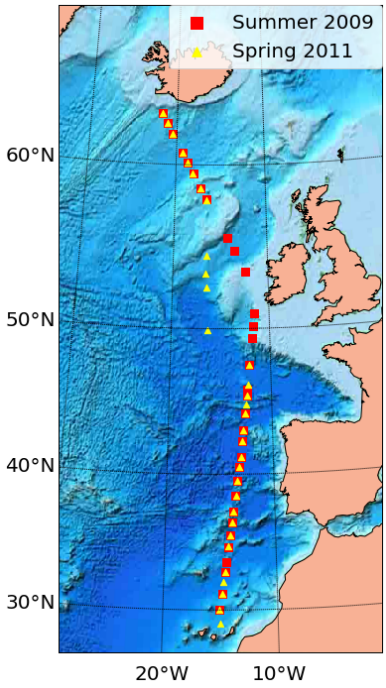

Figure 3.1: Bathymetric map of the Northeast Atlantic ocean depicting station locations and station numbers for the spring 2011 (yellow triangles) and summer 2009 (red squares) STRATIPHYT cruises

3.1.1 Chlorophyll-a

The autofluorescence sensor measurements were calibrated with HPLC Chl a data, as described by van de Poll et al. (2013) [59] in order to estimate the total Chl a concentrations used in this study [43].

3.1.2 Nutrients

Water samples of 6ml were taken from multiple bottles, for nutrients: phosphate (PO_4), ammonium (NH_4), nitrate (NO_3) and nitrite (NO_2). The samples were filtered through 0.2μm Acrodisc filters and measured on-board for inorganic PO_4, NH_4, NO_2, and NO_2 + NO_3 using a Bran & Luebbe Quaatro autoanalyzer. The detection limits for the two cruises ranged from 0.06 to 0.10 μmol L^{-1} for NOx, 0.010 to 0.028 μmol L^{-1} for PO_4 and 0.05 to 0.09 μmol L^{-1} for NH_4 [43, 59].

3.1.3 Vertical Mixing

Vertical mixing measurements were performed with the Self Contained Autonomous Microprofiler (SCAMP). A more in-depth description of this method can be found in the publications by

Jurado et al. (2012a, b) [32, 31]. The device was used at 17 stations in spring 2011 and 14 stations in summer of 2009 and only down to 100m depth [43].

3.2 The NEMO-PISCES model

Two standalone runs of NEMO-PISCES were performed by the SMHI (Swedish Meteorological and Hydrological Institute), for the years 1958 to 2016 (run 1) and 1948 to 2009 (run 2). The version of NEMO used was v3.2 and had a horizontal resolution of 1^o and a vertical resolution of 75 levels (0.5m thickness at the surface to 610m at the bottom).

NEMO run 1 was forced at the surface using DFS 5.2 fields developed by the European collaboration, DRAKKAR [DRAKKAR Group, 2007]. This uses the ERA-interim (ERAi) reanalysis product, which provides precipitation and downward short-and long-wave radiation, 10 m wind and 2 m air humidity and temperature from 1958 until 2016. It is combined with ERA40 reanalysis for the 10 m wind and 2 m air humidity and temperature of years 1958 to 1978. ERA40 reanalysis records are interpolated to that of the ERAi: 3-hourly and 0.7^o. NEMO run 2 was forced at the surface using the protocol of the Coordinated Ocean-ice Reference Experiments (CORE) [22, 23, 16] interannually varying experiment (CORE-II). The forcing data set covers the years 1948 to 2009, the physical ocean fields are forced using the interannualy varying atmospheric state from Large & Yeager (2009) [36] combined with river runoff data from Dai and Trenberth (2002) and Dai et al. (2009) [14, 15]. The 2nd run was performed after changing 3 parameters: **a)** Snow Thermal Conductivity (rn_cdsn) from 0.30 (run 1) to 0.40 W K^{-1} M^{-1}, **b)** Ocean Turbulent Kinetic Energy (nn_etau) penetration depth from 1 (run 1) to 0 and **c)** Ocean Langmuir Waves Cell Size (rn_lc) from 0.15 (run 1) to 0.2. The aforementioned three changes will primarily affect the ocean vertical mixing.

PISCES v2 consists of 24 compartments in total. It includes 5 modeled limiting nutrients: nitrate (NO_3) and ammonium (NH_4), phosphate (PO_4), silicate (Si) and iron (Fe), with NO_3, NH_4 and PO_4 following a constant Redfield ratio in every organic compartment. Nitrogen (N) undergoes fixation and denitrification in the open ocean and the upper sediments. The external sources of nutrients, meaning river run-off and dust, are independent from the Redfield ratio. 4 living compartments are modeled, consisting of 2 phytoplankton (nanophytoplankton and diatoms) and 2 zooplankton size classes (microzooplankton and mesozooplankton). For phytoplankton, the Fe/C, Chl a/C and Si/C (only for diatoms) ratios are prognostically predicted by the model. Regarding zooplankton, only its total biomass is modeled. Overall, the $C/N/P/O_2$ ratios are constant and do not vary. The Redfield ratio used is 122/16/1 (C/N/P) and the O/C ratio is 1.34. Bacteria are not modeled. Three non-living compartments are modeled, including semi-labile dissolved organic matter, small sinking particles and large sinking particles. Additionally, PISCES simulates dissolved inorganic carbon, total alkalinity and dissolved oxygen. See Aumont et al. (2015) [2] for a full description of PISCES.

3.3 Combining the model with in situ measurements

The results of the 2 NEMO-PISCES v2 runs were provided by the SMHI, in NetCDF database format, and out of them the years 2009 & 2011 from run 1 and 2009 from run 2 were selected. Before any process, several "test" plots were created in order to see if these years had any extreme values (outliers) regarding the parameters of interest. Then, the 2009 and 2011 files were processed with CDO (Climate Data Operators), a software designed by the Max Planck meteorological institute (https://code.mpimet.mpg.de/projects/cdo/), in order to convert the coordinates to regular 1×1^o grids.

The STRATIPHYT I & II data were provided by Groningen University (RUG), by prof. dr. Anita Buma and dr. Willem van de Poll, in Microsoft Office Excel format. The model results (NetCDF files) and the field data (Excel files) were further processed and compared using the Python pro-

gramming language (https://www.python.org/). More specifically, the parameters of interest from NEMO-PISCES v2 and STRATIPHYT: Salinity, temperature, density, Chl a concentration, nutrient concentrations were plotted for the exact same coordinates as the 32 stations (see Fig. 3.1) and compared, using scatter plots, depth profiles and maps. Furthermore, remote sensing data regarding surface Chl a were additionally used in some cases (visualized on maps) in order to facilitate the comparison and the understanding of the North Atlantic phytoplanton dynamics. The remote sensing data were obtained from the European Space Agency (ESA) and National Aeronautics and Space Administration (NASA) websites. The ESA remote sensor used was the MEdium Resolution Imaging Spectrometer (MERIS, https://earth.esa.int/web/guest/missions/esa-operational-eo-missions/envisat/instruments/meris) and the NASA remote sensor was the Moderate Resolution Imaging Spectroradiometer (MODIS) Aqua (https://oceancolor.gsfc.nasa.gov/data/aqua/).

Chapter 4

Results

4.1 NEMO-PISCES run 1 compared to STRATIPHYT observations

4.1.1 Physical parameters

Since ocean biogeochemichal processes are modulated by ocean physics, 5 physical parameters are shown first (Fig.4.1) : Mixed layer depth (MLD), stratification index (SI), sea surface temperature (SST), sea surface salinity (SSS) and light attenuation coefficient (Kd). In 4.1**(a)** it is clear that model and observations do not diverge significantly, with MLDs fluctuating around 150m in the northern part of the transect, north of 55^{o}N for spring 2011. It needs to be mentioned that in the calculation of the STRATIPHYT MLDs, the same criterion as in the model was used: A difference of 0.01kg/m^3 in potential density ($\sigma\theta$) from the reference depth of 10m ($\Delta\sigma\theta$ = 0.01kg/m^3, reference: 10m), in order for the results to be comparable.

The measured stratification index ($\Delta\sigma\theta$ between 10m and 200m depth) [59] values of 2011 can be divided in two regions (Fig.4.1 **(b)**): one south of 50 ^{o}N with values ranging between 0.20-0.50 kg/m^3 and one north of 50 ^{o}N with density differences close to zero (density difference $<$0.125) [59], implying a well-mixed regime. In summer, the values are higher along the entire transect, which according to De Boyer Montegut et al. (2004) implies that all of the stations are stratified ($\Delta\sigma\theta > 0.125$ kg/m^3) [17].

The $\sigma\theta$ of sea water according to NEMO-PISCES, was calculated using the UNESCO equation of state [57], which for a temperature in the range of 0 to 40 ^{o}C, salinity in the range of 0 to 42 PSU and a given pressure, allows the determination of $\sigma\theta$. The model results follow a similar pattern but produce in general higher values for the first part, predicting slightly more stratified conditions. In 2011, the modelled density differences between surface and 200m depth follow quite closely the observations, translating into similar spring MLDs, as density plays a crucial role in the deep, convective mixing. The 2009 values are higher, as expected, meaning that all stations are stratified as discribed also by Van De Poll et al. (2013) [59]. NEMO-PISCES (UNESCO formula) follows once again the measured density differences closely, with slightly higher values in the northern part.

SST's measured by STRATIPHYT cruises and calculated by NEMO-PISCES (Fig.4.1**(c)**) fit very well for spring of 2011 and summer of 2009. The spring temperatures start from 18-20 ^{o}C in the first stations and drop to 8 ^{o}C at 63 ^{o}N while the summer ones start from over 22 ^{o}C and drop to 12 ^{o}C in the last station.

In the case of SSS (Fig. 4.1**(d)**) a different behaviour is observed: the STRATIPHYT measurements for 2009 and 2011 fit fairly well and both start from almost 37 PSU in the south, which drops to 35 PSU in the north (63 ^{o}N). The model results for 2009 and 2011 fit with each other and are constantly 0.5 PSU lower than the measurements. The problem here is that model and observations do not agree. One more thing needs to be pointed out: Model results exhibit a decrease in salinity between 52-60 ^{o}N, at the stations over the Irish continental shelf implying a possible fresh water input.

Light attenuation coefficient (Kd) was measured along the transect (Fig.4.1**(e)**) and for 2011

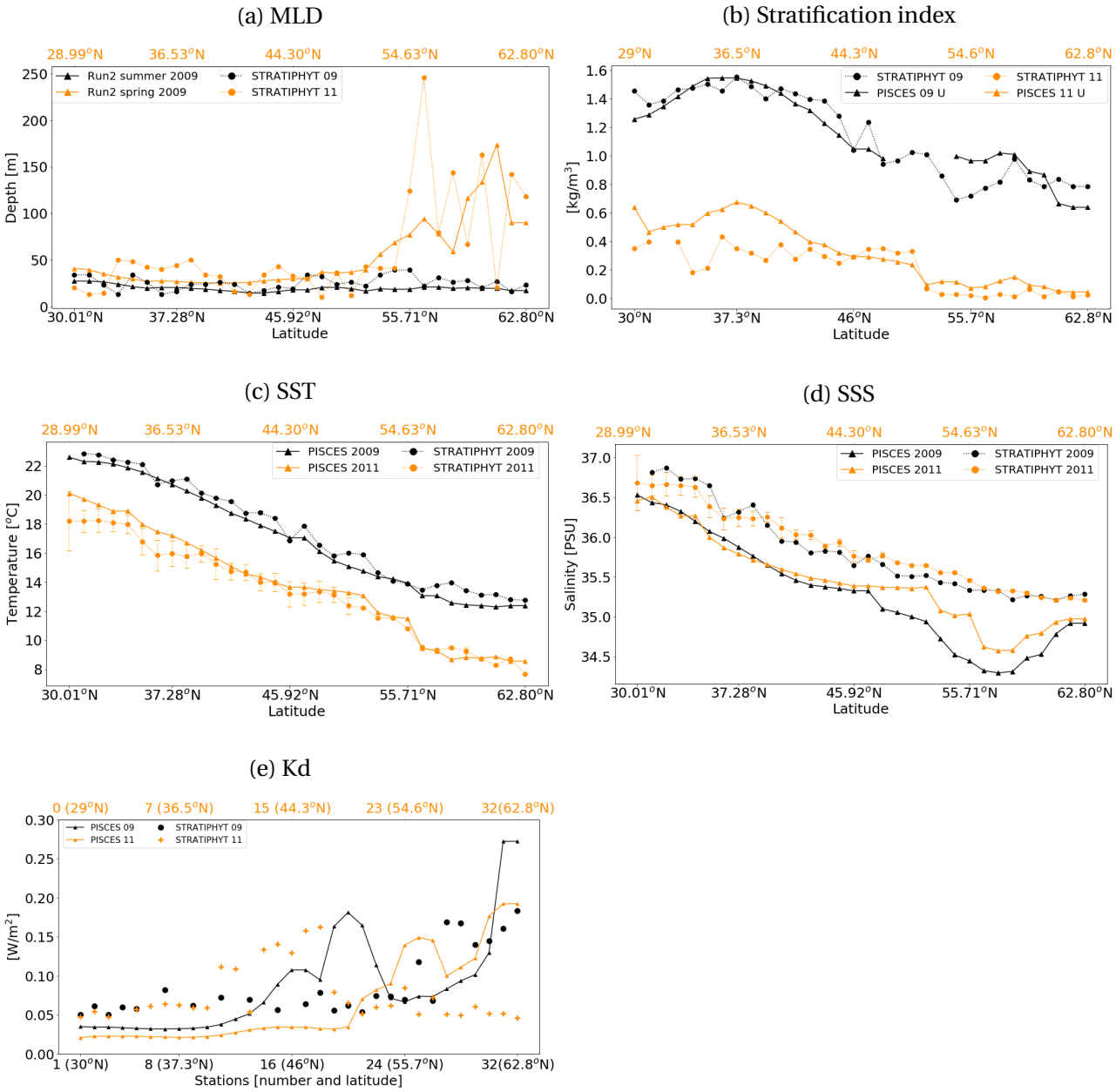

Figure 4.1: Physical parameters (MLD, SI, SST, SSS and Kd) as measured by STRATIPHYT cruises (orange dots for 2011 and black for 2009) and model results as April-May (orange triangles) and July-August (black triangles) averages along the transect shown in Fig. 3.1. Standard deviation is plotted as errorbars around the STRATIPHYT curves (orange and black color). Latitude is along the x-axis with orange (for 2011) and black color (for 2009).

Spring it was found to have low values south of 40 ^{o}N, in the southern part of the transect where Deep Chlorophyll Maxima (DCM) states dominate. North of 50 ^{o}N, in the northern part of the transect where deep mixing distributes chl a over the water column, Kd was again low. The values were almost quadruple in the middle of the transect, between 40-55 ^{o}N, were the chlorophyll is concentrated at the surface because of the Upper Chlorophyll Maxima (UCM) states observed in that region. The modelled Kd (calculated by linear regression of natural log - transformed PAR plotted against depth, from 0 to 100m) for spring 2011 follows a different pattern as it has values close to 0 south of 50 ^{o}N, which increase gradually up to 0.20 in the last station, following the modelled, spring Chl a distribution which is different than the observed one: the northern part of the transect exhibits deep UCM states instead of deeply mixed phytoplankton.

The measured Kd of summer 2009 maintains low values until 55 ^{o}N along the former (spring) DCM and UCM stations which in summer have lower chl a concentrations because of the ML

nutrient depletion. It starts to increase above that latitude, along the UCM group of stations which are now formed were in spring there was deeply mixed phytoplankton, until reaching maximum values (0.20) in the last stations. The summer 2009 model results give a very low Kd until 40 ^{o}N which fits with the observations for this part of the transect where STRATIPHYT and NEMO-PISCES agree on the DCM state of the stations. In the northern part, the increase captured by the cruise is not reproduced by the model because it predicts weak DCM states in this region. This can be traced back to the different spring Chl a distribution predicted by the model, which now causes further implications in the summer Chl a distribution. The Kd can be affected by waves, air bubbles, phytoplankton, sediments and dissolved organic material [25]. In this case mainly the phytoplankton was taken in to consideration as waves and air bubbles are very localized. Nevertheless, a possible contribution of sediments and dissolved organic matter should not be excluded for the stations close to Ireland and Iceland (19-23 and 31-32 respectively), especially for NEMO-PISCES results.

The four stations in Fig. 4.2 were selected from a total of 32 along the transect. An effort was made for the stations to be as representative as possible of all the different parts from 29 up to 63 ^{o}N, resulting to two "southern" stations with shallow MLDs but deeper bathymetry and four "northern" with deeper MLDs but shallower sea bottom depths. For all of the stations, the same pattern can be seen for spring 2011 (Fig.4.2**(a)**) with measured (1028-1030 kg/m^3) and modelled (1027 kg/m^3) potential density being almost a straight line from surface down to 500m depth, illustrating a homogeneous water column. There is one significant difference: The model constantly underestimates the density by 1-3 kg/m^3, most likely because of the salinity underestimation as explained in the following paragraph. In summer, the model succeeds in predicting the density of the upper layer which clearly shows the formation of the ML. Below 50m though, it has the same problem as in spring: underestimation of density. Station 25 shows a divergence between modelled and measured potential density in the upper 200m.

Salinity (Fig.4.2**(b)**) can be described as homogeneous, with field data and model results producing straight lines around 36 PSU (stations 5 and 17) and 35 PSU (stations 25 and 32). Two remarks must be made: (a) modelled salinity is always 0.5 PSU lower than the measured one, as mentioned in the previous paragraph and (b) in station 25, shallower than 200m a decrease is observed in the model results giving values close to 34 PSU, something that agrees with the SSS decrease around 55^{o}N (Fig.4.1) which implies fresh water input. These four plots also indicate that the stratification is caused by an increase in temperature and is not connected to salinity decrease via precipitation or fresh water input (except for station 25).

In the temperature depth profile (Fig.4.2**(c)**) an almost perfect match between field and model data can be seen. Spring 2011 temperatures are almost homogeneous along the water column (down to 500m) with a general decrease observed from south (15^{o}C) to north (9^{o}C). The summer warming of the surface water that leads to the formation of a surface layer is, indeed, apparent in the summer data (black circles) and model results (black lines). The same remark as with salinity has to be made again: In station 25, shallower than 200m slight fluctuations are observed in the model results, probably because of cold fresh water input.

Measured temperature, salinity and density depth profiles follow the expected succession from a warmer and saltier southern region to a colder and fresher one in the north and the measured values are within the range of northeast Atlantic typical values [58]. The potential temperature–salinity relation indicates that the water sampled by STRATIPHYT cruises belongs to the Eastern North Atlantic Central Water (ENACW) [31]. Moreover, the profiles are constant with depth and show that the winter deep convective mixing took place not long before the sampling dates [31]. So far, after paying attention to the physical parameters' graphs, a pattern emerges: salinity is underestimated by the model, density is subsequently underestimated and there is fresh water input in the upper layer of the northern stations. All of these observations indicate a possible problem with the deep, convective winter mixing calculation by NEMO-PISCES, something vital in the North Atlantic which is dominated by this type of mixing [42].

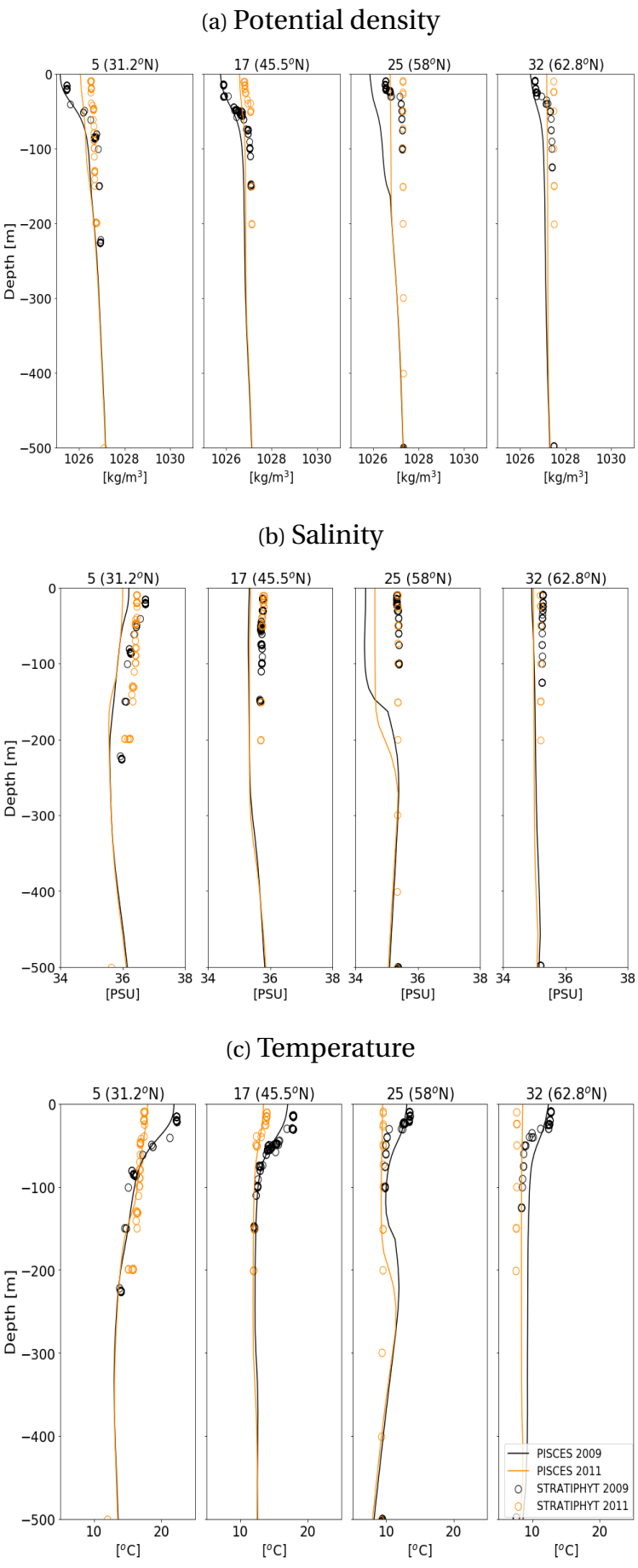

Figure 4.2: Depth profiles of four stations along the transect, for density, salinity and temperature, as measured by STRATIPHYT cruises (dots and crosses) and model results (lines) as April-May and June-August averages along the transect shown in Fig. 3.1. Orange color for 2011 and black for 2009.

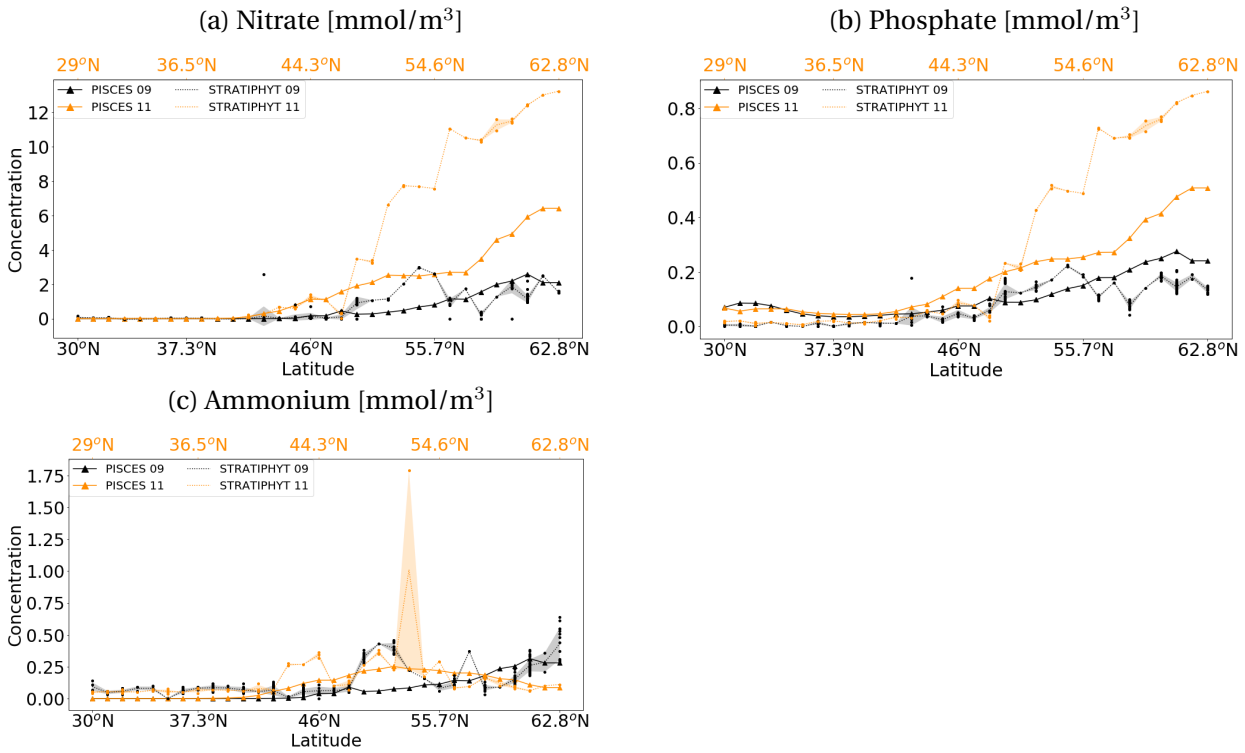

Figure 4.3: Basic nutrient surface concentrations (top 15m) measured by STRATIPHYT cruises (dots) and model results (triangles) along the transect shown in Fig. 3.1. The cruise of 2011 is plotted in orange color and the one of 2009 in black. Model results are 2011 April-May average (orange color) and 2009 July-August average (black color). Standard deviation is plotted as shade around the STRATIPHYT curves (orange and black color) and multiple dots show the multiple samples at each sampling location.

4.1.2 Nutrients

Measurements and model results (Fig.4.3) agree that surface nitrate is depleted in latitudes south of 43 ^{o}N, in the first 10, nutrient-limited stations of the transect which are located close to the oligotrophic gyre [50]. In spring, north of this latitude, in the less stratified, northern part of the transect, nitrate concentrations at the surface start increasing until a maximum value of 13 mmol/m^3 in the last station. The 2011 model results follow the same pattern, only fail to picture the magnitude of nutrient increase in the upper layers of these nutrient-rich stations: the modelled maximum NO_3 concentration (6 mmol/m^3) is less than half of the measured one, most likely due to mixing depth issues or/and consumption from early phytoplankton growth. The bottom concentrations of NO_3 are similar between measurements and model (Fig.4.8), so the low surface concentrations cannot be attributed to this. For summer 2009, model and STRATIPHYT cruise agree fairly well, with an increase starting at 50 ^{o}N this time, as spring blooms have consumed the ML nutrients and reaching values of 2 mmol/m^3. A bump can be seen in the observations, only during the summer 2009 cruise, at 50-55 ^{o}N (stations 20-22) where the sampling stations were on the continental shelf of Ireland and close to its coast, implying possible land input.

A similar pattern can be described for surface phosphate as well, with maximum measured concentrations (0.9 mmol/m^3) of more than double than the modelled ones for spring and a relatively good match between NEMO-PISCES and field data for summer. It is interesting that in the PO_4 - depleted ML's south of 45 ^{o}N, the model still predicts - low - concentrations. As a general remark, it is fair to say that the "real-life" (measured ones) algae have possibly twice as much nutrients available compared to the modelled algae, which leads to an underestimation of their growth by the model.

In general, surface ammonium concentrations follow a similar pattern to the Chl a distribution, as remineralization is the main source of this nutrient. South of 40 ^{o}N, in the nutrient-limited part of the transect, both STRATIPHYT cruises measured concentrations of around 0.1

mmol/m^3 at the surface and the model calculates zero. North of 40 ^{o}N, during spring, a bump is observed (0.4 mmol/m^3) right where the spring bloom (UCM) stations are located, between 40-48 ^{o}N. Further north, intermediate values were measured at the deeply mixed stations. The model fails to capture these spring patterns, following its own, different Chl a distribution, as mentioned before (4.1(**e**)). In summer, the STRATIPHYT transect is subdivided in a southern, surface ammonium-depleted part (DCM's) and a northern part with UCM states which enhance the remineralization process in the upper layer. More specifically the increase close to the Irish coast is larger than the rest of UCM stations and could be attributed partially to sediment release. Surprisingly the model produces very low values between 47-55 ^{o}N regardless of the bloom predicted in these latitudes. It does a good job though at predicting the ammonium concentrations north of 55 ^{o}N even if it fails to illustrate the magnitude of the blooms.

As a general conclusion regarding the nutrients, it is clear that in spring their surface concentrations in the North are underestimated either by winter mixing issues or/and consumption by an early bloom. As mentioned earlier, in section 4.1.1, the density issues might indeed affect the deep winter convective mixing and cause a limited nutrient supply to the upper layer creating further problems to the phytoplankton growth and unexpected results in the summer. It should be also noted that in the deeply-mixed stations (22-32) winds are not significant contributors to the winter mixing [31, 42], which in this area is mainly convective.

4.1.3 Chlorophyll-a

Remote sensing data

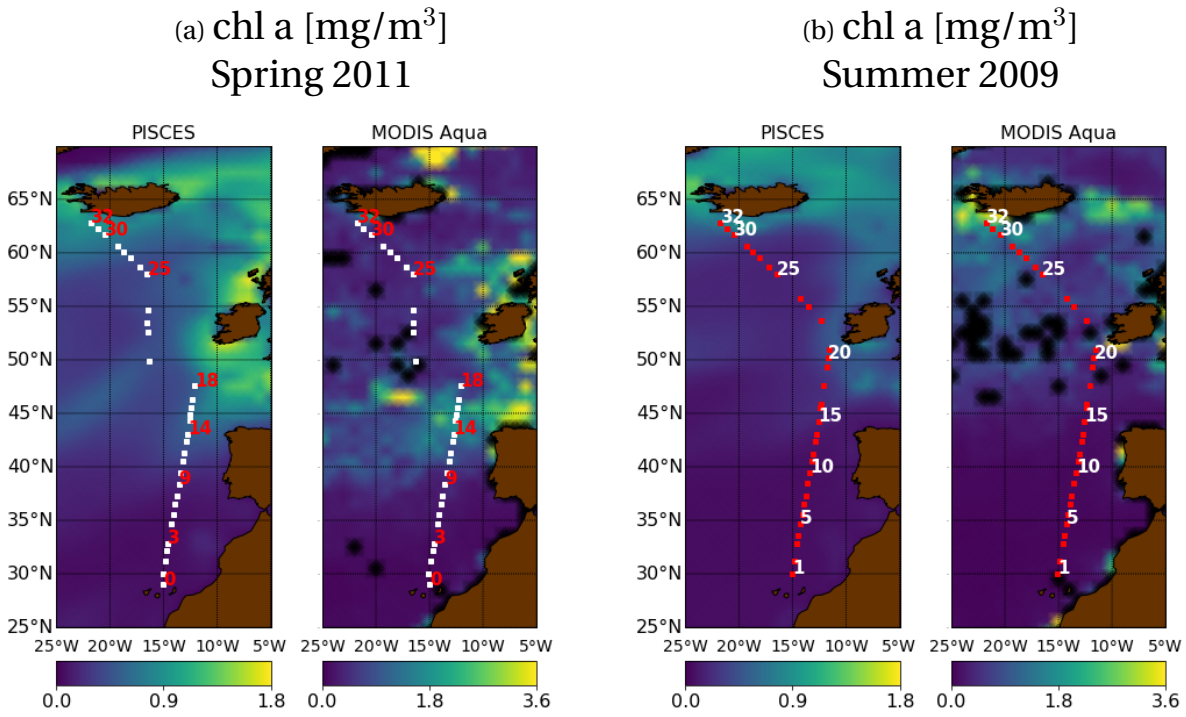

Figure 4.4: Map of the NE Atlantic with model results and MODIS-aqua remote sensor measurements for surface chlorophyll-a concentration as April-May average (spring) and July-August average (summer). Sampling station locations for the spring 2011 STRATIPHYT cruise are depicted with white squares and for summer 2009 with red squares.

Chlorophyll a (Chl a) is a good indicator for phytoplankton abundance and is used for the primary productivity estimation in the ocean [6]. Chl a biomass (mg/m^3) for both phytoplankton groups is calculated by NEMO-PISCES v2 with the use of the photo-adaptive model by Geider et al. (1997) [2, 21]. The satellite derived Chl a measurements cover a depth of more than 20m in oligotrophic regions but they can be as shallow as 1m in highly productive waters (http://esa-oceancolour-cci.org/).

Model results (Fig.4.4) follow the same pattern as the satellite observations for the southern part of the transect during Spring 2011 and summer 2009: DCM stations south of 40 ^{o}N with low surface Chl a concentrations and UCM stations between 40-55 ^{o}N with higher surface concentrations for the spring, while for summer low surface Chl a concentrations are found between 40-50^{o}N. Model and observations start diverging, as mentioned before, in the northern part of the transect: In spring, although it follows quite well the observations between Spain, Ireland and Britain, the model overestimates the surface Chl a concentrations north of 55 ^{o}N and especially around Iceland and along the 65 ^{o}N parallel of latitude. This discrepancy has been described before and could be attributed to possible winter mixing problems. In summer, the model exhibits a gap in Chl a between Ireland an Iceland, because of the model's failure to predict a correct spring phytoplankton growth and distribution. This time the observations show a summer bloom around Iceland and along the 65 ^{o}N parallel of latitude (the model predicted this bloom in the spring) while the modelled bloom expands even more to the north. This suggests that the model is always "one step ahead" of the observations, predicting the blooms earlier in the season than they actually occur (Fig.4.22) and implying once more problems with the convective winter mixing.

In general, the model agrees with the satellite observations below 50 ^{o}N and between Spain - Ireland, diverges north of this latitude and constantly underestimates the Chl a concentrations: almost 50% compared to the observations. Moreover, there are numerous patches of extremely high values in the ocean or close to Ireland, Spain or Iceland coasts, in the MODIS-aqua maps (up to 12 mg/m^3 in spring and 20 mg/m^3 in summer, bright yellow color), which might represent regional blooms induced by eddies [37, 40] or coastal upwelling.

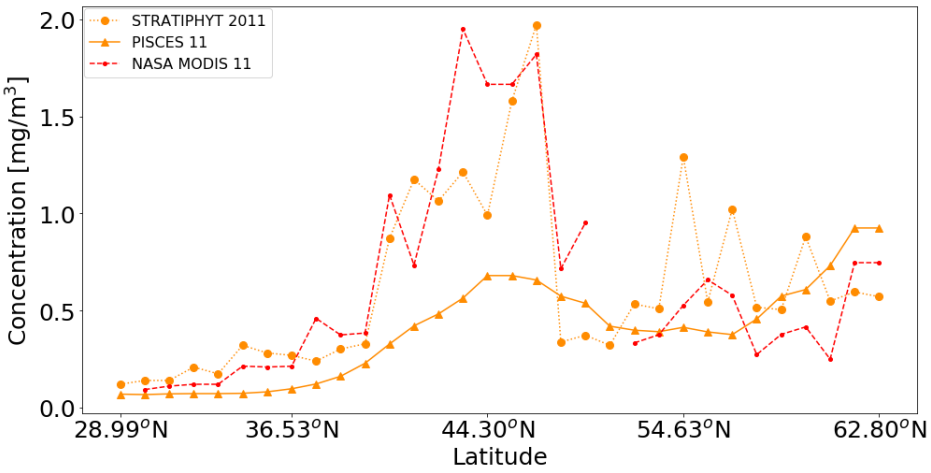

Figure 4.5: Surface chlorophyll-a concentration measured by STRATIPHYT spring 2011 cruise (top 20m, orange dots), MODIS aqua sensor (red dashed line) and 2011 model results (top 30m, orange triangles) along the transect shown in Fig. 3.1.

Measured surface Chl a by the STRATIPHYT 2011 cruise (Fig. 4.5) starts with low concentrations at the southern-deep part of the transect, where the DCM stations are located. It increases rapidly between 40-48 ^{o}N (UCM stations) with concentrations up to 2 mg/m^3. The third part of the curve (well-mixed stations) north of 48 ^{o}N has intermediate values as Chl a is diluted over the water column (probably even below 250m). A similar pattern is observed in the MODIS aqua observations, with comparable values. The model results are close to zero for the first part of the curve and show an increase at the same latitude as STRATIPHYT data but with values only up to 0.75 mg/m^3, underestimating the magnitude of the spring bloom by almost three times. In the third part, a decrease in surface Chl a concentration is apparent, although here are located the model-estimated deep UCM stations. Maximum concentrations are reached close to the coast of Iceland, at 63 ^{o}N (0.9 mg/m^3).

Measured surface Chl a by STRATIPHYT 2009 (Fig. 4.6) cruise starts with concentrations close to zero at the southern DCM stations and reaches maximum values of 1.6 mg/m^3 at the

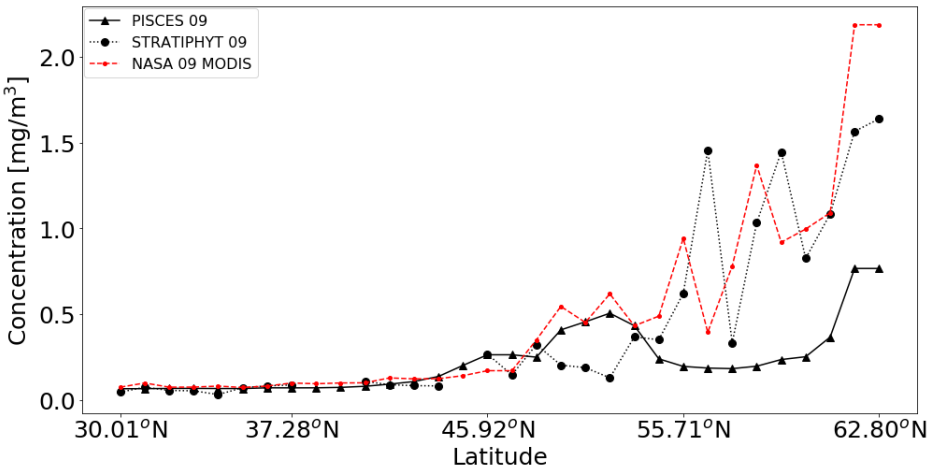

Figure 4.6: Surface chlorophyll-a concentration measured by STRATIPHYT summer 2009 cruise (black dots), MODIS aqua sensor (red dashed line) and 2009 model results (black triangles) along the transect shown in Fig. 3.1.

northern UCM stations. More specifically Chl a shows a sharp increase above 50 ^{o}N. A similar pattern is observed in the MODIS aqua measurements, with one main difference: the remote sensor measures a significant concentration of Chl a between 47-52 ^{o}N (Ireland's continental shelf) where STRATIPHYT measurements are close to zero, probably because of the Chl a patch located close to station 20 (Fig.4.4, bright yellow color). The model results capture well the near-zero surface concentrations south of 47 ^{o}N. It also manages to capture the increase close to the Irish coast (47-52 ^{o}N) with concentrations close to those of the remote sensor. Where the model diverges is north of 52 ^{o}N, where it estimates surface concentrations much lower than the observed ones, exhibiting a surface Chl a gap in this region.

The surface concentrations of Chl a (Fig.4.7) are separated into diatom (top) and nanophytoplankton (bottom) Chl a as well as in spring 2011 (left) and summer 2009 (right). According to the STRATIPHYT and NEMO-PISCES, Chl a concentrations south of 40^{o}N are almost zero, so there is no meaning in describing the phytoplankton composition in this region of DCM stations. In spring, between 40-48 ^{o}N (UCM stations) diatoms have a small contribution in the total Chl a although the conditions are favourable with abundant nutrients and irradiation. In the third part, north of 48^{o}N diatom Chl a contributes almost equally with nanophytoplankton Chl a to the total Chl a of the well-mixed stations, as diatoms are associated with homogeneously-mixed waters, with high nutrient concentrations because of their lower half-saturation constants for nutrient uptake and nutrient-limited growth [43]. According to the 2011 spring model results, in the second part of the transect, there is a considerable increase in diatom-originated Chl a, implying that most of the Chl a in the spring bloom comes from diatoms and connects them to high-nutrient, high-irradiance conditions. In the third part of the deep-UCM stations NEMO-PISCES fails to picture the importance of diatoms as it estimates high values only for the stations on Iceland's continental shelf, showing that the model does not predict diatoms in this deep UCM state, with MLD's around 150m. All these results contradict the Mojica et al. (2015) observations, which say that diatoms dominate only between 50-58^{o}N [43], meaning that they don't contribute significantly to the blooms and the Icelandic coast's Chl a composition. Regarding nanophytoplankton (Fig.4.7**(b)**) it can be stated that the model constantly underestimates its contribution to the total Chl a.

Diatom Chl a concentrations are very close to zero almost for the entire transect, according to the STRATIPHYT 2009 measurements, meaning that the high-latitude summer bloom consists almost entirely of nanophytoplankton. This comes as no surprise since the contribution of diatoms, according to Van de Poll et al. (2013) was at its highest in the northern part during spring [59] and diatoms contributed with very low percentages north of 60^{o}N in summer [43]. The model results show similar concentrations but with two differences: a bump around 50 ^{o}N (coast of Ireland) and an increase up to 0.4 mg/m^3 in the last two stations (Icelandic coast).

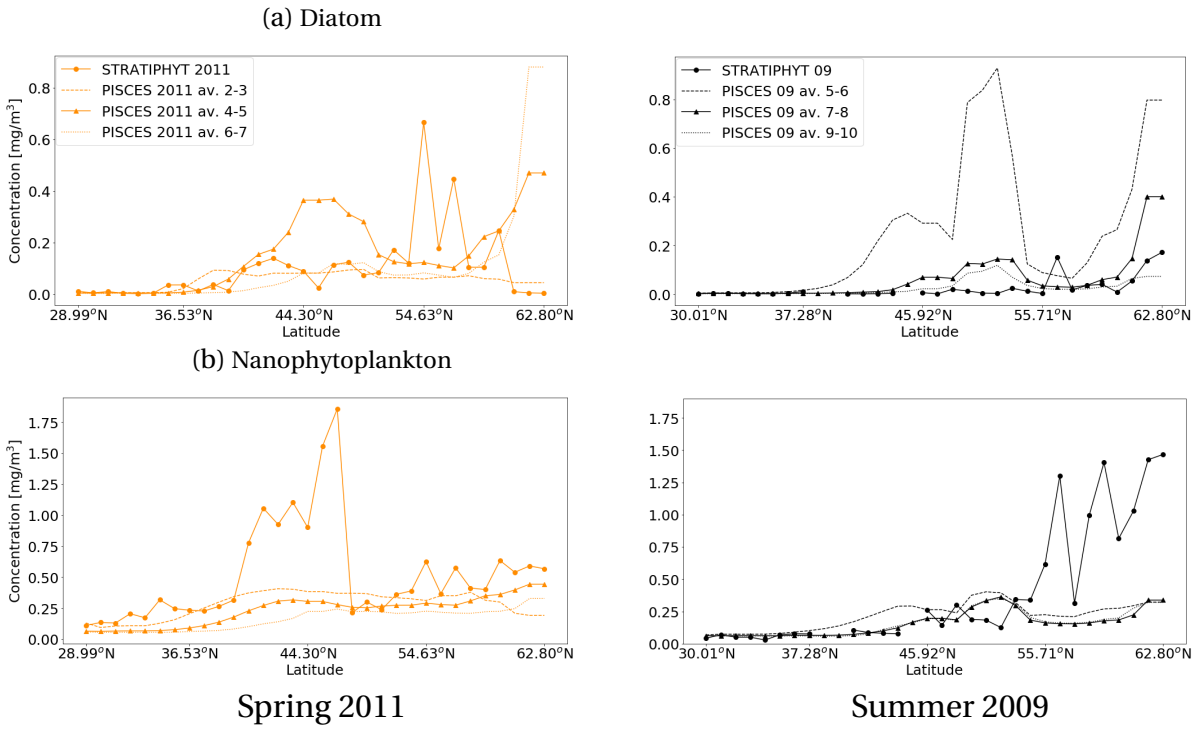

Figure 4.7: Surface diatom (**a**) and nanophytoplankton (**b**) chlorophyll-a concentration for spring 2011 (left, orange color) and summer 2009 (right, black color). 2011 STRATIPHYT measurements are depicted in dots, 2011 spring model results (April-May average) in triangles, 2011 winter model results (February-March average) are plotted with a dashed line and the 2011 summer model results (June-July average) with a dotted line. 2009 STRATIPHYT measurements are depicted in dots,2009 summer model results (July-August average) in triangles, 2009 spring model results (May-June average) are plotted with a dashed line and the 2009 Autumn model results (September-October average) with a dotted line.

Nanophytoplankton surface Chl a concentrations from STRATIPHYT 2009 (Fig.4.7**(b)**), are very low south of 50 ^{o}N. A sharp increase is observed north of 50 ^{o}N (up to 1.5 mg/m^3) which means that small phytoplankton species dominate completely in the northern, UCM stations. Model results show very low concentrations and a small increase close to 50^{o}N and in the two last stations.

A few general conclusions can be drawn regarding the concentration and composition of surface Chl a: (a) In spring, the model follows the pattern of the field measurements, with lower concentrations and an overestimation of diatoms. (b) In summer the model fails to reproduce the observed pattern and also underestimates the nanophytoplankton contribution to the total Chl a. (c) During both seasons, the modelled Chl a surface concentrations are constantly lower and only increase in coastal areas, with a very large contribution of diatoms.

Depth profiles

The eight stations in Fig. 4.8 were selected from a total of 32 along the transect. An effort was made for the stations to be as representative as possible of all the different parts from 29 up to 63 ^{o}N, resulting to four southern stations with shallow MLD's but deeper bathymetry and four northern with deeper MLD's but shallower sea bottom depths.

STRATIPHYT 2011 Chl a measurements reveal DCM states at station 1 and 5, south of 40^{o}N, which gradually become UCMs in the next two stations (between 40-48^{o}N) with stratification, light availability and shallow nutriclines favouring blooms (maximum Chl a concentration: 2mg/m^3). In the next four, northern, stations the situation changes: MLDs become deeper and Chl a together with nutrients is homogeneously mixed over the water column. Chl a in this region is diluted and reaches concentrations of less than 1 mg/m^3. Station 23 exhibits a clear, shallow nutricline and at the same time it has a deep MLD (120m), which is something that makes this

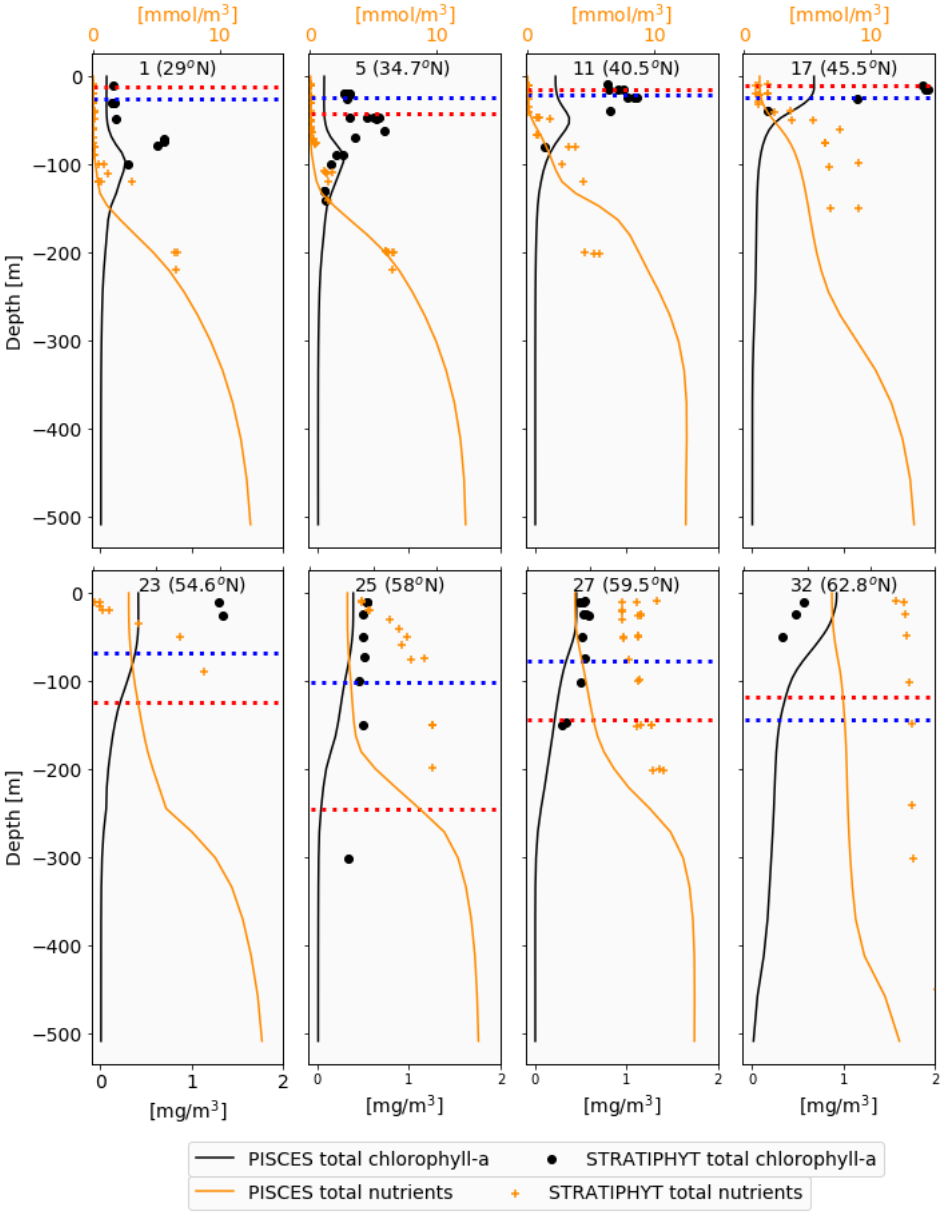

Figure 4.8: Measurements by the STRATIPHYT 2011 cruise (dots and crosses) and model results (lines) calculated as 2011 April-May average, for 8 stations along the transect shown in Fig. 3.1. Total chlorophyll-a is plotted in black color and total nutrients in orange. Red dashed lines indicate the MLD as measured by the 2011 STRATIPHYT cruise and blue dashed lines the MLD as estimated by the model for spring 2011.

station “transitional” between the winter deep mixing and the spring stratification.

The model manages to capture fairly well the distribution and concentration of nutrients in the southern stations. Chl a maxima are calculated slightly deeper than the measured ones and with much lower values (1/3 of the measured concentration). In the northern part of the transect, the model manages to capture only chlorophyll’s concentration but gives a different distribution pattern: deep UCM’s instead of homogeneously-mixed conditions. Another discrepancy is found in the transitional station 23, where the model gives the image of a well-mixed station with low Chl a concentrations. What NEMO-PISCES fails to predict, is the nutrient distribution and concentration in this part of the cruise: it produces curves that show low concentrations in the first 200m and then a nutricline at this depth coupled with low Chl a content, distributed down to 200m as well. There seems to be a timing issue: where the cruise clearly illustrates well-mixed conditions, the model is “one step ahead” (Fig.4.22) and predicts a shoaling ML and the onset of the algal bloom.

The eight stations in Fig. 4.9 have the same coordinates as in Fig. 4.8 but were sampled dur-

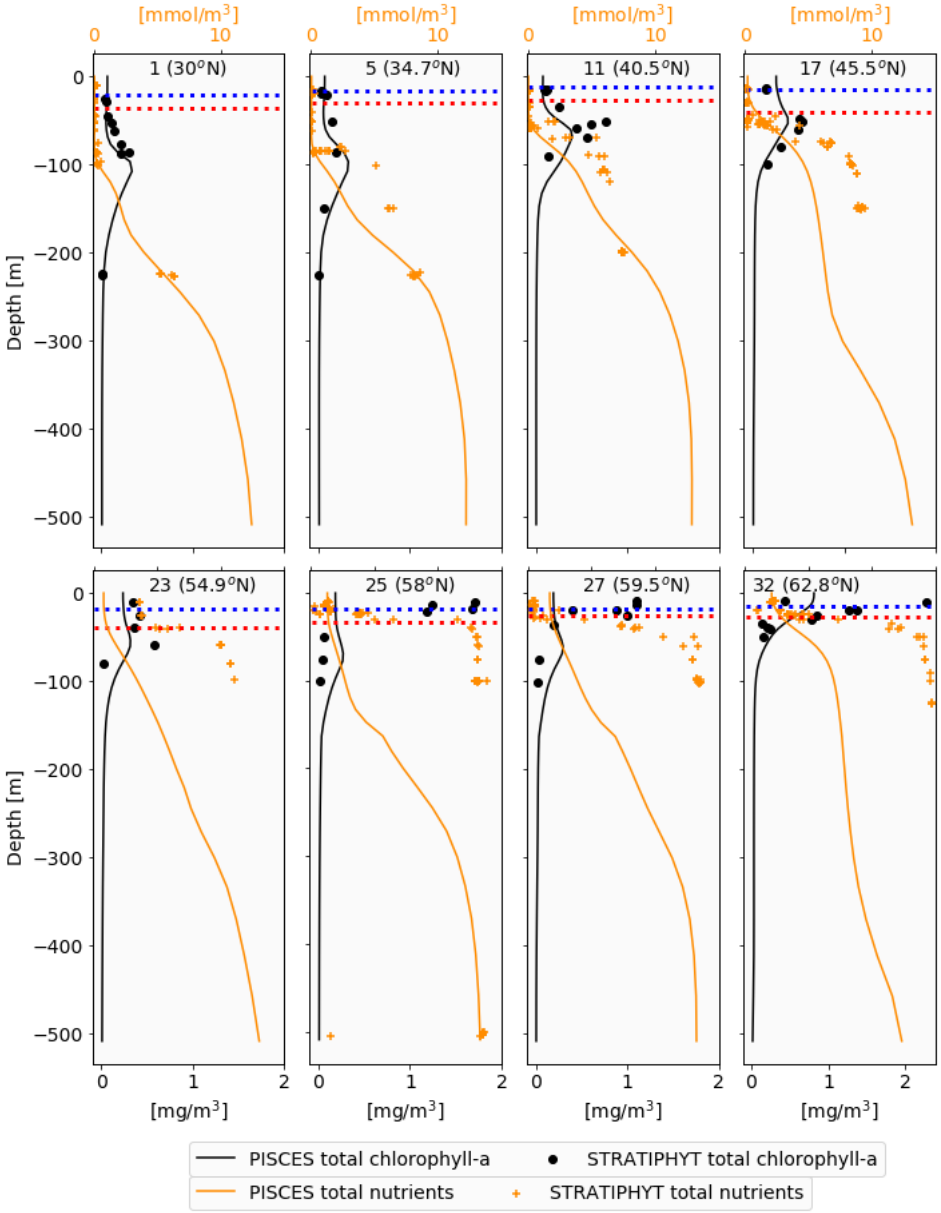

Figure 4.9: Measurements by the STRATIPHYT 2009 cruise (dots and crosses) and model results calculated as 2009 July-August average (lines), for 8 stations along the transect shown in Fig. 3.1. Total chlorophyll-a is plotted in black color and total nutrients in orange.Red dashed lines indicate the MLD as measured by the 2009 STRATIPHYT cruise and blue dashed lines the MLD as estimated by the model for Summer 2009.

ing the 2009 STRATIPHYT summer cruise. MLD's are shallower than in the spring of 2011, with depths ranging from 25 to 40m for STRATIPHYT and 12 to 25m for the model. The eight stations can be divided again in to four "southern" stations with DCMs and four "northern" with UCM states. The model results agree fairly well with the field data in the first four stations in terms of depth and concentrations, both for Chl a and nutrients: They both give the image of DCM state which moves gradually close to the MLD (station 17), followed closely by the nutricline. Model and observations start to diverge in the second part of the transect, where STRATIPHYT data give a clear picture of UCMs with high Chl a concentrations (higher than 2 mg/m^3) and shallow nutriclines. NEMO-PISCES fails to capture this image, probably because of the early spring blooms: Instead of UCMs, DCMs dominate in this area as phytoplankton sinks deeper leaving the nutrient-depleted surface. What does not make sense is the absence of a clear nutricline and the existence of a gradient down to 400m. The only exception is the last station (Icelandic coast) where according to what has been written in page 17: *"During both seasons, the modelled Chl a surface concentrations are constantly lower and only increase in coastal areas"*.

Phytoplankton composition

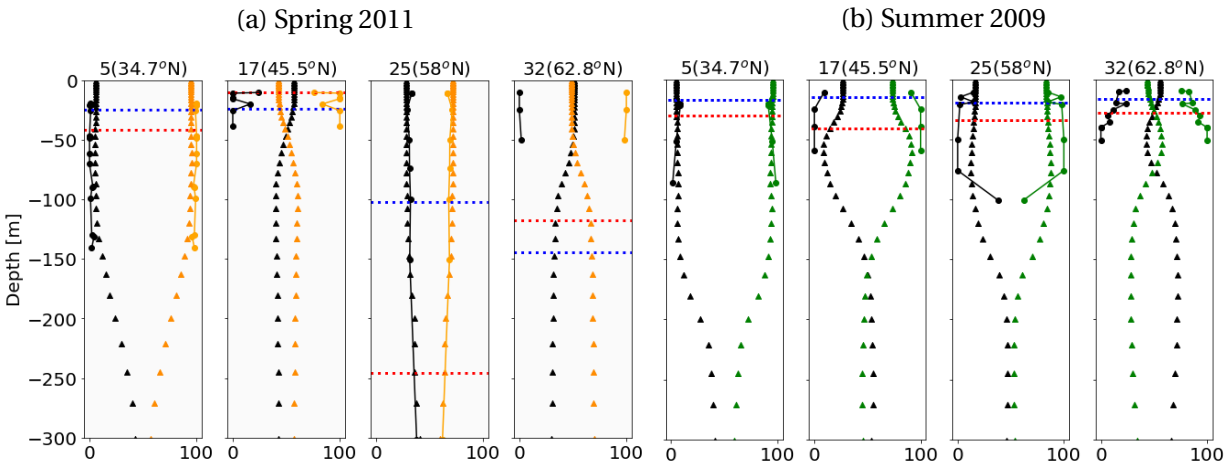

Figure 4.10: Measurements by the STRATIPHYT 2011 (left) and 2009 (right) cruise (dots) and model results calculated as 2011 April-May (left) and 2009 July-August (right) average (triangles), for 4 stations along the transect shown in Fig. 3.1. Diatom chlorophyll-a is plotted in black color and nanophytoplankton chlorophyll-a in orange (for 2011) and green (for 2009). Both are expressed as percentage of total chlorophyll-a.

The phytoplankton composition can be seen in depth for four stations along the transect (spring and summer) according to the STRATIPHYT measurements and model results (Fig.4.10). In spring,in the nutrient-depleted station (5) according to measurements and model results the diatom contribution is almost 0% for the top 150m, which is expected as the low nutrient availability of the oligotrophic gyres results in the dominance of cyanobacteria and other small-size phytoplankton species [59]. In station 17 (UCM) the measured diatom contribution is higher, almost 1/3 of the total Chl a, as the shallow MLD combined with abundant nutrients favours the growth of larger species [13, 38]. NEMO-PISCES overestimates diatom population in this case, estimating a contribution of over 50% at the surface. In station 25 measurements and model results agree almost completely, as they both show a ratio of nanophytoplankton:diatoms close to 2:1 in the top 250m. This is something expected as *"At unstratified stations, diatoms were found in the surface layers and they have an association with colder water temperatures, higher nutrient concentrations and higher potential for light limitation"* (Hahn-Woernle et al., 2014) [26]. In the last station, the largest divergence between the model and the field data is observed: almost 0% diatom contribution according to STRATIPHYT, while the model gives a completely different image with a 50% contribution, once again close to the coast.

In summer of 2009 (Fig.4.10**(b)**) model results and field data agree for the first station, with diatom Chl a percentages close to 0% for the first, nutrient-depleted 150m. In the next two stations (17 and 25) model and field data show a diatom contribution of 20-30% close to the surface, something expected as the beginning of stratification and consequent spring bloom leads to a shift towards smaller species compared to Fig.4.10**(a)** [59]. In the coastal area of station 32, measurements show an increased diatom percentage (30%) at the bloom while the model makes an overestimation once again at this location: 50%.

Description of stations

Figure 4.11 gives an overview of the 32 stations along the transect, in terms of chlorophyll-a and nutrient concentration (as measured by the STRATIPHYT cruises) and distribution over the water column. Figure 4.11**(a)** shows the chlorophyll-a concentration measured during the spring and summer cruise, respectively. The spring cruise can be separated roughly in three parts: (a) South of 40 ^{o}N Chl a (1.5 mg/m^3) is found in Deep chlorophyll maxima (DCM), meaning Chl a concentrated below the mixed layer (ML), because of nutrient limitation in the ML. Maximum growth depth and the nutricline are coupled, meaning that phytoplankton grow where they find

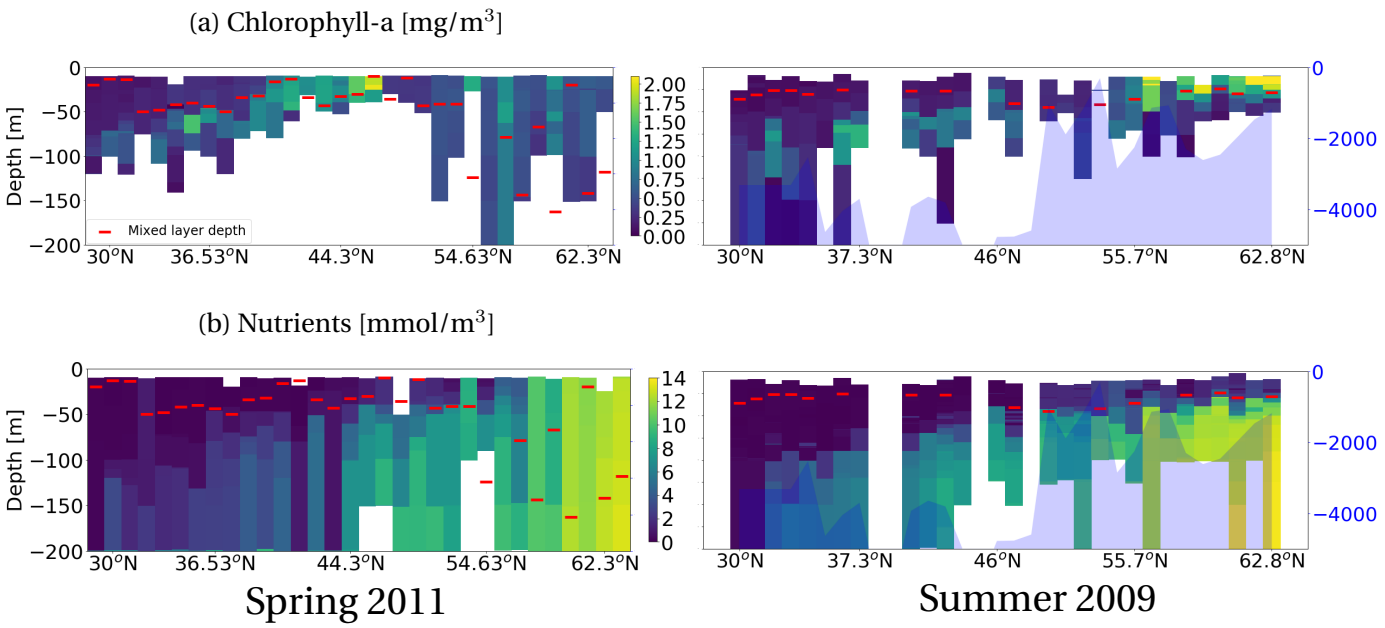

Figure 4.11: Measured profiles of **(a)** chlorophyll-a and **(b)** total nutrients for the spring 2011 (left) and summer 2009 (right) STRATIPHYT cruises. The MLD is indicated by the red dashes and the bathymetry (where available) by the blue shade. Data is plotted from south (left) to north (right) along the transect shown in Fig. 3.1

nutrients [26]. b) Between 40 - 48 ^{o}N it is concentrated in upper chlorophyll maxima (UCM), which is Chl a mainly concentrated inside the ML, as in this latitude the shallow mixed layer depths (MLD) in combination with the shallow nutricline provide enough nutrients and irradiance to the phytoplankton to grow up to a Chl a concentration of 2 mg/m^3. (c) Further north the deep MLD's distribute Chl a over the well-mixed water column and regardless of the abundance of nutrients, Chl a concentration remains low (1 mg/m^3) due to light limitation and dilution. This state is vital to maintaining a viable population through the winter, which will later give way to the spring bloom that dominates the total annual production of organic carbon [42].

Jurado et al. (2012) described the water column in the northern stations during spring as being right at the beginning of the ML's shoaling process and the onset of the spring bloom. Moreover, they state that the two most important mixing parameters values, temperature eddy diffusivities (K_T) and turbulent kinetic energy dissipation rates (ϵ) are representative of early spring upper ocean waters [31].

In summer, two different behaviours can be observed: (a) DCMs (1 mg/m^3) at latitudes below 47 ^{o}N, following the nutricline. Where there used to be a spring bloom (40 - 48^{o}N) the surface nutrients were consumed and the phytoplankton migrated deeper, creating a DCM state in summer. (b) UCMs dominate at latitudes above 55 ^{o}N, where the deep spring mixing brings nutrients to the surface and together with the decrease in MLDs as a result of stratification, contribute to the summer bloom (2 mg/m^3). This division in low, mid and high latitudes based on Chl a follows the fact that bloom formation is associated with stratification in mid- and high latitude North Atlantic [59]. What must be noted is that more stratified conditions do not necessarily result in higher phytoplankton biomass in this region [59], meaning that the depth-integrated Chl a in spring can be higher than the one during the summer bloom.

Nutrient concentrations (Fig. 4.11**(b)**) are very low in the upper euphotic zone (0-50m) south of 40 ^{o}N in spring and 48 ^{o}N in summer, as also reported by Mojica et al. (2015) [43], causing the DCMs described in the previous paragraph. Further north this changes, as concentrations increase at depth and in the upper euphotic zone, making it easier to inject nutrients in the ML and trigger blooms. In the northern stations (above 47 ^{o}N) deep spring mixing provides abundant nutrients (15 mg/m^3) to the mixed layer which are depleted under the more stratified summer conditions due to phytoplankton consumption. Measured MLDs can be seen in Figure 4.11 as red dashes.

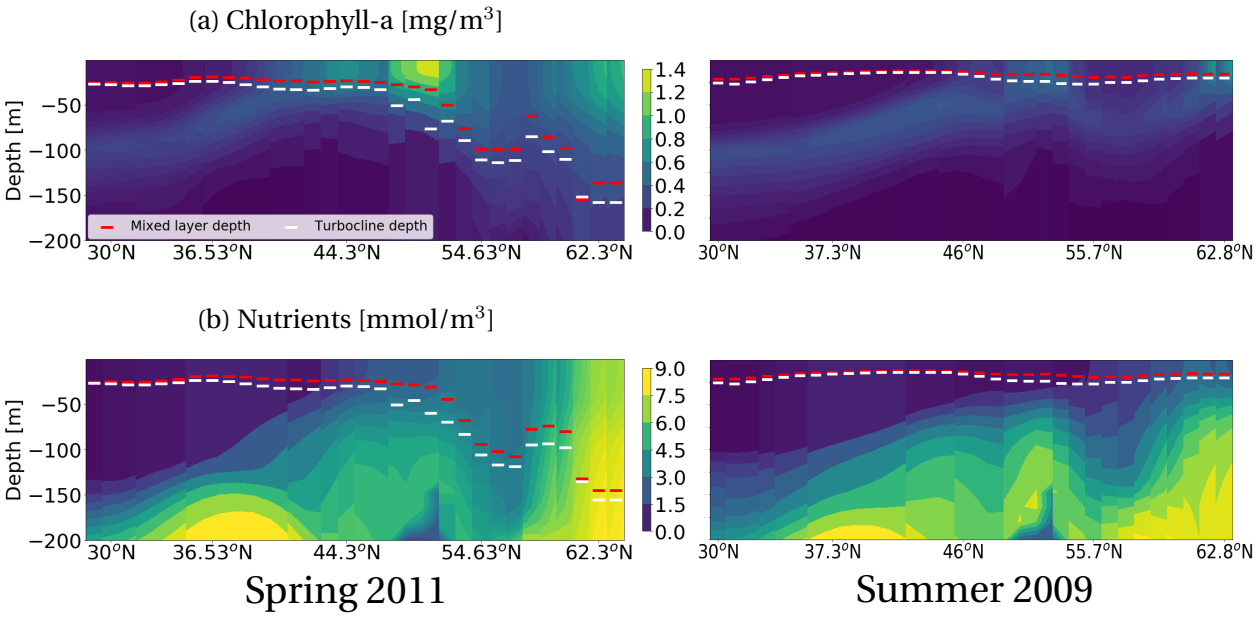

Figure 4.12: Calculated profiles of **(a)** chlorophyll-a and **(b)** total nutrients by NEMO-PISCES for spring of 2011 (left, April-May average) and summer of 2009 (right, July-August average). The MLD is indicated by the red dashes and the turbocline depth by the white dashes. Data is plotted from south (left) to north (right) along the transect shown in Fig. 3.1.

Figure 4.12 gives an overview of the 32 stations according to the NEMO-PISCES model. Figure 4.12**(a)** shows the chlorophyll-a concentration calculated by the NEMO-PISCES model as April-May average for spring and July-August average for the summer. The spring model results can be separated in three parts again: South of 40 ^{o}N Chl a is found in DCMs (1 mg/m^3) up to 100m depth, as a result of the nutrient-depleted surface and between 40-55 ^{o}N it is concentrated in UCMs (1 mg/m^3), again as a result of shallow MLDs and shallow nutricline. Further north the model gives a different image of that part of the transect: Instead of diluted Chl a over the water column, UCMs appear to be formed earlier in the season (Fig. 4.22), probably due to the already mentioned possible winter mixing issues. In the opposite case, when models overestimate the MLD, surface Chl a concentrations increase too late in the season and too strongly compared to field measurements and satellite observations [26, 2].

In summer the pattern is different than the one observed in STRATIPHYT 2009 cruise: Although the southern half is similar, the northern part exhibits -weak- UCMs limited in the coast of Ireland (50-55^{o}N) and Iceland (63^{o}N). The northern part of the transect is dominated by DCMs, as a result of nutrient depletion (early spring bloom). The model calculates a maximum concentration of 1 mmol/m^3 along the transect in the summer.

Modelled nutrient concentrations (Fig. 4.12**(b)**) follow the same pattern as the measured ones: very low in the upper euphotic zone (0-50m) south of 40-45 ^{o}N and increase further north at the surface and at depth. In the northern stations modelled mixing provides nutrients to the mixed layer, only here less effectively (8 mmol/m^3) than in the measured data because it is shallower. A gap in the nutrient distribution is observed between station 20-22 or latitude 50-53 ^{o}N. This gap is located close to Ireland's continental shelf and might be caused by the bathymetry, resulting in low nutrient concentrations between 180-200m depth.

4.1.4 Run 1 conclusions

As a general remark it can be said that NEMO-PISCES run 1 systematically underestimates Chl a concentrations in comparison to the STRATIPHYT data and also calculates lower nutrient concentrations in the upper 200m (slightly more than half of the measured ones). It also fails to capture the phytoplankton dynamics in the northern section of the transect. Behrenfeld et al. (2006) and Polovina et al.(2008) concluded, with the use of remote-sensing data, a negative relationship

between density differences in the upper ocean and Chl a concentration [6, 47], meaning that non-stratified winter conditions (small density differences) produce stronger spring blooms. All of these symptoms can have a common cause: vertical mixing issues. Mixing problems probably originate from an underestimation of the winter convective mixing, caused by salinity and density miscalculations, which can trigger a "chain reaction": changes in the onset of stratification can change nutrient availability and the spectral composition and intensity of irradiance [35], resulting in weaker phytoplankton blooms earlier in the season (Fig.4.22).

Another possible reason for these issues could be the use of the $\Delta\sigma\theta$=0.01kg/m^3 as MLD calculation criterion by NEMO. This rather "sensitive" MLD definition could cause problems with the estimation of MLs in the northern stations as in this region the termination of convection and the onset of stratification is of crucial importance for the phytoplankton bloom [59]. It was shown by Brainerd and Gregg (1995), for example, that the ΔT=0.2^{o}C definition of the ML gives a good estimate of the depth at which recent mixing has occurred [9].

Another discrepancy was observed in the phytoplankton composition, as calculated by PISCES: diatoms are always overestimated, especially in regions with nutrient abundance and close to coasts.

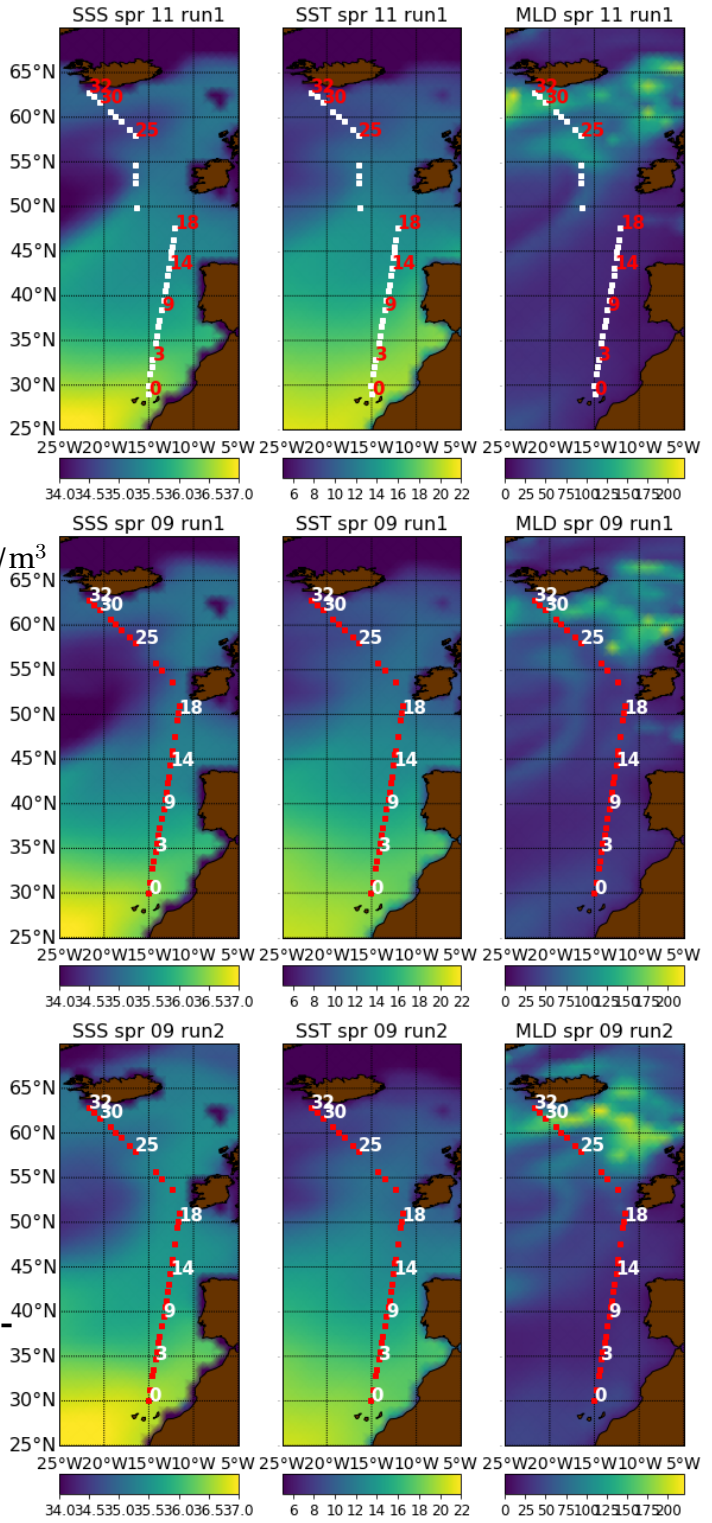

Figure 4.13: Map of the NE Atlantic with model results for SSS, SST and MLD as April-May average (spring), for NEMO run1 (2009 and 2011) and NEMO run 2. Sampling stations are depicted with with red and white squares.

4.2 NEMO-PISCES run 1 compared to NEMO-PISCES run 2

Fig.4.13 summarizes one of the main reasons behind the underestimation of MLDs in the northern part of the transect and the changes after the adjustment of 3 NEMO parameters. In run 1, during spring of 2009 and 2011 there was a fresh and cold water input from the West in the northern part of the transect between 45 and 60 ^{o}N. This resulted in density being underestimated by the model and eventually in an un-

derestimation of the deep, convective winter mixing. In the 2nd run (spring) it is clear that the cold fresh water input has been reduced considerably, giving also deeper MLDs in that area.

Since the beginning of 2017 there has been a discussion on the EC-Earth Development Portal (https://dev.ec - earth.org/) regarding this issue: The input of fresh and cold water in the North Atlantic. Following many trials it has been decided to perform a 2nd run after changing 3 NEMO (physical) parameters: **a)** Snow Thermal Conductivity (rn_cdsn) from 0.30 to 0.40 $W\,K^{-1}\,M^{-1}$, **b)** Turbulent Kinetic Energy (nn_etau) penetration depth from 1 to 0 and **c)** Langmuir Waves Cell Size (rn_lc) from 0.15 to 0.2.

4.2.1 Physical parameters

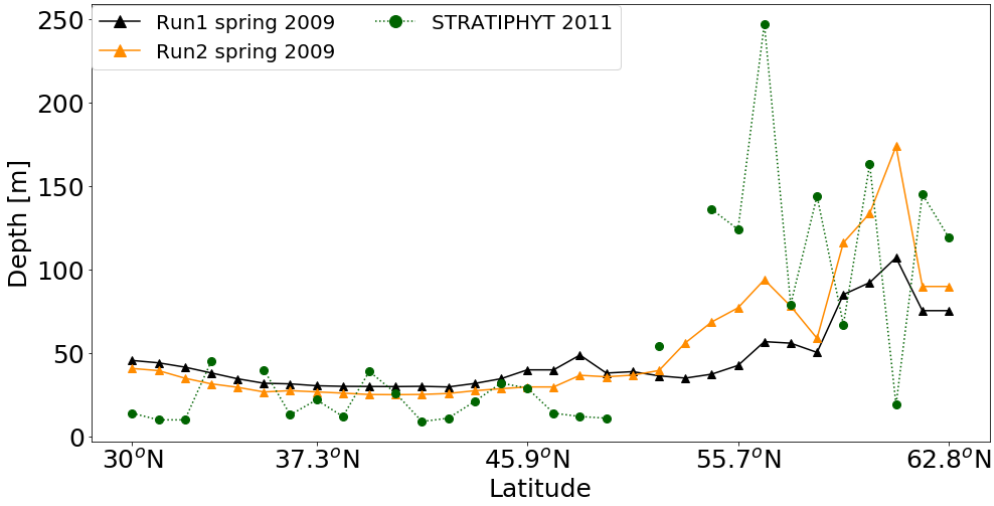

Figure 4.14: MLDs as measured by the spring 2011 STRATIPHYT cruise (green dots) and 2009 spring model results as April-May (black triangles for NEMO run 2 and orange triangles for NEMO run 2) averages along the transect shown in Fig. 3.1.

The changed NEMO parameters resulted in a small increase of the spring MLDs in the Northern part of the transect (above 55°N, Fig.4.14). The difference is not big, since the maximum MLD is now around 200m instead of 150m (first run). Potential density (Fig.4.15) has increased along the transect both in Spring and summer, approaching the STRATIPHYT values. Not only it is now higher but it also shows a more clear pycnocline in summer, close to the surface, following the same pattern as the field data (Fig.4.2 **a**). Salinity (Fig.4.16) has also increased along the transect both in Spring and summer approaching the STRATIPHYT values, except for station 25 where there is still a density underestimation. Moreover, the unexpected decrease in station 25 (both in spring and summer) that has been attributed to a possible fresh water influx (Fig.4.2 **b**), has been decreased. It is safe to say that the density increase is due to the increase of salinity, as temperature in NEMO-PISCES run 2 (Fig.4.16) shows no clear difference in values compared to run 1. Salinity is still underestimated in the top 200m (fresh water input) of station 25, causing the density problem mentioned in Fig.4.16. It is interesting though to point out that the pycnocline observed in summer, is caused by a clear temperature increase close to the surface. This was not so obvious in NEMO-PISCES run 1.

4.2.2 Nutrients

As mentioned in the previous paragraph (subsection 4.2.1), the improved convective mixing results in more nutrients (NO_3 and PO_4) being brought up to the surface, triggering a more intense bloom. In Fig.4.17 this is clear north of 55°N. Something worth mentioning is the slightly

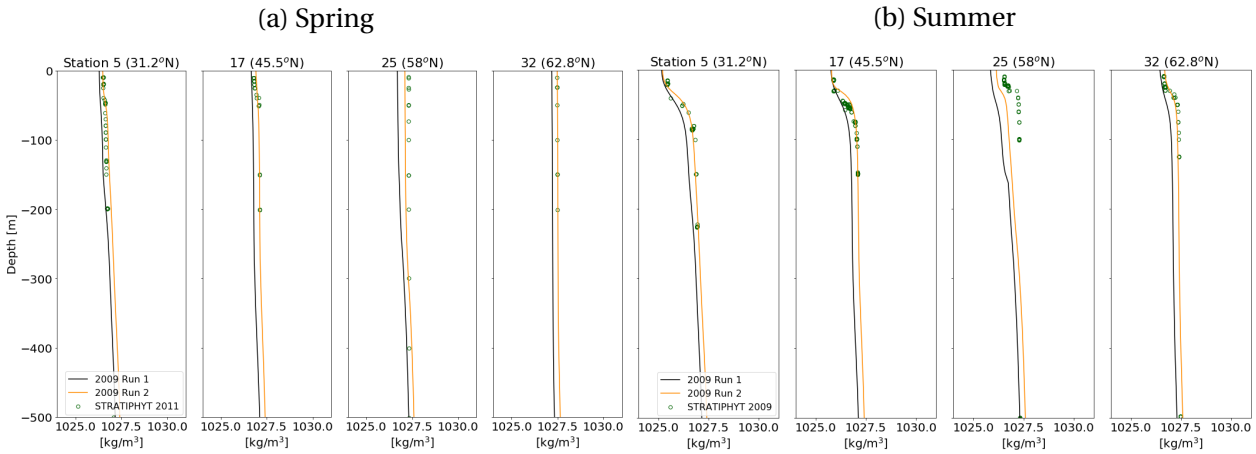

Figure 4.15: Calculated by NEMO-PISCES (continuous lines) and measured by STRATIPHYT (circles) profiles of 4 stations (5, 17, 25 and 32) for potential density, in spring (left, April-May average) and summer (right, July-August average). Model run 1 is indicated by black colour and run 2 by orange.

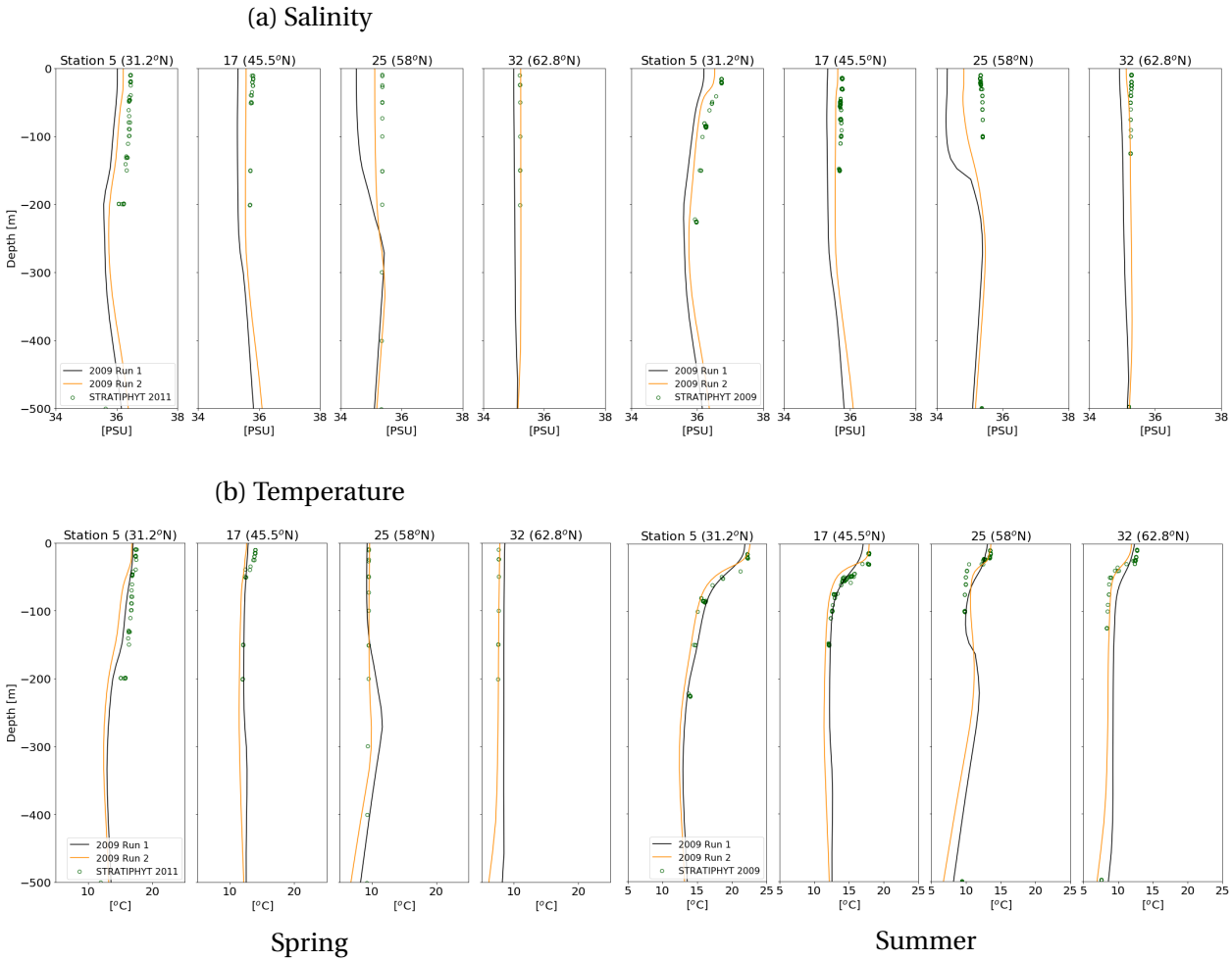

Figure 4.16: Calculated by NEMO-PISCES (continuous lines) and measured by STRATIPHYT (circles) profiles of 4 stations (5, 17, 25 and 32) for salinity (a) and temperature (b), in spring (left, April-May average) and summer (right, July-August average). Model run 1 is indicated by black colour and run 2 by orange.

decreased nutrient concentration between 40-55°N, probably due to consumption by the more intense spring bloom. In summer, increased phytoplankton population, has as a result almost complete depletion of surface waters from the main nutrients along the transect.

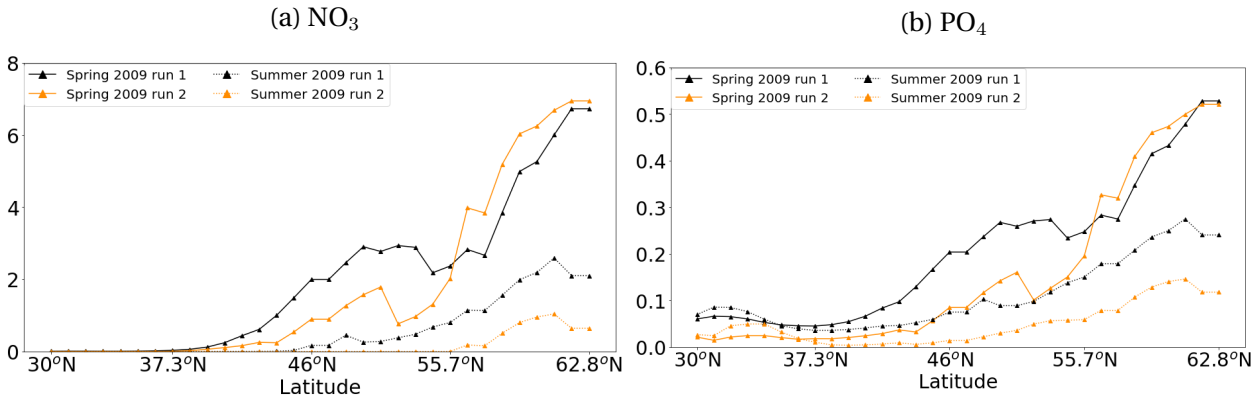

Figure 4.17: Nitrate (a) and phosphate (b) surface concentrations (top 15m) calculated by the model for spring 2009 (continuous lines) and summer 2009 (dotted lines). NEMO-PISCES run 1 results are depicted with black colour and run 2 results with orange.

4.2.3 Chlorophyll-a

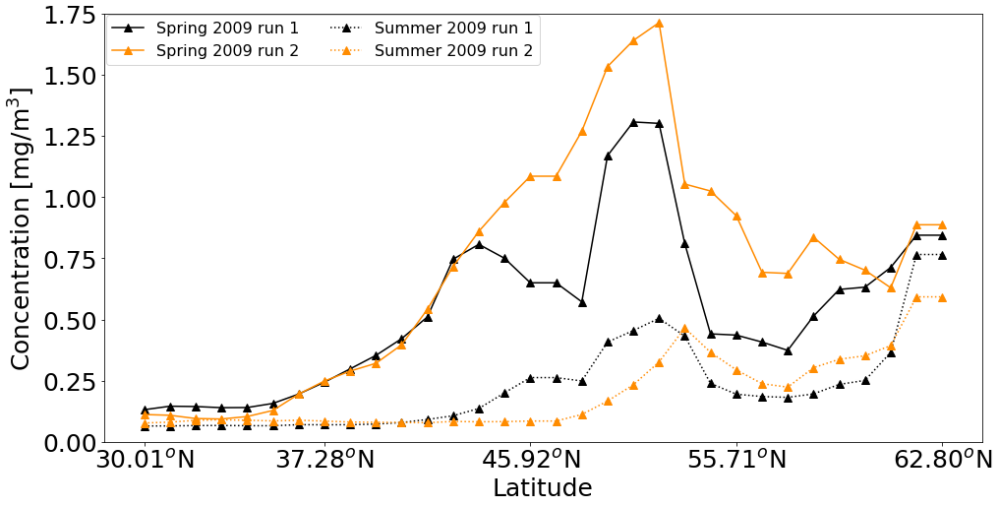

Figure 4.18: Chl a surface concentrations (top 15m) calculated by the model for spring 2009 (continuous lines) and summer 2009 (dotted lines). NEMO-PISCES run 1 results are depicted with black colour and run 2 results with orange.

The NEMO-PISCES adjustments have as a result a wider (between 43-53^oN) and more intense spring bloom for 2009, compared to the first run (Fig.4.18). The region where the mid-latitude bloom occurs is close to the coast of Ireland and has a maximum concentration of 1.75 mg/m^3. North of that point (53^{o}N) surface Chl a concentrations are higher in the region of deep spring mixing (northern part of the transect), implying a better convective mixing that results in more surface nutrients or even a different state of phytoplankton growth. In summer there is almost no surface Chl a up to the region where the spring bloom took place, according to run 2, because of the nutrient consumption by the algae. North of 53^{o}N and up to 63^{o}N surface Chl a concentrations are slightly higher, reducing the Chl a gap between Ireland and Iceland. This increase of surface Chl a in the northern part of the transect implies that the new MLDs might produce more realistic conditions for spring and as a consequence for summer too.

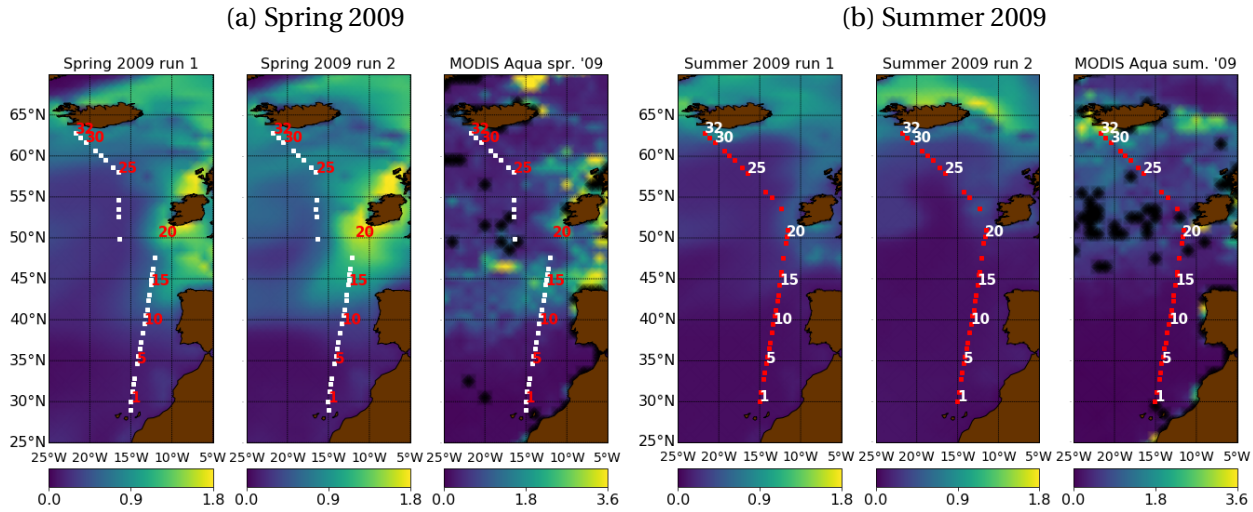

Figure 4.19: Map of the NE Atlantic with model results (run 1 and run 2) and MODIS-aqua remote sensor measurements for surface chlorophyll-a concentration as April-May average (spring, a) and July-August average (summer, b). Sampling station locations for the spring 2011 STRATIPHYT cruise are depicted with white squares and for summer 2009 with red squares.

Remote sensing data

During spring of 2009, the same general pattern is observed (Fig.4.19) for both runs: No surface Chl a south of $40^o N$, high concentrations between $40^o N$ and $50^o N$ (spring blooms) and intermediate concentrations north of Ireland until Iceland. The difference is that in run 2 the surface Chl a concentrations are higher and more spread to the West. An other considerable effect of the deeper winter MLDs in the North is the increase in Chl a between Ireland and Iceland, implying a more effective mixing of nutrients in that region.

In summer 2009 the pattern is once again similar between the two runs: Practically no surface Chl a below $50^o N$ and low concentrations above that latitude. Two things need to be pointed out regarding NEMO-PISCES run 2: a) The Chl a concentration between Ireland and Iceland is slightly increased, meaning that it is not depleted from the surface as in run 1 and b) The model in run 2 illustrates quite well a summer bloom along the $65^o N$ parallel, around Iceland. This result is in accordance with the MODIS aqua data as seen in Fig.4.4 (b).

Depth profiles

In spring (Fig.4.20), the Chl a distribution and concentration in the south is similar to run 1 but mid-latitude the spring bloom is now more intense with almost double the concentrations. The nutrients in general show higher concentrations in the upper 200m and seem to form a more clear nutricline below the DCMs and UCMs. In the northern stations both Chl a and nutrients show higher concentrations in the upper 200-300m but are still far from being homogeneous. In summer (Fig.4.20), not many things have changed in the southern and mid-latitude stations in terms of Chl a distribution and concentration. Nutrients seem to have slightly higher concentrations in the upper 200m and form a clearer nutricline below the DCMs. In the 3 last, northern stations the situation is slightly improved with higher Chl a concentrations and shallower DCMs (not still UCMs). The shallower and more intense DCMs imply an improvement in the winter mixing as deeper convective mixing brings more nutrients to the surface and triggers an intense bloom, which also reaches its peak later in the season (Fig.4.22).

Description of stations

The DCM and UCM states in the South and at mid-latitude respectively are similar between the 2 runs (Fig.4.21). There has been an improvement in the Northern part of the transect: The

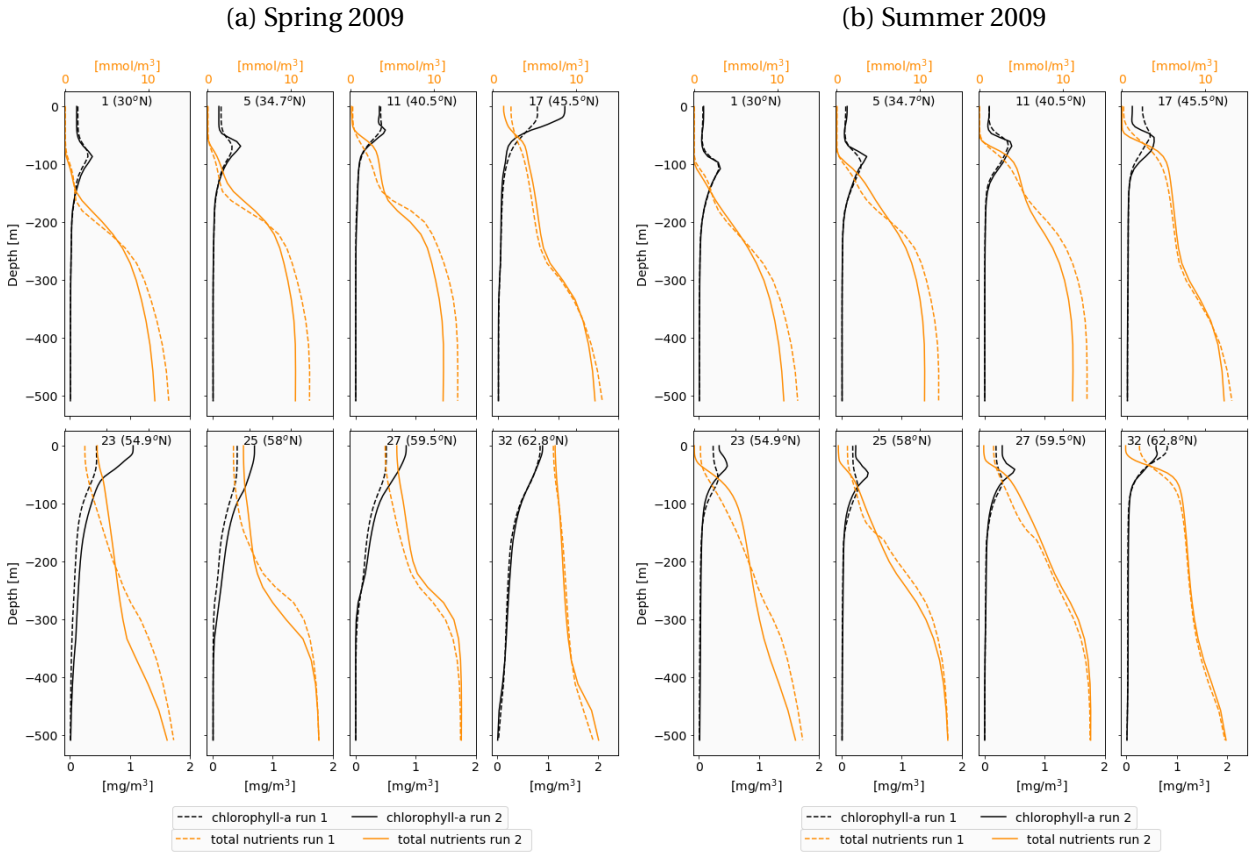

Figure 4.20: Calculated profiles of chlorophyll-a (black colour) and total nutrients (orange colour) by NEMO-PISCES for spring of 2009 (left, April-May average) and summer of 2009 (right, July-August average), for 8 stations along the transect shown in Fig. 3.1. Model run is depicted by dashed lines and run 2 by continuous.

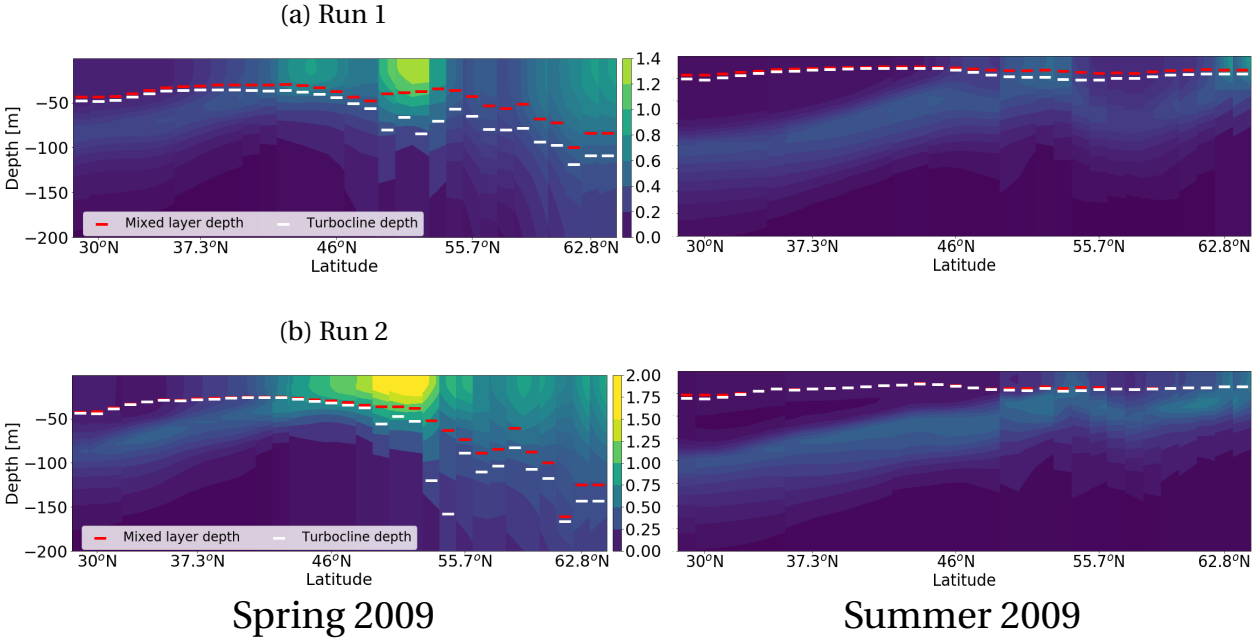

Figure 4.21: Calculated profiles of chlorophyll-a for model run 1 **(a)** and run 2 **(b)**, by NEMO-PISCES for spring of 2009 (left, April-May average) and summer of 2009 (right, July-August average). The MLD is indicated by the red dashes and the turbocline depth by the white dashes. Data is plotted from south (left) to north (right) along the transect shown in Fig. 3.1.

deeper MLDs and turboclines (or mixing layer depth), bring more nutrients to the surface and create a growth state which is deeper than in the 1st run. This state has more nutrients, higher Chl a concentrations and the bloom (when the ML is shallow enough) will happen slightly later in the season than in run 1 (Fig.4.22). The results of this change can also be witnessed in summer where there is still some Chl a left in the ML.

4.2.4 Run 2 conclusions

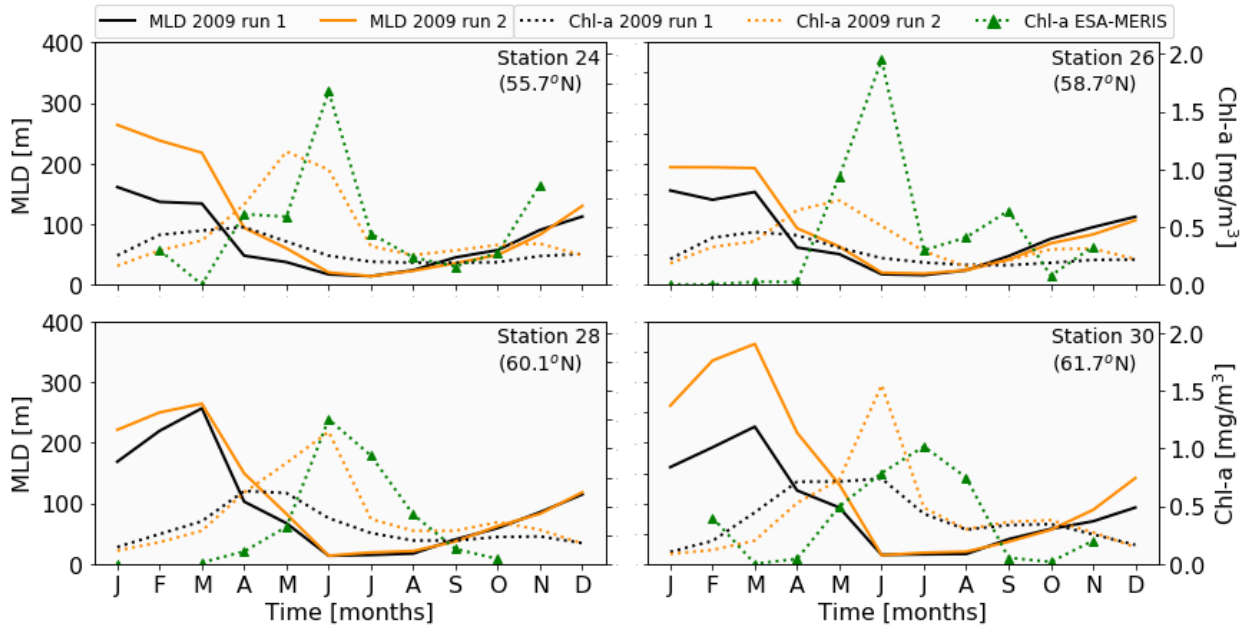

Figure 4.22: Chl a surface concentrations (top 15m, dotted lines) and MLDs (continuous lines) calculated by the model run 1 for 2009 (black colour), model run 2 for 2009 (orange colour) and ESA-MERIS remote sensor data for 2009 (green colour). The results are presented over the entire year (from January to December - November for ESA-MERIS) and for 4 "Northern" stations (24, 26, 28, 30).

The impact of the 2nd run changes over four northern stations can be better described in Fig.4.22. The winter MLDs have increased considerably from 150-200m in run 1 to 250-350m in run 2. This has resulted in more nutrients being brought to the upper layers and almost in a doubling of the Chl a maximum concentrations and a shift of its peak to 2 months later in the season. The NEMO 2nd run adjustments have resulted in more realistic but still not perfect phytoplankton dynamics: The Chl a peak has shifted closer to the observed one (June-July according to ESA MERIS remote sensor data) but in most cases still takes place 1 month earlier. Moreover, Chl a concentration is now higher but still not in accordance with the observations, in 3 out of 4 stations. Aumont et al. (2015) did not face similar problems with their PISCES validation: the timing of the North Atlantic spring bloom was in accordance with observations. It has to be noted that they did not couple PISCES with NEMO in their study but with the ORCA2-LIM v3.2 ocean general circulation model [2]. This shows that phytoplankton growth can be predicted correctly by PISCES if the correct physical parameters are used.

Along with timing, Chl a and nutrient distribution and concentrations have also improved in the depth profiles (Fig.4.20), suggesting that the adjustments made in the second run might have not fixed all of the problems but are a step in the right direction. The drawback of STRATIPHYT's sampling strategy is the limited number of depth profiles in each station, according to Jurado et al. (2012) [31] and the limited amount of time spent (one day per station) which makes it difficult to obtain robust measurements over a longer time period and more specifically over the winter. The winter is a crucial period as the ML shoaling is a very fast process and the division rates of cells increase very rapidly [42], meaning that one day of sampling per station is not enough to

produce safe conclusions regarding the timing of phytoplankton growth.

Chapter 5

Discussion

Winter mixing

In NEMO-PISCES run 1 there was a clear problem in the estimation of Chl a and nutrient concentrations and distribution in the northern part of the transect (above 55^{o}N) which according to Jurado et al. (2012) is seasonally stratified and dominated by convective (not wind) mixing [31]. The problem was at first apparent in spring and consequently affected summer. The constant underestimation of nutrients and Chl a concentrations was combined with a tendency of the model to predict everything earlier in the year: earlier onset of spring blooms, earlier summer blooms, earlier depletion of surface nutrients and shift to DCM states. These two indications suggested that there was a problem in the deep, convective winter mixing that can cause a chain reaction: shallower winter MLDs $\rightarrow$ less light limitation $\rightarrow$ less nutrients are brought in the upper layers $\rightarrow$ weaker and earlier phytoplankton blooms [26]. This hypothesis was also supported by the fact that density and salinity were underestimated, which is something that can definitely influence the deep convective mixing taking place in winter.

Timing

Moreover, the beginning of ML's shoaling is an extremely important process which triggers the onset of the spring bloom. Changes in the onset of stratification can alter nutrient abundance, light intensity and light spectral composition and affect the overall phytoplankton dynamics [35]. Jurado et al. (2012) stated that the $K\tau$ and turbulent kinetic energy dissipation rates (ϵ) were representative of early spring waters. They also concluded based on the temperature profiles and the difficulties they faced while defining the MLDs, that most likely it was the beginning of the thermocline formation [31]. As it is clear in Fig.4.22, NEMO-PISCES estimates the onset of ML shoaling two months earlier, in March, creating possible timing issues in the phytoplankton dynamics. This was also observed by Aumont et al. (2015) during a PISCES validation, when they concluded that the timing of the phytoplankton bloom was driven by the timing of stratification [2].

MLD criterion

Another possible source of the mixing problems is the MLD criterion used by NEMO: 0.01 ref.10m, which means that NEMO defines the MLD as the depth at which the difference in potential density ($\Delta\sigma_\theta$) between that point and 10m depth is 0.01kg/m^3. This "sensitive" criterion seems to work well in the southern, stratified stations but in the deeply-mixed, northern stations it predicts unrealistically shallow MLDs which could possibly have an impact on biology, causing an earlier onset of the spring bloom which will lead to low surface Chl a [26]. Alternative suggestions are made in the following chapter (Outlook).

Model run 2

Run 2, as shown in Fig.4.22, improved many things regarding phytoplankton dynamics. The increase of the winter MLDs and the changes in sea ice resulted in higher Chl a concentrations during the summer bloom in the northern stations. Additionally, the spring bloom is more clear now and is depicted by a peak instead of an almost three-month straight line. In run 1, this three-month plateau was beginning too early (2 months before the run 2 peak) and before the MLD was at its shallowest point, meaning that for almost 3 months there was a depletion of nutrients. This nutrient consumption, resulted in an absence of a peak at the MLD's shallowest point and in an absence of Chl a concentrations increase although the ML was shoaling, from March to June. Constant surface Chl a concentrations while the ML is getting shallower mean that there is phytoplankton loss during that period, instead of increasing growth rates, probably because of nutrient depletion or other factors like grazing. The onset of the spring bloom in run 1 was also not synchronized with the beginning of stratification, and was starting one month earlier. This is fixed in the 2nd run. Finally, the bloom seems to be taking place a few months later than in the previous run, something which is closer to reality and proves that winter mixing problems can result in timing issues for the phytoplankton dynamics.

Unfortunately, it was not possible to collect literature using the same MLD criterion ($\Delta\sigma\theta$ = 0.01kg/m^3, ref.=10m) for the eastern north Atlantic region, so a comparison of the new winter MLDs with literature was not possible. The STRATIPHYT cruise data may be valuable but they are only a "snapshot", since they were collected within one day for each station. Thus, it was not possible to make any comparisons between the NEMO-PISCES run 2 improved convective mixing with observations. It is in general very challenging to observe vertical phytoplankton profiles from autumn to spring, because ships can only sample limited regions for a few weeks, while the bloom stretches over months and is heterogeneous in space[42]. Remote sensing products are also limiting, since they only measure surface Chl a concentrations and, especially at high latitudes, produce incomplete maps because of cloud coverage[42].

Model resolution

NEMO's resolution in both runs was 1^o by 1^o. Aumont et al. (2015) used the ocean physical model ORCA2-LIM version 3.2 for a PISCES evaluation. The model's resolution was 2^o by 2^o and they concluded that it failed to reproduce correctly the phytoplantkon dynamics in coastal areas and in open water regions in which mesoscale and submesoscale processes stimulate biological productivity[2]. A model study by Koné et al. (2009), which used PISCES coupled to a higher resolution version of NEMO (0.5^o by 0.5^o), achieved Chl a concentrations and distribution in much better agreement with the observations[34]. Although there was certainly an improvement, the model still failed to reproduce the blooms in some areas where mesoscale processes play major role in the dynamics of phytoplankton. An increase in the model's spatial resolution would improve things, but there are always practical limits.

PISCES

An important aspect that has not been studied during the present Thesis is related to PISCES: An extremely quick response of phytoplankton to the MLD shoaling, could have the same effects as wintermixing problems in spring Chl a and nutrients. This early phytoplankton growth onset could enhance or even cause the earlier and weaker blooms.

Another PISCES-related issue is the constant overestimation of diatoms in nutrient-rich and coastal regions compared to STRATIPHYT measurements. The contribution of diatoms to total primary production is very broad and uncertain, with values ranging from 17% [2] up to 40% [45] although according to Aumont and Bopp (2006), this is an overestimation [3]. Unfortunately neither remote sensing methods can give a more clear image [10], as their estimations range from as low as 7% to as high as 32% of the total phytoplankton primary production [54, 28]. Finally, ocean biogeochemical models estimate a diatom contribution between 15 and 30% [2]. For the

STRATIPHYT cruise stations, both van de Poll et al. (2013) and Mojica et al. (2015) conclude that diatom's contribution was important only in spring and only between 50-58^{o}N [59, 43], as it is common for them to become Si limited after the stratification of the water column [1]. Probably PISCES' approach to phytoplankton is simplistic and predicts diatoms wherever there is nutrient abundance, from deep mixing or land input. As a result of this, nanophytoplankton are underestimated, especially at the surface blooms. An effort to further investigate this phytoplankton composition issue was done in the experimental report, by comparing 2 species, a diatom (*Thalassiosira oceanica*) and a haptophyte (*Emiliania huxleyi*), under 3 different irradiance - temperature regimes as observed by the STRATIPHYT cruises.

There are certainly many aspects of PISCES that have not been covered by this study, which could possibly play an important role in the growth and distribution of phytoplankton. It seemed logical that the main physical parameters controlled by NEMO (MLD, salinity, density) should be given priority. If the physical model (NEMO) fails to predict the right conditions then it is obvious that the biogeochemical part (PISCES) will also deviate from observations. Clearly, evaluating the model in the Notheast Atlantic Ocean is quite challenging and requires a more thorough systematic analysis of both the model and the available data sets.

Chapter 6

Outlook

STRATIPHYT time limitations

It is not possible to study the deep, winter convective mixing based only on the limited STRATIPHYT data. It is in general very challenging to obtain cruise samples from this period and remote sensors are limiting due to cloud coverage and their ability to measure only surface values[42]. A promising way to overcome these difficulties is the use of biogeochemical-Argo (BGC-Argo) floats, which measure key variables: Oxygen concentration, Nitrate concentration, pH, Chl a concentration, suspended particles and downwelling irradiance (http://biogeochemical-argo.org). Additionaly, they create time series irrespective of the sea conditions and more importantly, Argo data are collected and made freely available by the international Argo Program and by the national programs that contribute to it [48]. As an example, Hosoda et al.(2010) created a global ocean map of MLDs, using Argo data [30] and Mignot et al. (2018) studied the processes that trigger the North Atlantic bloom [42]. Studying the convective winter mixing with the use of Argo data is therefore a very interesting and achievable prospect especially since the data are freely available.

High latitudes

The most prominent divergence between the model and the measurements was observed in the region between Ireland and Iceland and had as a result Chl a and MLD underestimation. It is very important that NEMO-PISCES improves in predicting the right physical conditions and phytoplankton dynamics in this region and possibly in high latitudes in general, where the homogeneous water column during winter causes problems. This becomes more urgent, if we take in to consideration the fact that the sub-polar North Atlantic bloom is the most dramatic seasonal increase in phytoplankton biomass globally [42]. This could be done by validating NEMO-PISCES with BGC-Argo floats data in combination with remote sensing products. Another possibility is the use of datasets compiled by sampling in high latitudes, which is what the DTU Aqua (Danish Institute for Fisheries Research) does with the DANA cruises in the Baltic sea (http://www.aqua.dtu.dk).

MLD criterion

What also needs to be studied further, is the effect of a possible change of the NEMO's MLD criterion in the North Atlantic region. The stations above 55^oN were the most sensitive ones, as even a slight change in the threshold resulted in big differences in the MLDs. The homogeneously mixed water column makes the finding of the correct MLD criterion a very challenging process, nevertheless it can be safely said is that the criterion which was used in the two model runs ($\Delta\sigma_\theta$=0.01kg/m^3, ref.=10m depth) is very sensitive. A different definition like $\Delta\sigma_\theta$=0.03kg/m^3, ΔT=0.2^{o}C or ΔT=0.5^{o}C might produce more realistic results in these problematic regions.

Model resolution

It would be interesting to perform a study using a finer-resolution version of NEMO, not only for studying the changes in primary producers but for two other phenomena as well: (a) Unexpected model results close to coastal areas and on continental shelves and (b) Anomalies in NEMO-PISCES results close to underwater formations. It has already been mentioned that Chl a concentrations (mostly diatoms) were too high close to coastal areas. Moreover, the physical values (salinity, temperature, density) were producing unexpected vertical profiles for the stations located on the Irish continental shelf (19 to 22, STRATIPHYT 2009). Finally, similar problems were observed with the physical values, close to underwater formations (see Fig.4.12). All of the above issues might be improved by a finer model resolution.

Phytoplankton composition

Phytoplankton composition issues have already been documented by Aumont et al. (2015), as they state that in the future, PISCES needs to improve in two aspects: (a) a more sophisticated treatment of phytoplankton physiology and (b) inclusion of mixotrophic organisms [2]. It is very important to perform a more detailed study of PISCES ability in predicting the correct phytoplankton composition under various conditions, which unfortunately was not possible by the present study due to time limitation.

Zooplankton

A major parameter that was beyond the scope of this study is zooplankton. The effect of grazing can have a major impact on phytoplankton dynamics as mesozooplankton alone grazes about 9% of total primary production [2, 12]. It is easily understandable that the inclusion of micro- and mesozooplankton in the validation of NEMO-PISCES can give new insights.

Fe and Si

Another parameter that was not taken into account from this study were two important nutrients: silica (Si) and iron (Fe). Iron is a component of many algal proteins and it is responsible the synthesis of chlorophyll and the electron transport reactions of respiration and photosynthesis [27]. It can affect diatom productivity and growth by reducing the rates of CO_2 fixation and inorganic N assimilation as it limits the capacity of photosynthesis to provide the necessary energy for these processes [11, 20]. Iron limitation is the main reason for low growth rates and productivity in about 30% of the ocean, in high-nutrient, low-chlorophyll regions (HNLC) [11]. The silica cycle is intertwined with the carbon cycle, affecting the carbon export to the deep sea and the atmosphere's CO_2 content [53]. Silicon, is one of the most abundant elements on the planet and is required for the growth of diatoms as it is the "building block" of their cell walls [53, 61].

Spin-up run

The deep ocean gets ventilated on very long timescales, i.e. hundreds of years. This slow process can cause significant drifts in multiple ocean properties [24] creating a problem which needs to be addressed. A few cycles of atmospheric forcing, as it was done for the 2 NEMO-PISCES v2 runs used in this study (358 & 310 years), are usually not enough for the deep ocean to reach an equilibrium. It would be very interesting to perform a similar study in the future, using runs which have been spun-up for a much longer time period (thousands of years).

PISCES

There are certainly many aspects of PISCES that have not been covered by this study. Among those is the response of phytoplankton to the ML's shoaling, meaning how fast they respond to

the decreasing MLDs. Also, the nutrient transfer between the nutricline and the ML is a major factor for the blooms. Moreover, this study did not focus on mortality rates, light penetration (euphotic depth and light attenuation coefficient), remineralization processes etc. All of these variables, could possibly play an important role in the growth and distribution of phytoplankton and should be given more attention in following studies.

Bibliography

[1] Alkire, M. B., D'Asaro, E., Lee, C., Jane Perry, M., Gray, A., Cetinić, I., … González-Posada, A. (2012). Estimates of net community production and export using high-resolution, Lagrangian measurements of O2, NO3-, and POC through the evolution of a spring diatom bloom in the North Atlantic. Deep-Sea Research Part I: Oceanographic Research Papers, 64, 157–174. https://doi.org/10.1016/j.dsr.2012.01.012

[2] Aumont, O., Ethé, C., Tagliabue, A., Bopp, L., & Gehlen, M. (2015). PISCES-v2: An ocean biogeochemical model for carbon and ecosystem studies. Geoscientific Model Development, 8(8), 2465–2513. https://doi.org/10.5194/gmd-8-2465-2015

[3] Aumont, O., & Bopp, L. (2006). Globalizing results from ocean in situ iron fertilization studies. Global Biogeochemical Cycles, 20(2), 1–15. https://doi.org/10.1029/2005GB002591

[4] M. J. Behrenfeld and E. S. Boss. Resurrecting the Ecological Underpinnings of Ocean Plankton Blooms. Annual Review of Marine Science, Vol 6, 6:167–U208, 2014

[5] Behrenfeld, M. J., & Falkowski, P. G. (1997). Photosynthetic rates derived from satellite-based chlorophyll concentration. Limnology and Oceanography, 42(1), 1–20. https://doi.org/10.4319/lo.1997.42.1.0001

[6] Behrenfeld, M. J., O'Malley, R. T., Siegel, D. A., McClain, C. R., Sarmiento, J. L., Feldman, G. C., … Boss, E. S. (2006). Climate-driven trends in contemporary ocean productivity. Nature, 444(7120), 752–755. https://doi.org/10.1038/nature05317

[7] Bessières, L., Leroux, S., Brankart, J. M., Molines, J. M., Moine, M. P., Bouttier, P. A., … Sérazin, G. (2017). Development of a probabilistic ocean modelling system based on NEMO 3.5: Application at eddying resolution. Geoscientific Model Development, 10(3), 1091–1106. https://doi.org/10.5194/gmd-10-1091-

[8] Bintanja, R., Nederlands, K., Instituut, M., Hazeleger, W., Haarsma, R., Nederlands, K., … Instituut, M. (n.d.). EC-EARTH: goals, developments and scientific perspectives, (January 2015).

[9] Brainerd, K. E., & Gregg, M. C. (1995). Surface mixed and mixing layer depths. Deep-Sea Research Part I, 42(9), 1521–1543. https://doi.org/10.1016/0967-0637(95)00068-H

[10] Brewin, R. J. W., Hardman-Mountford, N. J., Lavender, S. J., Raitsos, D. E., Hirata, T., Uitz, J., … Gentili, B. (2011). An intercomparison of bio-optical techniques for detecting dominant phytoplankton size class from satellite remote sensing. Remote Sensing of Environment, 115(2), 325–339. https://doi.org/10.1016/j.rse.2010.09.

[11] Buitenhuis, E., & Geider, R. J. (2010). A model of phytoplankton acclimation to iron – light colimitation. Methods, 55(2), 714–724.

[12] Calbet, A. (2001). Mesozooplankton grazing effect on primary production: A global comparative analysis in marine ecosystems. Limnology and Oceanography, 46(7), 1824–1830. https://doi.org/10.4319/lo.2001.46.7.1824

[13] Claustre, H. (2005). Toward a taxon-specific parameterization of bio-optical models of primary production: A case study in the North Atlantic. Journal of Geophysical Research, 110(C7), C07S12. https://doi.org/10.1029/2004JC002634

[14] Dai, A., & Trenberth, K. E. (2002). Estimates of Freshwater Discharge from Continents: Latitudinal and Seasonal Variations. Journal of Hydrometeorology, 3(6), 660–687. https://doi.org/10.1175/1525-7541(2002)003¡0660:EOFDFC¿2.0.CO;2

[15] Dai, A., Qian, T., Trenberth, K. E., & Milliman, J. D. (2009). Changes in continental freshwater discharge from 1948 to 2004. Journal of Climate, 22(10), 2773–2792. https://doi.org/10.1175/2008JCLI2592.1

[16] Danabasoglu, G., Yeager, S., Bailey, D., Behrens, E., Bentsen, M., Bi, D., ... Wang, Q. (2014). North Atlantic Simulations in Coordinated Ocean-ice Reference Experiments phase 2 (CORE-II). Part 1: Mean States. Ocean Modelling, 73, 76–107. https://doi.org/10.1016/j.ocemod.2013.10.005

[17] de Boyer Montégut, C., Madec, G., Fischer, A. S., Lazar, A., & Iudicone, D. (2004). Mixed layer depth over the global ocean: An examination of profile data and a profile-based climatology. Journal of Geophysical Research C: Oceans, 109(12), 1–20. https://doi.org/10.1029/2004JC002378

[18] de Boyer Montégut, C., Mignot, J., Lazar, A., & Cravatte, S. (2007). Control of salinity on the mixed layer depth in the world ocean: 1. General description. Journal of Geophysical Research: Oceans, 112(6), 1–12. https://doi.org/10.1029/2006JC003953

[19] Falkowski, P. (1996). The role of phytoplankton in the global carbon cycle. S.It.E. Atti, 17, 3–6.

[20] Franck, V. M., Brzezinski, M. A., Coale, K. H., & Nelson, D. M. (2000). Iron and silicic acid concentrations regulate Si uptake north and south of the Polar Frontal Zone in the Pacific Sector of the Southern Ocean. Deep-Sea Research Part II: Topical Studies in Oceanography, 47(15–16), 3315–3338. https://doi.org/10.1016/S0967-0645(00)00070-9

[21] Geider, R. J., MacIntyre, H. L., & Kana, T. M. (1997). Dynamic model of phytoplankton growth and acclimation: Responses of the balanced growth rate and the chlorophyll a:carbon ratio to light, nutrient-limitation and temperature. Marine Ecology Progress Series, 148(1–3), 187–200. https://doi.org/10.3354/meps148187

[22] Griffies, S. M., Biastoch, A., Böning, C., Bryan, F., Danabasoglu, G., Chassignet, E. P., ... Yin, J. (2009). Coordinated Ocean-ice Reference Experiments (COREs). Ocean Modelling, 26(1–2), 1–46. https://doi.org/10.1016/j.ocemod.2008.08.007

[23] Griffies, S. M., Winton, M., Samuels, B., Danabasoglu, G., Yeager, S., Marsland, S., Drange., H., and Bentsen, M., 2012: Datasets and protocol for the CLIVAR WGOMD Coordinated Ocean-sea ice Reference Experiments (COREs), WCRP Report No. 21/2012, pp. 21

[24] Griffies, S. M., Danabasoglu, G., Durack, P. J., Adcroft, A. J., Balaji, V., Böning, C. W., ... Yeager, S. G. (2016). OMIP contribution to CMIP6: Experimental and diagnostic protocol for the physical component of the Ocean Model Intercomparison Project. Geoscientific Model Development, 9(9), 3231–3296. https://doi.org/10.5194/gmd-9-3231-2016

[25] Hahn-Woernle, L., Dijkstra, H. A., & Van Der Woerd, H. J. (2014). Sensitivity of phytoplankton distributions to vertical mixing along a North Atlantic transect. Ocean Science, 10(6), 993–1011. https://doi.org/10.5194/os-10-993-2014

[26] Hahn-Woernle, L. (2016). Estimation of upper ocean vertical mixing from surface ocean colour observations. PhD Thesis, IMAU, Utrecht.

[27] Harrison, G. I., & Morel, F. M. M. (1986). Response diatom Thalassiosira of the marine weissflogii to iron stress '. Limnology and Oceanography, 31(5), 989–997. https://doi.org/10.4319/lo.1986.31.5.0989

[28] Hirata, T., Aiken, J., Hardman-Mountford, N., Smyth, T. J., & Barlow, R. G. (2008). An absorption model to determine phytoplankton size classes from satellite ocean colour. Remote Sensing of Environment, 112(6), 3153–3159. https://doi.org/10.1016/j.rse.2008.03.011

[29] Holte, J., & Talley, L. (2009). A new algorithm for finding mixed layer depths with applications to argo data and subantarctic mode water formation. Journal of Atmospheric and Oceanic Technology, 26(9), 1920–1939. https://doi.org/10.1175/2009JTECHO543.1

[30] Hosoda, S., Ohira, T., Sato, K., & Suga, T. (2010). Improved description of global mixed-layer depth using Argo profiling floats. Journal of Oceanography, 66(6), 773–787. https://doi.org/10.1007/s10872-010-0063-3

[31] Jurado, E., Dijkstra, H. A., & Van Der Woerd, H. J. (2012). Microstructure observations during the spring 2011 STRATIPHYT-II cruise in the northeast Atlantic. Ocean Science, 8(6), 945–957. https://doi.org/10.5194/os-8-945-2012

[32] Jurado, E., Van Der Woerd, H. J., & Dijkstra, H. A. (2012). Microstructure measurements along a quasi-meridional transect in the northeastern Atlantic Ocean. Journal of Geophysical Research: Oceans, 117(4), 1–12. https://doi.org/10.1029/2011JC007137

[33] Kara, A. B. (2003). Mixed layer depth variability over the global ocean. Journal of Geophysical Research, 108(C3), 3079. https://doi.org/10.1029/2000JC000736

[34] Koné, V., Aumont, O., Lévy, M., & Resplandy, L. (2009). Physical and biogeochemical controls of the phytoplankton seasonal cycle in the Indian Ocean: A modeling study. Geophysical Monograph Series, 185, 147–166. https://doi.org/10.1029/2008GM000700

[35] Kulk, G., De Vries, P., Van De Poll, W. H., Visser, R. J. W., & Buma, A. G. J. (2012). Temperature-dependent growth and photophysiology of prokaryotic and eukaryotic oceanic picophytoplankton. Marine Ecology Progress Series, 466, 43–55. https://doi.org/10.3354/meps09898

[36] Large, W. G., & Yeager, S. G. (2009). The global climatology of an interannually varying air - Sea flux data set. Climate Dynamics, 33(2–3), 341–364. https://doi.org/10.1007/s00382-008-0441-3

[37] Lévy, M., Ferrari, R., Franks, P. J. S., Martin, A. P., & Rivière, P. (2012). Bringing physics to life at the submesoscale. Geophysical Research Letters, 39(14), 1–13. https://doi.org/10.1029/2012GL052756

[38] Litchman, E., Klausmeier, C. A., Schofield, O. M., & Falkowski, P. G. (2007). The role of functional traits and trade-offs in structuring phytoplankton communities: Scaling from cellular to ecosystem level. Ecology Letters, 10(12), 1170–1181. https://doi.org/10.1111/j.1461-0248.2007.01117.x

[39] Madec, G., & NEMO team. (2016). NEMO Ocean Engine, (27).

[40] Mahadevan, A., D'Asaro, E., Lee, C., & Perry, M. J. (2012). Eddy-driven stratification initiates North Atlantic spring phytoplankton blooms. Science, 336(6090), 54–58. https://doi.org/10.1126/science.1218740

[41] Marshall, J., & Schott, F. (1999). Open-ocean convection: Observations, theory, and models. Reviews of Geophysics, 37(98), 1–64. https://doi.org/10.1029/98RG02739

[42] Mignot, A., Ferrari, R., & Claustre, H. (2018). Floats with bio-optical sensors reveal what processes trigger the North Atlantic bloom. Nature Communications, 9(1), 190. https://doi.org/10.1038/s41467-017-02143-6

[43] Mojica, K. D. A., van de Poll, W. H., Kehoe, M., Huisman, J., Timmermans, K. R., Buma, A. G. J., ... Brussaard, C. P. D. (2015). Phytoplankton community structure in relation to vertical stratification along a north-south gradient in the Northeast Atlantic Ocean. Limnology and Oceanography, 60(5), 1498–1521. https://doi.org/10.1002/lno.10113

[44] Mulder, C., & Hendriks, A. J. (2014). Half-saturation constants in functional responses. Global Ecology and Conservation, 2, 161–169. https://doi.org/10.1016/j.gecco.2014.09.006

[45] Nelson, D. M. (1995). Revised global estimates, comparison with regional data, 9(3), 359–372.

[46] Oschlies, A., & Garçon, V. (1998). An Eddy-Permitting Coupled Physical-Biological Model of the North Atlantic. Sensitivity to Advection Numerics and Mixed Layer Physics, 13(1), 135–160. Retrieved from http://www.agu.org/pubs/crossref/1999/98GB02811.shtml

[47] Polovina, J. J., Howell, E. A., & Abecassis, M. (2008). Ocean's least productive waters are expanding. Geophysical Research Letters, 35(3), 2–6. https://doi.org/10.1029/2007GL031745

[48] Roemmich, D., Johnson, G., Riser, S., Davis, R., Gilson, J., Owens, W. B., ... Ignaszewski, M. (2009). The Argo Program: Observing the Global Oceans with Profiling Floats. Oceanography, 22(2), 34–43. https://doi.org/10.5670/oceanog.2009.36

[49] S. Sathyendranath, R. Ji, and H. I. Browman. Revisiting Sverdrup's critical depth hypothesis. ICES Journal of Marine Science: Journal du Conseil, 72:1892–1896, 2015.

[50] Signorini, S. R., Franz, B. A., & McClain, C. R. (2015). Chlorophyll variability in the oligotrophic gyres: mechanisms, seasonality and trends. Frontiers in Marine Science, 2(February), 1–11. https://doi.org/10.3389/fmars.2015.00001

[51] Sverdrup, H. U. (1953). On conditions for the vernal bloom of phytoplankton. J.Cons.Perm.Int.Explor.Mer, 18, 287–295.

[52] Thomson, R. E., Fine, I. V. (2003). Estimating mixed layer depth from oceanic profile data. Journal of Atmospheric and Oceanic Technology, 20(2), 319–329. https://doi.org/10.1175/1520-0426(2003)020¡0319:EMLDFO¿2.0.CO;2

[53] Tréguer, P. J., & De La Rocha, C. L. (2013). The World Ocean Silica Cycle. Annual Review of Marine Science, 5(1), 477–501. https://doi.org/10.1146/annurev-marine-121211-172346

[54] Uitz, J., Claustre, H., Morel, A., & Hooker, S. B. (2006). Vertical distribution of phytoplankton communities in open ocean: An assessment based on surface chlorophyll. Journal of Geophysical Research: Oceans, 111(8). https://doi.org/10.1029/2005JC003207

[55] Vage, K., Pickart, R. S., Thierry, V., Reverdin, G., Lee, C. M., Petrie, B., ... Ribergaard, M. H. (2009). Surprising return of deep convection to the subpolar North Atlantic Ocean in winter 2007-2008. Nature Geoscience, 2(1), 67–72. https://doi.org/10.1038/ngeo382

[56] Popova, E. E., Yool, A., Coward, A. C., Dupont, F., Deal, C., Elliott, S., ... Zhang, J. (2012). What controls primary production in the Arctic Ocean? Results from an intercomparison of five general circulation models with biogeochemistry. Journal of Geophysical Research: Oceans, 117(1), 1–16. https://doi.org/10.1029/2011JC007112

[57] UNESCO, 1983: Algorithms for computation of fundamental property of sea water. Techn. Paper in Mar. Sci, 44, UNESCO.

[58] Van Aken, H. M. (2000). The hydrography of the mid-latitude Northeast Atlantic Ocean II: The intermediate water masses. Deep-Sea Research Part I: Oceanographic Research Papers (Vol. 47). https://doi.org/10.1016/S0967-0637(99)00112-0

[59] Van De Poll, W. H., Kulk, G., Timmermans, K. R., Brussaard, C. P. D., Van Der Woerd, H. J., Kehoe, M. J., … Buma, A. G. J. (2013). Phytoplankton chlorophyll a biomass, composition, and productivity along a temperature and stratification gradient in the northeast Atlantic Ocean. Biogeosciences, 10(6), 4227–4240. https://doi.org/10.5194/bg-10-4227-2013

[60] Wunsch, C., & Ferrari, R. (2004). Vertical Mixing, Energy, and the General Circulation of the Oceans. Annual Review of Fluid Mechanics, 36(1), 281–314. https://doi.org/10.1146/annurev.fluid.36.050802.122121

[61] Yool, A., & Tyrrell, T. (2003). Role of diatoms in regulating the ocean's silicon cycle. Global Biogeochemical Cycles, 17(4), n/a-n/a. https://doi.org/10.1029/2002GB002018

Master's thesis part 2:

Growth of *Emiliania huxleyi* and *Thalassiosira oceanica* under 3 irradiance regimes

Utrecht University

university of groningen

Royal Netherlands Meteorological Institute
Ministry of Infrastructure and the Environment

Nomikos Skyllas

Supervisors:

prof. dr. Jack Middelburg (UU)

prof. dr. Anita Buma (RUG)

prof. dr. Richard Bintanja (KNMI - RUG)

dr. Willem van de Poll (RUG)

July 10, 2018

Abstract

Two phytoplankton species, a diatom and a haptophyte, typical for the North Atlantic ocean were acclimated to three different irradiance - temperature regimes, simulating stable (5 μmol m^{-2} s^{-1} / 17 ^{o}C) and dynamic water column conditions (0-20 μmol m^{-2} s^{-1} / 9^{o}C and 50-1250 μmol m^{-2} s^{-1} / 13.5^{o}C). An effort has been made to simulate as closely as possible the conditions observed during the summer 2009 and spring 2011 STRATIPHYT cruises. Specific growth rates were estimated using microscopy, fluorescence, Chlorophyll a (Chl a) extraction and spectrophotometry. Furthermore, the photoacclimation abilities of the two species were assessed by maximum PSII efficiency (f_v/f_m), Chl a content per cell and optical density (OD) per cell.

Results showed no distinct differences between the studied species, *Thalassiosira oceanica* and *Emiliania huxleyi*. On one hand, based on growth rates and photoacclimation characteristics it is not possible to tell if one species would dominate over the other in any of the three completely different conditions that were studied. On the other hand clear differences in growth and photoacclimation responses were observed between the constant low irradiance and the dynamic low and dynamic high irradiance experiments. These results imply that although both species exhibited high photoacclimation potential under extreme and fluctuating irradiance conditions, this did not translate into significantly different growth rates. We can conclude that light intensity is not sufficient to explain the differences in the occurrence of these species in the field.

Contents

List of Figures

List of Tables

Chapter 1

Theory

1.1 Irradiance and phytoplankton growth

Phytoplankton experiences irradiance fluctuations, which range from seasonal patterns down to the scale of minutes or even seconds [24], because of seasonal and diurnal variations, weather changes and vertical mixing in the water column [28]. On top of these factors, there is also the attenuation of light by water, by suspended particles and by the substances dissolved in it [4]. In permanently stratified regions, the phytoplankton cells are confined, because of mixing and the density difference with the underlying layer (thermocline), within a shallow Mixed Layer (ML). This means that they are exposed to strong, dynamic sunlight [28] but in a nutrient-depleted environment or they can be found in a Deep Chlorophyll Maximum (DCM) state, under very weak and limiting irradiance conditions but with abundant nutrients. In seasonally stratified regions, the stratification is followed by a season of deep, convective mixing which is usually light-limiting for the phytoplankton as they are distributed over the entire column down to aphotic depths of 400 or even 600m [13].

The process of vertical mixing modulates the exposure of cells to Photosynthetically Active Radiation (PAR) and UV light [28]. Different species have different growth optima, meaning light intensity and spectral composition, and consequently an advantage or disadvantage over other species [13]. The competitive success of a species depends not only on the irradiance regime but on the abundance of nutrients as well [13]. These dynamic light changes between high (surface) and low (euphotic depth limit or deeper) intensities require an adaptation mechanism on behalf of phytoplankton, which adjust their light harvesting and photoprotection pigments along with other cell components. The extent of this adjustment defines the fate of the species under these extreme conditions, with some organisms having a greater potential than others [28, 13]. As a result, certain species have an advantage in shallow MLs while others dominate in DCMs [13].

Whenever phytoplankton is exposed to irradiance variations it responds by using a series of cellular mechanisms which allow the optimum utilization of the available light and the protection against excess radiation [4, 28, 24]. These responses, which allow the adaptation of phytoplankton cells in new light environments, are called “photoacclimation” [28, 4]. Photoacclimation includes alterations in physiological processes and the biochemistry of the cell: pigment composition, PSII reaction center abundance and activity of the Calvin cycle [24, 28]. The result is stable photosynthetic performance under extreme light fluctuations and utilization of very low irradiance, provided there are adequate nutrients available [4].

Under low irradiance conditions, the light-harvesting pigments (chlorophylls, phycobilins, fucoxanthin and peridinin) increase, causing the phytoplankton cells to change colour. The exact opposite happens under high light conditions resulting in almost transparent cells [4]. A second type of pigments takes part in the photoacclimation process too: the photoprotective pigments, β-carotene, astaxanthin and the xanthophyll cycle elements [4, 28]. Xanthophyll pigments have a dual role: the epoxidized diadinoxanthin (DD) contributes to light harvesting while the de-epoxidized diatoxanthin (DT) helps in dissipating excessive irradiance as thermal energy, protecting the cell from viability loss [28, 4]. Another photoacclimation mechanism is

the formation of antioxidant enzymes (catalase, superoxydismutase and ascorbate peroxidase) which protect the PSII from free radicals, created by the excess radiation [4]. Furthermore, algal cells can increase the number of thylacoids per granum, resulting in an increased area for the extra pigment molecules [4]. Finally, some species can increase the number or the size of the photosynthetic units (PSU) as a response to light fluctuations [4].

1.2 *Emiliania huxleyi* and *Thalassiosira oceanica*

Emiliania huxleyi is a cosmopolitan species, numerous in eutrophic (following diatom blooms) and oligotrophic regions [27]. It is the most important and well-studied of the coccolithophores (division haptophyta), a climatically important group because of dimethylsulphide (DMS) and inorganic carbon (calcium carbonate coccoliths) formation [18, 19, 30]. *E. huxleyi* can be found almost in every ocean (except for the Southern) and it is capable of forming vast blooms which contain low Chl a concentrations, because of its small cell size (5 - 10 μm) [27, 18]. It is one of the most eurythermal and euryhaline species as it occurs in waters ranging from 2 to 28^{o}C, accounting for 20-50% of the total coccolithophore community in most oceans [27, 30]. The majority (if not all) of the blooms occur in temperate waters always in highly stratified waters, with MLDs shallower than 30m and usually between 10 - 20m [27, 30, 18]. *E. huxleyi* seems to have a competitive advantage at high light conditions due to fast pigment adjustments and highest resistance to photoinhibition [18, 27]. It is a fast-growing species and under favorable conditions, meaning high irradiance and Si limitation, it is very likely that it will dominate towards the end of the spring diatom bloom [27].

Thalassiosira is the genus with the highest diversity of all temperate, marine diatoms, including approximately 100 species which contribute significantly in the diatom - dominated spring blooms [10]. *Thalassiosira oceanica* is a relatively small (3-12μ), cosmopolitan diatom species occuring mostly in warm waters [10]. It has been reported off the coasts of Chile, California, west coast of Africa, NE America, Norway, Australia and in the Sargasso Sea [8]. In many temperate regions, during winter, a deep convective mixing takes place. During this mixing nutrients and phytoplankton cells (low concentrations) are homogeneously mixed over the entire water column at depths that can reach hundreds of meters. At the beginning of spring a ML shoaling process begins, creating favourable conditions (abundant nutrients, mixing in the euphotic zone) for the diatoms to grow [8]. *Thaslassiosira* species take advantage of these bloom - inducing conditions thanks to their ability to grow under low temperatures, weak irradiance and well-mixed waters [8].

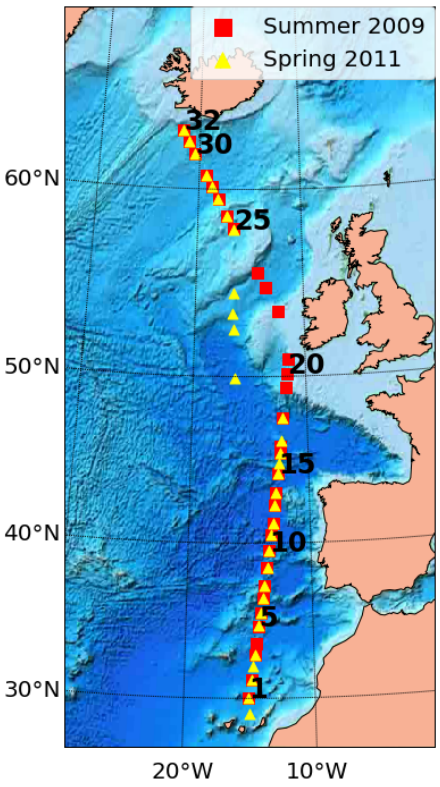

Figure 1.1: Bathymetric map of the North-east Atlantic ocean depicting station locations and station numbers for the spring 2011 (yellow triangles) and summer 2009 (red squares) STRATIPHYT cruises. The bold, black numbers represent the stations numbers.

1.3 STRATIPHYT cruises

The North Atlantic ocean provides an opportunity to study in depth the phytoplankton dynamics under each of the 3 already mentioned states: DCM, growth close to the surface and slow growth because of deep mixing. It provides a meridional stratification gradient from 29 ^{o}N (Canary islands) to 63 ^{o}N (Iceland) with permanently

stratified conditions in the South, seasonally stratified conditions mid-latitude and deep, convective winter mixing in the North [17, 29]. This region also plays a key role in the global climate and the ocean circulation because of the deep water formation which results in a large amount of CO_2 uptake (20% of the total ocean uptake) [17].Two cruises were performed onboard the RV Pelagia, in the summer of 2009 (July/August) and spring of 2011 (April/May), covering a transect between the Canary islands and Iceland (Fig.1.1). The transect was divided in 32 stations at which CTD measurements were performed (conductivity, temperature, depth) and samples were collected. The samples were analyzed for macronutrients, pigments, chlorophyll specific absorption and excess light experiments were performed [11, 17, 29].

1.4 Objective

In the present study, a comparison of the growth of *Thalassiosira oceanica* (diatom) and *Emiliania huxleyi* (haptophyte) was performed, under 3 different irradiance regimes. More specifically, it was decided to cultivate a diatom and a haptophyte (coccolithophore) in order to mimic the division of phytoplankton into 2 classes (diatoms and nanophytoplankton) by the NEMO-PISCES v2 model. Consequently, an effort was made to simulate as closely as possible the conditions (mixing, irradiance and temperature) from 3 different parts of the STRATIPHYT cruise which were used for the validation of the same model: Upper Chlorophyll maximum (UCM), Deep Chlorophyll Maximum (DCM) and Well-Mixed (WM) conditions. Thus the results of this study were comparable to the ones of the NEMO-PISCES v2 validation study, regarding the biogeochemical component (PISCES) and its ability to predict the phyoplankton composition. Growth was assessed after photoacclimation, using 4 different methods (photometry, fluorescence, cell counts and chl a extraction) and the results are discussed in the context of ecophysiological differences between a diatom and a haptophyte with similar sizes.

Chapter 2

Methods

2.1 Culture conditions

Batch cultures of *Emiliania huxleyi* (strain: CCMP 2112) and *Thalassiosira oceanica* (strain: CCMP 1616) were grown in f2 - enriched [7] autoclaved seawater (salinity 35) in a temperature - controlled cabinet (16 ^{o}C) in low irradiance (9 μmol m^{-2} s^{-1}), provided by Osram biolux lamps during a 16 : 8 h light : dark (LD) cycle. The cultures were regularly diluted in new medium for 3 weeks and served as back-up starting material in case an experiment needed to be repeated.

2.2 Experimental design

Triplicate Erlenmeyer flasks containing 400 ml of f2 medium were used and were inoculated with 10 ml of the low light - acclimated cultures and grown for 5 days under the Deep Chlorophyll Maximum (DCM) constant irradiance, 4 days under the Well Mixed (WM) dynamic irradiance and 1 day under the Upper Chlorophyll Maximum (UCM) dynamic light conditions. Two of the three irradiance conditions (WM and UCM) were simulated using a U-shaped lamp setup [28] which contains 12 fluorescent biolux lamps. The lamp setup was also equipped with Doublelux reflectors and was connected to Osram dimmers. Inside the U-shaped lamp a transparent, UV and PAR tramsmissive water bath was placed. The cultures were submerged (for a few cm) in to the water bath and the different temperatures were controlled by a cryostat: 17^{o}C for the DCM, 9^{o}C for the WM and 13.5^{o}C for the UCM experiment. The dimmers were controlled by a computer with the use of LabVIEW (National Instruments) software. The irradiance was dynamic in 2 out of the 3 setups (WM and UCM) and ranged between 0 and 1,250 μmol m^{-2} s^{-1} without changing spectral composition. It was measured using a QSL-100 (Bio- spherical Instruments).

In the DCM treatment (Fig.2.1, Table2.1), an effort was made to simulate the conditions dominating the southern, constantly stratified stations of the STRATIPHYT transect. Both species were cultivated under a low, constant irradiance of 5 μmol m^{-2} s^{-1} and were covered by a transparent, blue-coloured plastic screen in order to mimic the Deep Chlorophyl Maximum light intensity and spectrum composition in that depth (100m). The flasks were placed in a non-transparent plastic box, with an open top. The water bath was kept at a constant temperature of 17^{o}C and the daily irradiance was provided from the top (open side of the box) as a block function (on–off) during a 14 : 10 h LD cycle.

In the WM dynamic irradiance treatment (Fig.2.1, Table2.1), the two species were cultivated under electronically modulated irradiance, with mixing speed (one cycle in 15.5 h), mixing depth (330 m), and attenuation (K_d = 0.058 for PAR) superimposed on the diurnal cycle (16 : 8 h LD). The field values were combined with the calculated mixing speed and with the help of LabVIEW (National Instruments) software were used to manipulate irradiance levels in the 2 dynamic light experiments (WM and UCM). Neutral density screens were used in order to achieve the extremely low irradiance conditions required. It was decided to simulate the deep convective mixing conditions of the Northern STRATIPHYT stations during the 2011 cruise, which experienced deep winter mixing down to a few hundred meters during the time of sampling by the RV

Pelagia. The average value of 330m for the Mixed Layer Depth (MLD) and the K_d value of 0.058 m^{-1} were calculated from stations 22 to 30 and the highest vertical eddy diffusivity coefficient (K_T) value estimated by Jurado et al. (2012) was chosen [11]. The reason for this choice was practical: Only the highest K_T value produced a mixing speed that was reproducible in the lab (15.5 h) considering the equipment and time limitations. The mixing speed was then calculated based on the Lande & Wood (1987) equation for the time needed by a neutrally buoyant particle to reach the thermocline [14]. A number of assumptions were made: phytoplankton cells are almost neutrally buoyant (sinking speed is negligible), the cells remain inside the Mixed Layer (ML) and don't sink below the thermocline, the time that a cell needs to be resuspended to the surface is equal to the time that it needs to reach the thermocline. Finally, one more assumption was made, related to the irradiance curve: 24 curves were produced, representing 24 different possible hours of the day that the phytoplankton might come to the surface. Eventually all of the 24 curves were averaged to 1, which was used for the experiment and represented the average daily irradiance curve for a phytoplankton cell.

In the UCM dynamic irradiance treatment (Fig.2.1, Table2.1), the two species were cultivated under electronically modulated irradiance, with mixing speed (one cycle in 3 h), mixing depth (20 m), and attenuation (K_d = 0.16 for PAR) superimposed on the diurnal cycle (14 : 10 h LD). It was decided to simulate the Upper Chlorophyll Maximum (UCM) conditions of the seasonally stratified station 17 from STRATIPHYT 2011 cruise, which exhibited a clear and strong phytoplankton blooom at the time of sampling by the RV Pelagia. Values for MLD, K_T and K_d were taken from the STRATIPHYT dataset and Jurado et al. (2012) [11]. The mixing speed was then calculated based on the Lande & Wood (1987) equation as described in the previous paragraph.

Table 2.1: Experimental setup details: Simulated light regime, irradiance, simulated depth, temperature, mixing speed (how often the pytoplankton complete a full mixing cycle), attenuation coefficient (K_d), vertical eddy diffusivity coefficient (K_T), daylength, light setup, used screens for irradiance modification, STRATIPHYT station conditions that were simulated by the experiment.

	DCM	WM	UCM
Light regime	stable	dynamic	dynamic
Irradiance (μmol m^{-2} s^{-1})	5	0 - 20	50 - 1250
Depth (m)	100	0 - 330	0 - 20
Temperature (^{o}C)	17	9	13.5
Mixing speed (h/cycle)	-	15.5	3
K_d (m^{-1})	0.055	0.058	0.16
K_T (m^2/s)	-	2	0.02
Daylength (h)	14	16	14
Setup	box	U-shaped	U-shaped
Screens	blue plastic	neutral density	-
STRATIPHYT station	Southern (1-11) average	Northern (22-30) spring average	17 (spring 2011)

2.3 Growth measurements

Sampling process

Samples of 25 ml were collected every 2 days, after several acclimation days (5 for DCM, 4 for WM and 1 for UCM). An effort was made to obtain samples during the exponential and the beginning of the stationary growth phase. 5ml were used for cell counts, 5ml for Pulse Amplitude modulation fluorometeter (PAM), 5ml for the spectrophotometer and 15 for Chl a extraction.

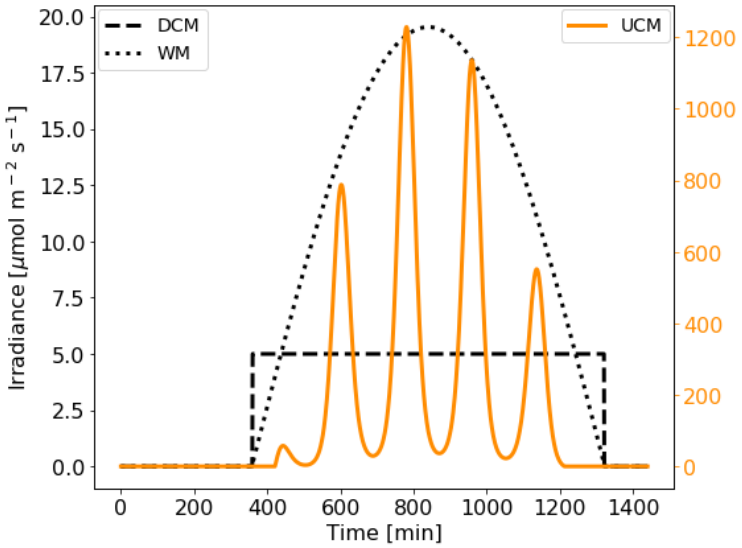

Figure 2.1: Irradiance (μmol m^{-2} s^{-1}) during the low stable light (DCM) and low and high dynamic light conditions (WM, UCM).

Cell counts

Cell concentrations were determined by light microscopy observations on fixed samples. Observations were made on an Olympus IMT-2 inverted microscope, using 40 times magnification (both species cell size was around 10μm). Sedgewick Rafter counting chambers were used, using samples of 2ml that were fixed with Lugol. Growth rates (d^{-1}) of the exponential growth phase were calculated by linear regression of natural log - transformed cell numbers for all replicates (3 - 5 data points).

Pulse Amplitude Modulation fluorometer (PAM)

Minimum fluorescence in darkness (f_0) and maximum photochemical efficiency of photosystem II (f_v/f_m) were measured using a water - PAM fluorometer (Waltz GmbH), for every sample. Growth rates (d^{-1}) of the exponential growth phase were calculated by linear regression of natural log - transformed f_0 for all replicates (3 - 5 data points).

Spectrophotometer

Light absorption of a specific wavelength (750 nm) was measured using a spectrophotometer for every sample. Growth rates (d^{-1}) of the exponential growth phase were calculated by linear regression of natural log - transformed absorption for all replicates (3 - 5 data points).

Chl a extraction

15 ml from each sample were filtered with 25mm GF/F filters (Whatman), frozen immediately in liquid nitrogen and stored at -80^{o}C until the extraction. Before the analysis, the filters were freeze-dried for 48 h and Chl a was immediately extracted in 3ml 90% acetone (v/v, 48 h, 4 ^{o}C). Chl a was measured using a Turner Designs Trilogy fluorimeter, calibrated with chl- a standard (Sigma). Growth rates (d^{-1}) of the exponential growth phase were calculated by linear regression of natural log - transformed fluorescence values for all replicates (3 - 5 data points).

Statistical analysis

Differences among replicates and species were tested for significance with a single-factor analysis of variance (ANOVA). Regression analysis was performed using the PYTHON programming language.

Chapter 3

Results

3.1 Growth

Under the DCM conditions, both species exhibited extremely low growth rates (Table 3.1). *E. huxleyi* specifically did not show any or even showed negative growth in the 1st and the 3rd replicate according to the PAM and Chl a extraction methods. Therefore, only the 2nd replicate of *E. huxleyi* from the DCM experiment (EDCM2) is used in this study which exhibited values between 0.05 and 0.07 d^{-1} according to all methods. *T. oceanica* showed growth for all of its replicates, only at very low rates: between 0.03 ± 0.01 (fluorescence) and 0.06 ± 0.02 d^{-1} (spectrophotometry).

Growth under the dynamic light conditions of WM was higher for both species: the haptophyte fluctuated between 0.17 ± 0.02 d^{-1} (spectrophotometry) and 0.33 ± 0.01 (cell counts). The diatom grew with rates of as low as 0.16 ± 0.01 d^{-1} (spectrophotometry) and as high as 0.29 ± 0.01 d^{-1} (fluorescence and cell counts). Non exponential growth, probably caused by nutrient limitation, was observed on the last 2 sampling days (data not shown), therefore the samples are considered to have been taken in the exponential and stationary growth phase. Finally, under the dynamic light of the UCM experiment both organisms showed their highest growth rates, with *E. huxleyi* ranging from 0.22 ± 0.03 d^{-1} (spectrophotometry) to 0.58 ± 0.04 d^{-1} (cell counts), while *T. oceanica* ranged between 0.19 ± 0.02 d^{-1} (spectrophotometry) and 0.55 ± 0.02 d^{-1} (cell counts). Once again, nutrient limitation was observed in the last 2 sampling days (data not shown), therefore the samples are considered to have been taken on the exponential and stationary growth phase.

Table 3.1: Growth rates, μ, (d^{-1}) $\pm$ standard deviation (SD) of the 3 replicates of *E. huxleyi* (E) and *T. oceanica* (T) under all irradiance regimes (DCM, WM and UCM). Growth rates of all methods used (Chl a, fluorescence, spectrophotometry and cell counting are shown in this table. *Only the 2nd replicate was taken into account.

	EDCM*	TDCM	EWM	TWM	EUCM	TUCM
Chl a	0.07	0.05±0.01	0.28	0.25±0.02	0.45±0.02	0.38±0.03
Fluorescence	0.05	0.03±0.01	0.29±0.01	0.29±0.01	0.36±0.03	0.39±0.02
spectrophotometry	0.06	0.06±0.02	0.17±0.02	0.16±0.01	0.22±0.03	0.19±0.02
Cell count	0.06	0.04±0.01	0.33±0.01	0.29±0.01	0.58±0.04	0.55±0.02

Growth rate differences among replicates and species were tested for significance ($p < 0.05$) with a single-factor analysis of variance (ANOVA). During cultivation in low irradiance (DCM), the growth of the two species was not significantly different (Table 3.2), with p-values between 0.29 (Chl a) and 0.66 (cell counts). Under the dynamic light conditions of the WM experiment, the μ of *E. huxleyi* was significantly higher than the one of *T. oceanica* for two out of four methods: Chl a ($p = 0.04$) and cell counts ($p = 0.01$). The other two methods (spectrophotometry and fluorescence) gave p-values of around 0.5. Finally, under the dynamic irradiance regime of the UCM setup, only the Chl a method calculated - μ showed significant difference between the

two organisms (p = 0.03) with the haptophyte growing faster once again. The other three methods produced much higher p-values (0.18 - 0.37), meaning that according to them there is no significant difference between the growth of the two organisms.

Table 3.2: p-values from a single-factor ANOVA, performed for μ as calculated by all four methods in order to test the significance of μ differences between replicates and species.

	DCM	WM	UCM
Chl a	0.29	0.04	0.03
Fluorescence	0.36	0.42	0.18
spectrophotometry	0.54	0.56	0.19
Cell count	0.66	0.01	0.37

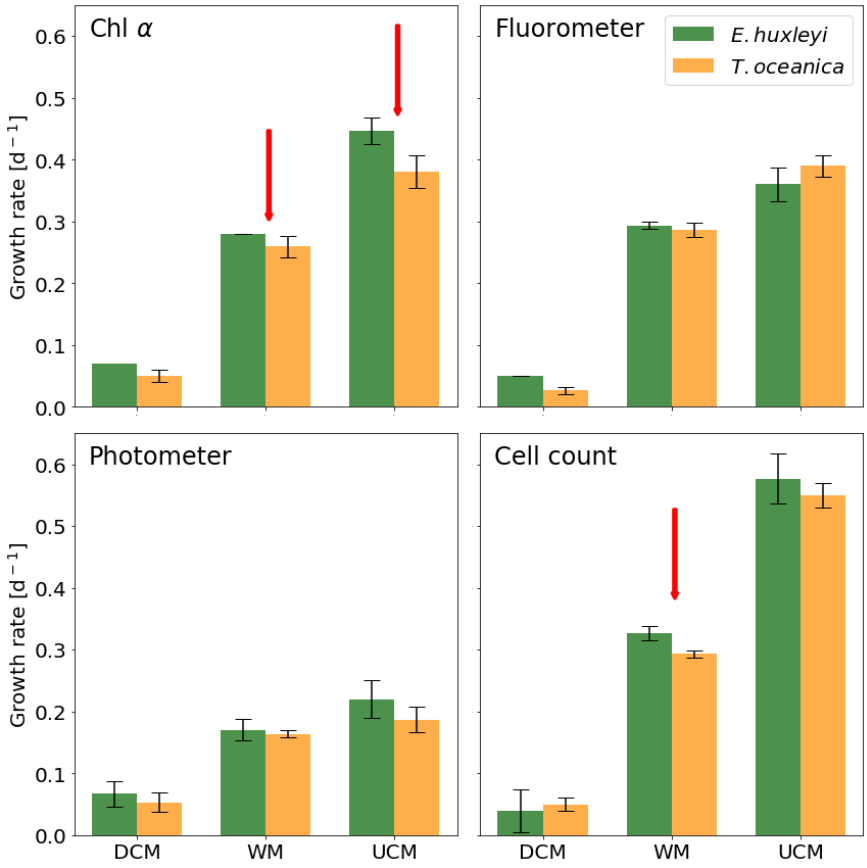

Figure 3.1: Growth rates (μ) of all methods used (Chl a, fluorescence, spectrophotometry and cell counting) presented as mean values of the 3 replicates (bars) $\pm$ standard deviation (errorbars), for *E. huxleyi* and *T. oceanica* under all irradiance regimes (DCM, WM and UCM). The red arrows depict the 3 measurements where statistically signifant difference ($p < 0.05$) between the 2 species has been observed. All units are d^{-1}.

The observed growth rates under the stable, extremely low irradiance of the DCM experiment are very low (below 0.1 d^{-1}) in all cases and both species (Table 3.1). It should also be reminded that *E. huxleyi* did not show any growth in two out of the three replicates, while *T. oceanica* exhibited (extremely low) growth in all replicates under these light-limited conditions (Fig.3.1).

It is obvious (Fig.3.1) that growth was much higher in the other two irradiance regimes (WM and UCM) in both species and ranged between 0.2 and 0.6 d^{-1}. In the low dynamic light experiment (WM) the haptophyte showed significantly higher ($p < 0.05$) growth according to the extracted Chl a measurements and the cell counts. Under the light-saturating and stressful high dynamic irradiance conditions (UCM), *E. huxleyi* exhibited once more higher growth rates according only to the Chl a measurements this time. In all other cases it was impossible to charac-

terize the observed differences as significant ($p > 0.05$).

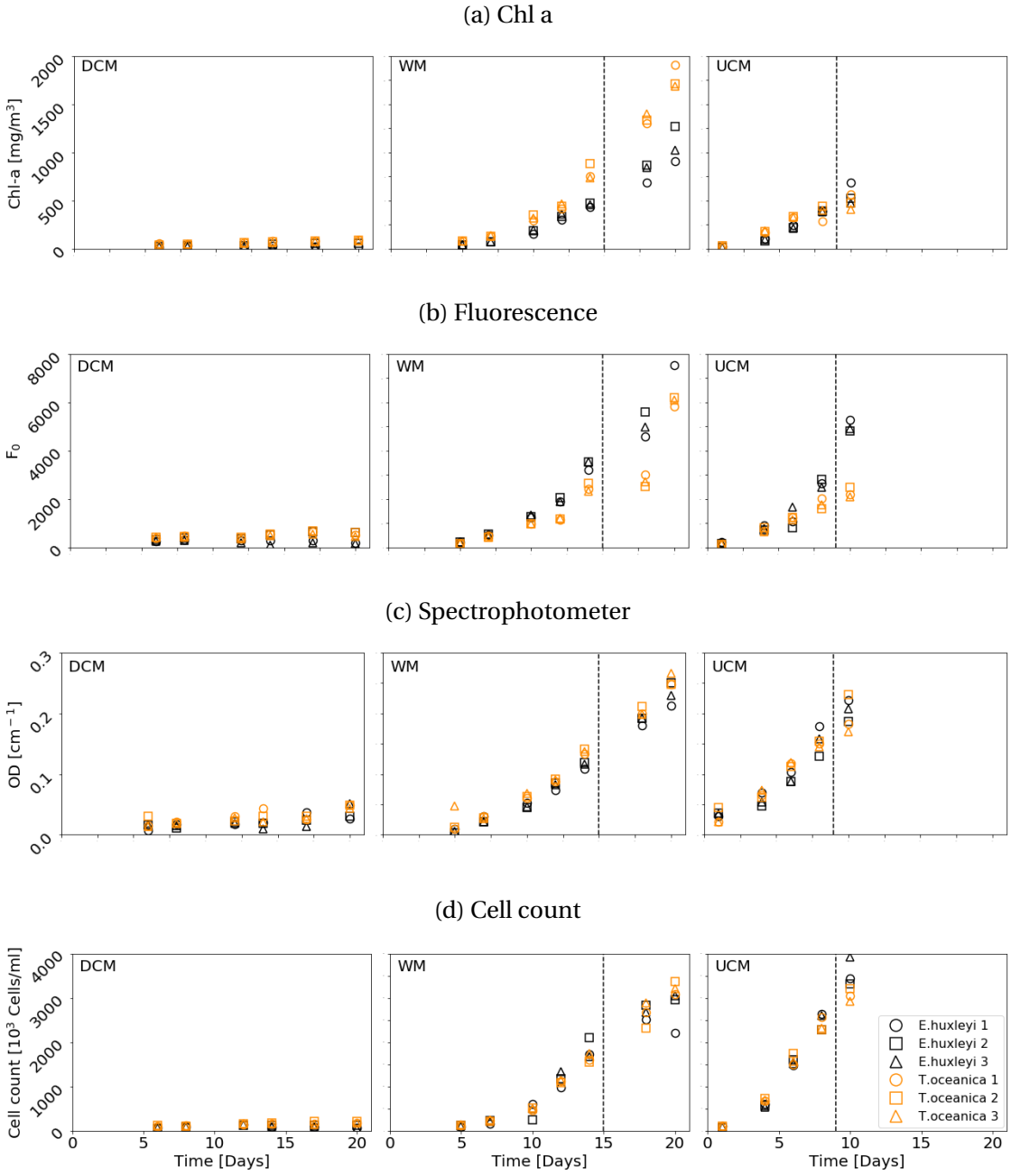

Figure 3.2: Growth according to all four different methods (Chl a extraction, fluorescence, spectrophotometry and cell counts) for the three experiments (DCM, WM and UCM) and both species (*E. huxleyi* and *T. oceanica*). All replicates are shown (3 per species) and are depicted with black colour for the haptophyte and orange for the diatom. In the WM and UCM experiments, only the measurements left of the dashed line were taken into account for the calculation of growth rates (μ).

In all four methods, Chl a extraction, fluorescence, spectrophotometry and cell counts (Fig.3.2), both species produced extremely low values under the stable, low irradiance regime which simulates Deep Chlorophyll Maximum conditions (DCM). On the contrary, important growth has been observed under the Well-Mixed (WM) and Upper Chlorophyll Maximum (UCM) irradiance regimes which simulate the convective deep mixing and the shallow mixing respectively.

Under the WM light conditions, there is a difference in the Chl a concentration of the two species (Fig.3.2(a)) after 20 days of culture, with values of almost 2 μg/L for *T. oceanica* and around 1 μg/L for *E. huxleyi* . The opposite is observed for the fluorescence measurements (Fig.3.2(b)) where *E. huxleyi* gives higher f_o values (around 8000) than *T. oceanica* (around 6000)

on the final sampling day. Yet another behaviour is observed according to the absorption of the species, with the diatom producing constantly slightly higher values from the first day. On the last, 20th day of the WM experiment, both species gave absorption values close to 0.25 cm^{-1}(Fig.3.2(c)). Cell counts (Fig.3.2(d)) tell a different story with both species having similar populations over the entire 20 days of the WM experiment, up to 3.5 $\times$ 10^6 cells/ml. What is common for both species, irrespective of the method, is that values start increasing after the first week of the experiment, under the WM irradiance regime.

In general, it can be said that under the UCM light conditions (Fig.3.2) values start increasing within the first few days of the experiment and after 10 days they reach numbers comparable to 20 days of the WM experiment (absorption and cell counts) or even almost half of them (Chl a content and fluorescence). The Chl a content of both species (Fig.3.2(a)) is around 0.5 $\times$ 10^6 ng/cell, which is almost two times higher compared to the WM values for the same day (around 0.25 $\times$ 10^6 ng/cell). Fluorescence measurements (Fig.3.2(b)) show a clear difference between the species, with *E. huxleyi* producing f_o values 2.5 times higher (5000) than *T. oceanica* (2000) on the 10th day. This value (5000) is almost 3 times higher than the one produced by *E. huxleyi* on the 10th day of the WM experiment. Absorption (Fig.3.2(c)) is similar for both species and reaches values around 0.25 cm^{-1} on the last day, a number almost 5 times higher than the one measured on the 10th day of the WM experiment. The same statement as with Chl a can be made for the cell counts (Fig.3.2(c)): There is no clear difference between the haptophyte and they both have a population almost 7 times higher than the one of the WM light conditions, after 10 days.

3.2 Photo-acclimation

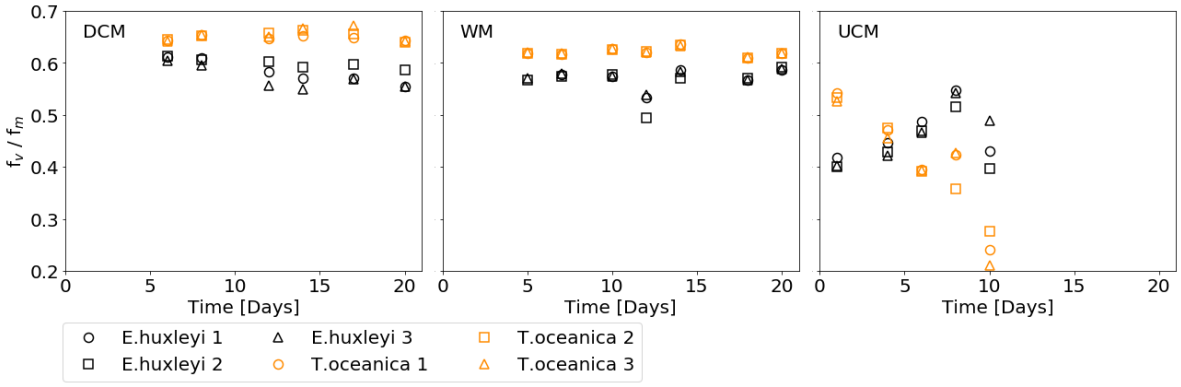

Figure 3.3: Maximum PSII efficiency (f_v/f_m), for all of the three experiments (DCM, WM and UCM) and both species (*E. huxleyi* and *T. oceanica*). All replicates are shown (3 per species) and are depicted with black colour for the haptophyte and orange for the diatom.

Maximum efficiency of PSII (f_v/f_m) was also measured for both species under every irradiance regime (Fig.3.3). During the DCM experiment, the f_v/f_m of *T. oceanica* was stable around the value of 0.65 and the same thing can be said for *E. huxleyi*, only for a slightly lower value (0.6). Under the dynamic light conditions of the WM experiment, f_v/f_m was once again stable for both organisms, slightly higher than 0.6 for *T. oceanica* and below 0.6 for *E. huxleyi*. Finally under the high irradiance conditions of the UCM setup, both organisms exhibited different behaviour: high values (0.55) at the beginning for the diatom, which decreased close to 0.2 on the 10th day of the experiment and lower values (0.4) for the haptophyte at first, which increased up to 0.6 in the end (10th day).

The Chl a content of the cells was calculated for both species under each irradiance regime (Fig.3.4, Table 3.3). During the extremely low light conditions (DCM) the Chl a content of the cells remained stable, around 400 to 500 ng/cell for *T. oceanica* and 300 to 400 ng/cell for *E. huxleyi* (only for the 2nd replicate). The haptophyte showed exactly the same behaviour under the

Table 3.3: Average of Chl a (ng/cell) and OD ($\times 10^{-4}$cm^{-1}cell^{-1}) per cell $\pm$ standard deviation (SD) of *E. huxleyi*, E, and *T. oceanica* ,T under all irradiance regimes, DCM, WM and UCM. The values are the average of the 3 replicates. *Only the 2nd replicate was taken into account.

	Chl a/cell	**OD/cell**
EDCM*	395±68	2.05±0.62
TDCM	450±49	1.94±0.49
EWM	345±100	0.86±0.36
TWM	547±96	1.07±0.47
EUCM	166±29	0.70±0.20
TUCM	208±55	0.74±0.16

low dynamic light conditions (WM) while the diatom produced more Chl a (500 to 600 ng/cell). Finally, the high dynamic light conditions (UCM) made both species compose significantly less Chl a: 300 ng/cell (diatom) and 200 ng/cell (haptopyte) at the beginning which decreased down to 100 ng/cell for both species on the final day of the experiment.

The Optical Density (OD) per cell was calculated for both species under every irradiance regime (Fig.3.5, Table 3.3). During the extremely low light conditions (DCM) the OD remained stable, around 2×10^{-4} cm^{-1}cell^{-1} for both species. The algae showed similar behaviour under the low dynamic light conditions (WM) with a stable OD of around 1×10^{-4} cm^{-1}cell^{-1} this time. Finally, the high dynamic light conditions (UCM) made both species exhibit an even lower OD: less than 1×10^{-4} cm^{-1}cell^{-1}. It has to be noted that the first measurement, on the second day of the experiment, showed OD values more than 4 times higher which immediately decreased after 2 days. These values were not included in the calculations of the average values and standard deviations.

The OD against Chl a content of the cells relationship was also examined for both species under every irradiance regime (Fig.3.6). During the stable low light conditions (DCM) the values were extremely low, making it impossible to perform regression analysis and reach to useful conclusions. The haptophyte showed a linear relationship (slope=2.5×10^{-4}) for Chl a concentrations of up to 500 mg/m^3. Above this concentration, OD started being underestimated. A similar behavior was observed from the diatom as well, only with a lower slope (2×10^{-4}) and once again underestimated OD values above 500 mg/m^3 of Chl a. Under the extreme fluctuations of the high, dynamic light conditions of the UCM experiment both species showed a linear relationship between OD and Chl a with similar slopes (3×10^{-4}).

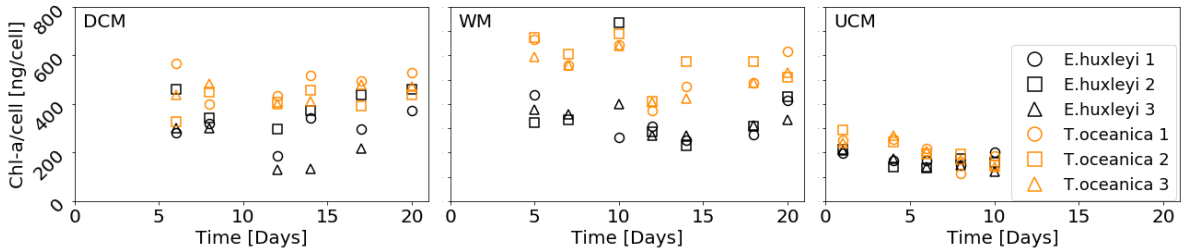

Figure 3.4: Results of Chl a content per cell calculations, for all of the three experiments (DCM, WM and UCM) and both species (*E. huxleyi* and *T. oceanica*). All replicates are shown (3 per species) and are depicted with black colour for the haptophyte and orange for the diatom.

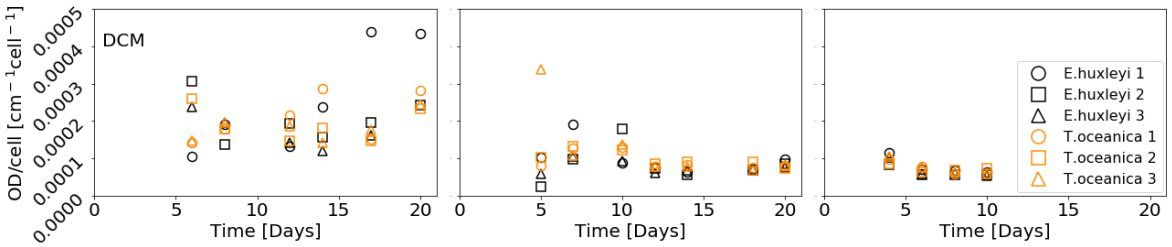

Figure 3.5: Results of Optical Density (OD) per cell calculations, for all of the three experiments (DCM, WM and UCM) and both species (*E. huxleyi* and *T. oceanica*). All replicates are shown (3 per species) and are depicted with black colour for the haptophyte and orange for the diatom.

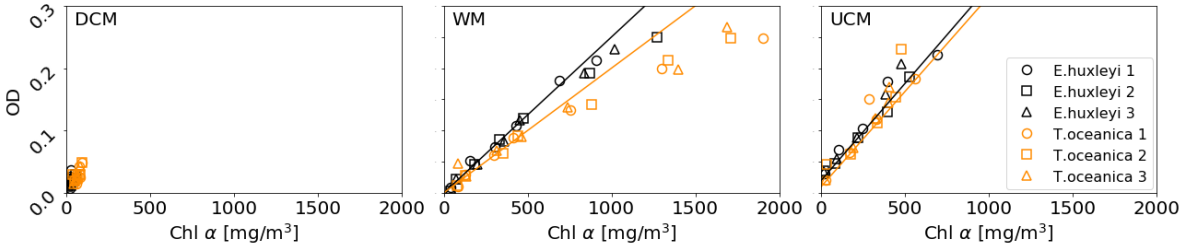

Figure 3.6: Results of Optical Density (OD) against Chl a content, for all of the three experiments (DCM, WM and UCM) and both species (*E. huxleyi* and *T. oceanica*). All replicates are shown (3 per species) and are depicted with black colour for the haptophyte and orange for the diatom. For the WM experiment the trendline slopes are: a_{EWM}=0.00025 and a_{TWM}=0.0002. For the UCM experiment the trendline slopes are: a_{EUCM}=0.0003 and a_{TUCM}=0.0003

Chapter 4

Discussion

DCM experiment

The extremely low irradiance of 5 μmol m^{-2} s^{-1} in combination with the position of the specific flasks in the setup (sides of the box), probably hindered the growth of the 1st and the 3rd replicates of *E. huxleyi* in the DCM experiment. The 2nd replicate was placed in the middle of the setup, thus receiving slightly higher irradiance and possibly allowing it to grow at a slow rate (0.05 - 0.08 d^{-1}). On the contrary, *T. oceanica* exhibited growth in all of 3 replicates, something expected as the specific species is able to exploit low-light regimes [24, 8]. These rates are comparable to the ones reported by Laws & Bannister (1980) [15] (0.06 - 0.13 d^{-1}) and by Eppley et al. (1973) [5] (0.14 - 0.21) for phytoplankton in DCM state, especially if the extremely low irradiance (5 μmol m^{-2} s^{-1}) is taken into account.

The diatom showed its photoacclimation potential by producing more Chl a per cell than the haptophyte, thus being able to exploit the extremely low light levels at the simulated depth (100m). Both species had quite high PSII efficiency values over the entire 20 days of the experiment, showing clearly that they were prepared to exploit the weak light. The extremely low growth rates might not have allowed the cells to complete a division over the 20 days of the experiment and it would be interesting to study their acclimation over longer time periods.

WM experiment

Under the WM light conditions both species showed higher μ by almost an order of magnitude in comparison to the DCM conditions. The conditions that were simulated might have been not representative of the North Atlantic convection. This is suspected because the growth rates seem to be higher than the ones expected from algae maintaining low populations through the winter, until the initiation of the spring bloom (close to zero according to Mignot et al. (2018) [16]). The μ might have been exaggerated because of the assumptions made (explained in the methods section) and mainly because of the averaged irradiance curve. This way, the cells received a relatively low light but on a daily cycle and without large fluctuations, which gave them the opportunity to acclimate better than they would normally do in situ. Another important factor could be the very high mixing speed chosen (15.5 h/cycle) which reduced the time spent in darkness to a minimum. The μ values derived from the WM experiment, are comparable to those by Schouten et al. (2006) [25], who estimated the growth rate to be 0.4 d^{-1}, for an *E. huxleyi* culture grown under 10^{o}C, 35.1 salinity, 16:8h L:D cycle and 300 μmol m^{-2} s^{-1} irradiance. On the other hand, Sakshaug et al. (1987) observed no growth of *T. oceanica* when cultivated under 15^{o}C, 32.5 PSU and continuous light of 17 μmol m^{-2} s^{-1} [24].

Under this low-light dynamic regime, the diatom is better acclimated (Chl a content per cell and f_v/f_m), confirming that *Thalassiosira* species are better adapted to low-light and well-mixed conditions [8]. Surprisingly, *E. huxleyi*'s μ (cell counts) is significantly higher than *T. oceanica*'s (Table 3.2), meaning possibly that in the absence of competition and provided abundant nutrients, it can grow at faster rates. In general, the differences in μ are very small and hardly significant, suggesting that factors other than light might influence their dominance in

the water column. What is surprising here is the lower OD/cell values of both species compared to the DCM experiment. Although Chl a/cell values remain high in the 2 low-light experiments, a different behavior is observed by OD showing a difference between the 2 methods used: fluorescence and spectrophotometry. Another interesting point are the low μ estimated by spectrophotometry for the UCM experiment, almost half of the other methods (Table 3.1). A look at the OD/Chl a ratio (Fig.3.6) reveals that this relationship is linear only for Chl a concentrations up to 500 mg/m^3. If only the OD values from the days when Chl a concentrations were lower than 500 mg/m^3 are taken into account, then the growth rates are higher: 0.24±0.05 for $E.huxleyi$ and 0.24±0.02 for $T.oceanica$, which are much closer to the values estimated using the other 3 methods.

UCM experiment

The μ (cell counts) of the haptophyte is, surprisingly, not significantly higher than the diatom's in the UCM experiment (Table 3.1). *E. huxleyi* is supposed to have a competitive advantage under high light regimes thanks to fast pigment adjustments and high photoinhibition resistance, according to literature [18, 27]. Both species exhibit almost double μ values than in the WM experiment (up to 0.58 d^{-1} based on cell counts), proving that they acclimated well to the extreme fluctuations of the light and achieved growth rates on the higher end of those estimated in the contemporary ocean for *E. huxleyi* [3, 21]. Schouten et al. (2006) estimated *E. huxleyi* μ of 0.56 and 0.68 d^{-1} for cultures grown under 21 and 15 ^{o}C respectively and salinity of 35.1 PSU. In general, maximum μ of *E. huxleyi* strains, cultivated in optimum conditions of irradiance and nutrient supply but with varying temperatures, range between 0.60 and 2.80 d^{-1} [19]. A similar range is also the case for *T. oceanica* with maximum rates between 0.45 and 2.80 d^{-1} [24, 20].

In the UCM experiment, the high, dynamic light conditions resulted in a much lower Chl a cell content (Fig. 3.4) forcing both species to adapt to the extreme irradiance fluctuations. The haptophyte showed an almost stable concentration (even after the 1st division) over the course of the experiment while the diatom started from a higher value and after roughly one week (almost 3 divisions later) reached the levels of *E. huxleyi*. This could show the "flexibility" of the haptophyte and the speed with which it acclimates to the new conditions by reducing its chlorophyll content. Regarding the photosynthetic competence, f_v/f_m (Fig. 3.3), *E. huxleyi* shows an increase during the first week which can be explained possibly by differences in the sampling process: Although the samples were always left in the dark before the PAM measurements, the time of sampling differed. The first samples were taken at a time when irradiance was relatively high, while the 3 last samples were collected early in the morning, when the light was very low. This might have had an effect on the stress imposed on the *E. huxleyi* cells, as reflected by the f_v/f_m. On the last day though, there is an obvious decrease most likely due to the nutrient depletion. *T. oceanica* on the other hand shows a clear decrease in f_v/f_m for the entire 10 days of the experiment. Exposure to high irradiance might have caused photodamage and significantly decreased the PSII potential efficiency. The cells also down-regulate the PSII reaction centers in order to avoid photodamage and as a result reduce f_v/f_m even further. Finally the nutrient depletion during the last two days probably played an additional role. It has to be noted that these results, f_v/f_m under UCM conditions, need to be used with caution for the aforementioned reasons.

The flexibility of *E. huxleyi* is once again apparent as it shows significantly higher growth rates based on Chl a ($p < 0.05$). In contrary to the WM experiment, the haptophyte did not show significantly higher cell division rates, meaning that the fast Chl a production is not the only factor that gives a competitive advantage and that low temperatures (13.5^{o}C in this case), salinity (35 in all experiments) and nutrient uptake should also be taken into account. Under the high irradiance condition the μ, as estimated by OD, is much lower (less than 50%) of the cell count-one. OD depends on cell numbers and pigment content, among other factors [12], and in this experiment the high populations in combination with the low Chl a cell content possibly led to low absorption measurements.

4 different methods

The different methods used in this study for the calculation of growth rates showed a similar trend with increasing values from DCM to WM and eventually to UCM conditions. The rates estimated by cell counts were the highest, followed by Chl a extraction and PAM methods and spectrophotometry producing the lowest values. It is clear that studies using different methods for the estimation of μ can not be compared.

Comparison with NEMO-PISCES v2

The results of this study show no clear difference between *T. oceanica* and *E. huxleyi* with their growth rates being comparable under each STRATIPHYT-simulated regime. Based on literature, an advantage of the diatom was expected under low-light and deep-mixing conditions while higher growth of the haptophyte was expected under high-irradiance conditions. These were not the findings of this study in any case. Furthermore, this experimental study contradicts the results of the modelling study, where there was a "*constant overestimation of diatoms in nutrient-rich and coastal regions compared to STRATIPHYT measurements*". This is indeed something that needs to be further investigated and is acknowledged by Aumont et al. (2015), as they state that in the future, PISCES needs to improve in two apects: (a) a more sophisticated treatment of phytoplankton physiology and (b) inclusion of mixotrophic organisms [1].

Chapter 5

Conclusion

E. huxleyi and *T. oceanica* showed very good photoacclimation abilities with fast regulation of the Chl a cell content and the maximum efficiency of PSII, which resulted in growth for seven out of the nine replicates under any irradiance - temperature regime implemented.

The growth rates of both species were similar in each of the experiments. Since the conditions simulated were at the extreme end of what was observed in the STRATIPHYT cruises, we can conclude that responses to irradiance are not a probable cause for differences in the occurrence of these species in the field.

Acknowledgements

First of all I would like to thank Anita and Richard for offering to me this amazing topic and for supporting me through the long process. Many thanks to Willem for his precious, daily supervision during my experiments in Groningen University, our discussions (and the eierballen) were crucial for this project. I would also like to thank Jack for his supervision and extremely helpful comments.

I had a great time during these 8 months, while working in KNMI and Groningen University, I met many friendly and very helpful people and made new friends. Thank you all! None of this would have been possible though, without the support of the most important person: Nikoleta.

Bibliography

[1] Aumont, O., Ethe, C., Tagliabue, A., Bopp, L., & Gehlen, M. (2015). PISCES-v2: An ocean biogeochemical model for carbon and ecosystem studies. Geoscientific Model Development, 8(8), 2465–2513. https://doi.org/10.5194/gmd-8-2465-2015

[2] Behrenfeld, M. J., Marañón, E., Siegel, D. A., & Hooker, S. B. (2002). Photoacclimation and nutrient-based model of light-saturated photosynthesis for quantifying oceanic primary production. Marine Ecology Progress Series, 228, 103–117. https://doi.org/10.3354/meps228103

[3] Bidigare, R. R., Fluegge, A., Freeman, K., Hanson, K. L., HAYES, J. M., Milero, F. G., … Wakeham, S. G. (1997). Consistent fractionation of 13C in nature and in the laboratory: Growth-rate effects in some haptophyte algae. Global Biogeochemical Cycles, 11(2), 279–292.

[4] Dubinsky, Z., & Stambler, N. (2009). Photoacclimation processes in phytoplankton: Mechanisms, consequences, and applications. Aquatic Microbial Ecology, 56(2–3), 163–176. https://doi.org/10.3354/ame01345

[5] Eppley, R. W., Renger, E. H., Venrick, E. L., & Mullin, M. M. (1973). a Study of Plankton Dynamics and Nutrient Cycling in the Central Gyre of the North Pacific Ocean. Limnology and Oceanography, 18(4), 534–551. https://doi.org/10.4319/lo.1973.18.4.0534

[6] Goto, N., Kihira, M., & Ishida, N. (2008). Seasonal distribution of photosynthetically active phytoplankton using pulse amplitude modulated fluorometry in the large monomictic Lake Biwa, Japan. Journal of Plankton Research, 30(10), 1169–1177. https://doi.org/10.1093/plankt/fbn073

[7] Guillard, R. R., and J. H. Ryther. 1962. Studies on planktonic diatoms 1. Cyclotella nana Hustedt and Detonula conferuacea (Cleve) Gran. Can. J. Microbiol. 8: 229–239.

[8] Harris, A. S. D., Lewis, J., Medlin, L. K., Harris, A. S. D., & Jones, K. J. (1995). Thalassiosira species (Bacillariophyceae) from a Scottish sealoch. European Journal of Phycology, 30(2), 117–131. https://doi.org/10.1080/09670269500650881

[9] Honeywill, C., Paterson, D. M., & Hagerthey, S. E. (2002). Determination of microphytobenthic biomass using pulse-amplitude modulated minimum fluorescence. European Journal of Phycology, 37(4), 485–492. https://doi.org/10.1017/S0967026202003888

[10] Hoppenrath, M., Beszteri, B., Drebes, G., Halliger, H., Van Beusekom, J. E. E., Janisch, S., & Wiltshire, K. H. (2007). Thalassiosira species (Bacillariophyceae, Thalassiosirales) in the North Sea at Helgoland (German Bight) and Sylt (North Frisian Wadden Sea) - A first approach to assessing diversity. European Journal of Phycology, 42(3), 271–288. https://doi.org/10.1080/09670260701352288

[11] Jurado, E., Dijkstra, H. A., & Van Der Woerd, H. J. (2012). Microstructure observations during the spring 2011 STRATIPHYT-II cruise in the northeast Atlantic. Ocean Science, 8(6), 945–957. https://doi.org/10.5194/os-8-945-2012

[12] Kain, J. M., & Fogg, G. E. (1958). Studies on the growth of marine phytoplankton: I. Asterionella japonica gran. Journal of the Marine Biological Association of the United Kingdom, 37(2), 397–413. https://doi.org/10.1017/S0025315400023778

[13] Kulk, G., de Poll, W. H. va., Visser, R. J. W., & Buma, A. G. J. (2011). Distinct differences in photoacclimation potential between prokaryotic and eukaryotic oceanic phytoplankton. Journal of Experimental Marine Biology and Ecology, 398(1–2), 63–72. https://doi.org/10.1016/j.jembe.2010.12.011

[14] Lande, R., & Wood, A. M. (1987). Suspension times od particles in the upper ocean. Deep-Sea Research, 34(1), 61–72. Retrieved from physical ecology

[15] Laws, E. A., & Bannister, T. T. (1980). Nutrient- and light-limited growth of Thalassiosira fluviatilis in continuous culture, with implications for phytoplankton growth in the ocean. Limnology and Oceanography, 25(3), 457–473. https://doi.org/10.4319/lo.1980.25.3.0457

[16] Mignot, A., Ferrari, R., Claustre, H. (2018). Floats with bio-optical sensors reveal what processes trigger the North Atlantic bloom. Nature Communications, 9(1), 190. https://doi.org/10.1038/s41467-017-02143-6

[17] Mojica, K. D. A., van de Poll, W. H., Kehoe, M., Huisman, J., Timmermans, K. R., Buma, A. G. J., … Brussaard, C. P. D. (2015). Phytoplankton community structure in relation to vertical stratification along a north-south gradient in the Northeast Atlantic Ocean. Limnology and Oceanography, 60(5), 1498–1521. https://doi.org/10.1002/lno.10113

[18] Nanninga, H. J., & Tyrrell, T. (1996). Importance of light for the formation of algal blooms by Emiliania huxleyi. Marine Ecology Progress Series, 136(1–3), 195–203. https://doi.org/10.3354/meps136195

[19] Paasche, E., & Box, P. D. (2002). E. contents, 40(January), 503–529.

[20] Popovich, C. a, & Gayoso, a M. (1999). Effect of irradiance and temperature on the growth rate of¡it¿Thalassiosira curviseriata¡/it¿ Takano (Bacillariophyceae), a bloom diatom in Bahía Blanca estuary (Argentina). Journal of Plankton Research, 21(6), 1101–1110. https://doi.org/10.1093/plankt/21.6.1101

[21] Popp, B. N., Kenig, F., Wakeham, S. G., Laws, E. A., & Bidigare, R. R. (1998). Does growth rate affect ketone unsaturation and intracellular carbon isotopic variability in Emiliania huxleyi? Paleoceanography, 13(1), 35–41. https://doi.org/10.1029/97PA02594

[22] Rickaby, R. E. M., Schrag, D. P., Zondervan, I., & Riebesell, U. (2002). Growth rate dependence of Sr incorporation during calcification of Emiliania huxleyi. Global Biogeochemical Cycles, 16(1), 6-1-6–8. https://doi.org/10.1029/2001GB001408

[23] Nutrient uptake and alkaline phosphatase (ec 3:1:3:1) activity of. (2000). Cell, 96, 87–96.

[24] Sakshaug, E., Demers, S., & Yentsch, C. M. (1987). Thalassiosira oceanica and T. pseudomonana: two different photoadaptational responses. Marine Ecology-Progress Series, 41, 275–282.

[25] Schouten, S., Ossebaar, J., Schreiber, K., Kienhuis, M. V. M., Langer, G., Benthien, A., & Bijma, J. (2006). The effect of temperature, salinity and growth rate on the stable hydrogen isotopic composition of long chain alkenones produced by Emiliania huxleyi and Gephyrocapsa oceanica. Biogeosciences, 3(1), 113–119. https://doi.org/10.5194/bg-3-113-2006

[26] Sunda, W. G., & Huntsman, S. A. (1995). Unknown - Unknown - Sunda, Huntsman - 1995 - Iron uptake and growth limitation in oceanic and coastal phytoplankton.pdf.pdf. Marine Chemistry, 50, 189–206.

[27] Tyrrell, T., & Merico, A. (2004). Emiliania huxleyi: bloom observation and the conditions that induce them. Coccolithophores: From Molecular Processes to Global Impact, 585–604. https://doi.org/10.1007/978-3-662-06278-4_4

[28] Van De Poll, W. H., Visser, R. J. W., & Buma, A. G. J. (2007). Acclimation to a dynamic irradiance regime changes excessive irradiance sensitivity of Emiliania huxleyi and Thalassiosira weissflogii. Limnology and Oceanography, 52(4), 1430–1438. https://doi.org/10.4319/lo.2007.52.4.1430

[29] Van De Poll, W. H., Kulk, G., Timmermans, K. R., Brussaard, C. P. D., Van Der Woerd, H. J., Kehoe, M. J., … Buma, A. G. J. (2013). Phytoplankton chlorophyll a biomass, composition, and productivity along a temperature and stratification gradient in the northeast Atlantic Ocean. Biogeosciences, 10(6), 4227–4240. https://doi.org/10.5194/bg-10-4227-2013

[30] Westbroek, P., Brown, C. W., Bleijswijk, J. van, Brownlee, C., Brummer, G. J., Conte, M., … Young, J. (1993). A model system approach to biological climate forcing. The example of Emiliania huxleyi. Global and Planetary Change, 8(1–2), 27–46. https://doi.org/10.1016/0921-8181(93)90061-R